UNIVERSIDADE ESTADUAL PAULISTA
"JÚLIO DE MESQUITA FILHO"
Faculdade De Ciências E Tecnologia
Campus Presidente Prudente
Programa De Pós-Graduação Em Ciências Cartográficas

LORAM SIQUEIRA

CONTRIBUTION OF UNESP ON BROADCAST EPHEMERIS AND PDOP MONITORING FOR GNSS IN THE IGMA- TRIAL PROJECT

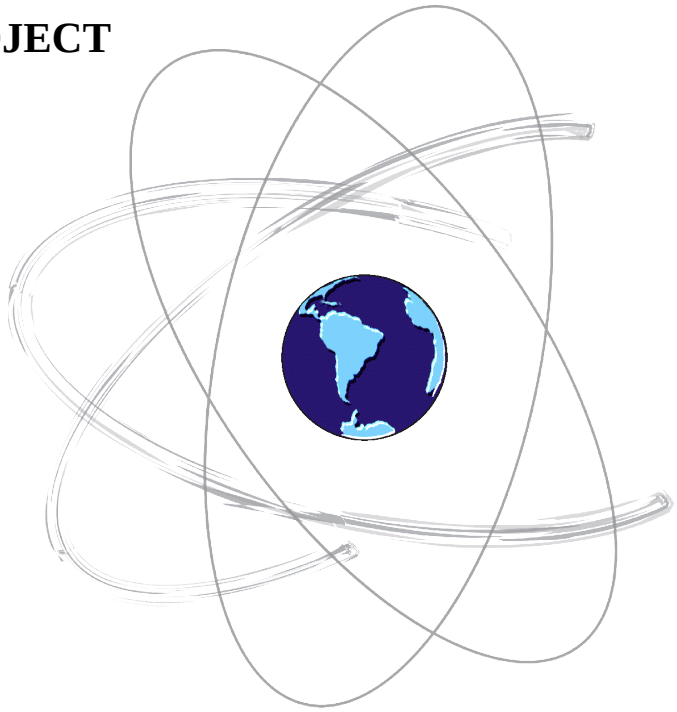

Presidente Prudente

2020

LORAM SIQUEIRA

CONTRIBUTION OF UNESP ON BROADCAST EPHEMERIS AND PDOP MONITORING FOR GNSS IN THE IGMA- TRIAL PROJECT

Master's degree dissertation report presented to the Cartographic Sciences Graduation Program from the Science and Technology College from the São Paulo State University

Supervisor: PhD João Francisco Galera Monico

PRESIDENTE PRUDENTE

2020

S618c

Siqueira, Loram
Contribution of Unesp on broadcast ephemeris and PDOP monitoring for GNSS in the IGMA - Trial Project / Loram Siqueira. -- Presidente Prudente, 2020
100 f. : il., tabs.

Dissertação (mestrado) - Universidade Estadual Paulista (Unesp), Faculdade de Ciências e Tecnologia, Presidente Prudente
Orientador: João Francisco Galera Monico

1. Efemérides transmitidas. 2. Acurácia. 3. PDOP. 4. WPDOP. 5. Multi-GNSS. I. Título.

Sistema de geração automática de fichas catalográficas da Unesp. Biblioteca da Faculdade de Ciências e Tecnologia, Presidente Prudente. Dados fornecidos pelo autor(a).

Essa ficha não pode ser modificada.

unesp

UNIVERSIDADE ESTADUAL PAULISTA

Câmpus de Presidente Prudente

ATA DA DEFESA PÚBLICA DA DISSERTAÇÃO DE MESTRADO DE LORAM SIQUEIRA, DISCENTE DO PROGRAMA DE PÓS-GRADUAÇÃO EM CIÊNCIAS CARTOGRÁFICAS, DA FACULDADE DE CIÊNCIAS E TECNOLOGIA - CÂMPUS DE PRESIDENTE PRUDENTE.

Aos 04 dias do mês de março do ano de 2020, às 14:00 horas, no(a) Sala de Apresentação de Projetos, reuniu-se a Comissão Examinadora da Defesa Pública, composta pelos seguintes membros: Prof. Dr. JOÃO FRANCISCO GALERA MONICO - Orientador(a) do(a) Departamento de Cartografia / Faculdade de Ciencias e Tecnologia de Presidente Prudente, Profa. Dra. DANIELE BARROCA MARRA ALVES do(a) Departamento de Cartografia / Faculdade de Ciencias e Tecnologia de Presidente Prudente, Prof. Dr. HAROLDO ANTONIO MARQUES do(a) Seção de Engenharia Cartográfica / Instituto Militar de Engenharia, sob a presidência do primeiro, a fim de proceder a arguição pública da DISSERTAÇÃO DE MESTRADO de LORAM SIQUEIRA, intitulada **Contributions on PDOP and broadcast ephemeris monitoring for GNSS in the IGMA trial project**. Após a exposição, o discente foi arguido oralmente pelos membros da Comissão Examinadora, tendo recebido o conceito final: APROVADO . Nada mais havendo, foi lavrada a presente ata, que após lida e aprovada, foi assinada pelos membros da Comissão Examinadora.

Prof. Dr. JOÃO FRANCISCO GALERA MONICO

Profa. Dra. DANIELE BARROCA MARRA ALVES

Prof. Dr. HAROLDO ANTONIO MARQUES

DADOS CURRICULARES

Loram Siqueira

Nascimento	26/10/1993
Filiação	Sebastiana Siqueira de Freitas
2011-2016	Graduação Bacharelado em Engenharia de Agrimensura e Cartográfica Universidade Federal Rural do Rio de Janeiro – UFRRJ
2017 – 2020	Pós-Graduação Mestrado em Ciências Cartográficas Faculdade de Ciencias e Tecnologias - Unesp

AGRADECIMENTOS

Agradeço ao universo, e a Deus por assim dizer, que em suas infinitas possibilidades me colocou em um lugar incrível rodeado por pessoas maravilhosas.

A minha mãe (*in memoriam*), uma mulher maravilhosa, forte e dedicada que moveu montanhas para que eu seguisse meus sonhos, que você esteja vendo das estrelas aonde o seu filho chegou. A minha prima Sandra Casati e ao meu irmão Edmilson que foram parte essencial durante os momentos tempestuosos da minha vida e a todos os meus familiares que de alguma forma foram parte importante desta fase da minha.

Agradeço a minha segunda família em Minas Gerais: Márcio, Miriam, Eduardo, Erick, Fátima por serem meu porto seguro quando eu precisei recarregar minhas energias pois acreditava não conseguiria mais caminhar.

Ao meu orientador professor Dr. João Francisco Galera Monico pela paciência durante esta jornada e por ser o principal motivador para que eu sempre seguisse em frente. A professora Drª Daniele Barroca Marra Alves por suas contribuições como banca do exame de qualificação e como membro da banca de defesa. Ao professor Dr. Haroldo Antônio Marques pelas contribuições como membro da banca da defesa.

Agradeço a todos do PPGCC por terem me acolhido como parte da família em especial Ana Lucia, Gabriel, Samara, Thainá, Luiz, Paulo Setti, Cris, Caio, Weverton, Fran, Vivi, Renato, Gabriela, Cida e Zilda.

Agradeço a minha família em Presidente Prudente: Sandra, Júlio, João, Maycon, Camila, Mônica, Lilian, Rodrigo, Letícia, Carlos, Carolina e André pelo apoio e companheirismo, pois foi a companhia de vocês que me permitiu chamar esta cidade de meu lar durante esses anos de mestrado.

Agradeço a UNESP, pela formação e estrutura oferecida. O presente trabalho foi realizado com apoio da Coordenação de Aperfeiçoamento de Pessoal de Nível Superior - Brasil (CAPES) - Código de Financiamento 001

RESUMO

A modernização do GNSS (Global Navigation Satellite System) com a inclusão de novas constelações e melhorias nos sistemas já disponíveis foi avaliada com grande interesse na última década. A combinação de diferentes constelações de satélite expande as aplicações possíveis; portanto, o termo multi-GNSS apareceu para designar o uso desses múltiplos sistemas. O IGS (International GNSS Service), observando a necessidade dos usuários que começaram a usar o multi-GNSS, lançou em 2011 a proposta de projeto experimental IGMA (International GNSS Monitoring Assessment). O projeto visa criar um sistema internacional de análise GNSS com resultados que apresentem confiabilidade para usuários em todo o mundo. Na chamada para a participação como centro de análise a FCT-Unesp foi aceita como parte do projeto para avaliar dois dos quatro parâmetros propostos: Diluição da Precisão da Posição (PDOP) e a acurácia das efemérides transmitidas. Dos sistemas disponíveis, quatro foram escolhidos: GPS, Galileo. GLONASS e BeiDou nessa pesquisa. Foi realizado um estudo sobre o estado da arte para as aplicações de PDOP e WPDOP (Diluição da precisão ponderada na posição). Nas análises de acurácia, foi utilizado a correção entre o centro de fase e o centro de massa do satélite para comparar corretamente as efemérides finais e as transmitidas durante 600 dias (os 120 primeiros dias de cada ano entre 2015 e 2019). O GPS apresentou um RMSE 3D de 1,94 m, Galileo 1,19 m, GLONASS 7,21 m e BeiDou 3,19 m. As análises do PDOP e WPDOP foram realizadas para avaliar a correlação desses elementos com a qualidade do posicionamento por ponto simples. Para o WPDOP foi utilizado um modelo de ponderação que considerou o ângulo de elevação do satélite já proposto na literatura. Uma estação da RBMC (BRAZ) foi escolhida para realização do experimento. Doze dias foram escolhidos, os quais representam variações nos elementos que influenciarão a transmissão do sinal na atmosfera: troposfera e ionosfera. O coeficiente de correlação entre o PDOP e o erro 3D foi classificada como não correlacionada em 25% dos dias, fracamente relacionada para o restante. O WPDOP teve uma correlação moderada com o erro 3D em 84% dos dias e fracamente correlacionada no restante. O projeto de teste da IGMA é uma boa oportunidade para a comunidade GNSS abordar tópicos importantes sobre a modernização dos sistemas de navegação. Sobre a precisão das efemérides transmitidas, esta pesquisa mostrou que cada sistema tem uma acurácia que precisa ser considerada ao combiná-los para o posicionamento. Para o PDOP, observa-se que o aumento no número de satélites e, portanto, o valor de PDOP diminuir não reflete em uma melhor qualidade do posicionamento. O WPDOP mostrou que a inclusão de informações com significado físico pode fornecer uma correlação mais alta entre esse valor e o erro 3D de um posicionamento de ponto simples.

Palavras-chaves: Efemérides Transmitidas, Acurácia, WPDOP

ABSTRACT

The modernization of GNSS (Global Navigation Satellite System) with the inclusion of new constellations and improvements in the already available systems has been assessed with great interest over the last decade. The combination of different satellite constellations expands the possible applications, so the term multi-GNSS appeared to designate the use of these multiple navigation systems. The IGS (International GNSS Service), observing the need of the users who started using multi-GNSS, launched in 2011 the proposal for the IGMA (International GNSS Monitoring Assessment) trial Project. It aims to create an international GNSS analysis system with results that present reliability for users around the world. In the call for participation as a center of analysis, FCT-Unesp was accepted as part of the trial project to evaluate the following parameters: Position Dilution of Precision (PDOP) and the accuracy of the broadcast ephemeris. Of the available systems, four were chosen: GPS, Galileo, GLONASS e BeiDou. A state-of-the-art study of PDOP and WPDOP (Weighted Position Dilution of Precision) applications was performed. On the accuracy analysis, it was used the phase center vector to correctly compare the final and broadcast ephemeris for 600 days (the first 120 days for each year between 2015 and 2019). The results show that GPS had an overall RMSE of 1.94 m, Galileo 1.94 m, GLONASS 7.21 m and BeiDou 3.19 m. The PDOP and WPDOP analyzes were carried out to evaluate the correlation of these elements with the quality of a standard point positioning. For WPDOP it was used a weighting model that considered the satellite elevation angle. A known station from the RBMC (BRAZ) was used for the analysis. Twelve days were chosen to represent variations on the elements that would influence the signal transmission in the atmosphere: Troposphere and Ionosphere. The correlation between the PDOP and the 3D error presented as no correlated for 25% of the days and weekly correlated remaining ones. The WPDOP had a moderate correlation with the 3D error on 84% of the days and strongly correlated to the other days. The IGMA trial project is a good opportunity for the GNSS community to address important topics on the modernization of navigation systems. On the broadcast accuracy this research showed that each GNSS has an accuracy that needs to be considered when combining them for positioning. For the PDOP it shows that increasing the number of satellites and therefore decreasing the PDOP value does not reflect in a higher reliability of the positioning. WPDOP showed that including information that have physical meaning can give a higher correlation between this value and the 3D error of a standard point positioning.

Keywords: Broadcast Ephemeris, Accuracy, WPDOP

LIST OF FIGURES

LIST OF TABLES

LIST OF ABBREVIATIONS

GNSS	Global Navigation Satellite System
GLONASS	Globalnaya Navigatsionnaya Sputnikovaya Sistema
BDS	BeiDou Navigation Satellite System
IGS	The International GNSS Service
QZSS	Quasi Zenith Satellite System
SIS	Signal in Space
UTC	Coordinated Universal Time
PDOP	Position Dilution of Precision
Unesp	São Paulo State University
GEGE	Grupo de Estudos em Geodésia Especial
WPDOP	Weighting Position Dilution of Precision
SPP	Standard Point Positioning
IGMA	International Monitoring and Assessment
LEO	Low Earth Orbit
AC	Analyses Centers
RMSE	Root Mean Squared Error
MGEX	Multi-GNSS Experiment
CoM	Center of Mass
CoP	Center of Phase
USA	United States of America
USSR	Union of The Soviet Socialist Republics
RNSS	Regional Navigation Satellite Systems
MEO	Medium altitude Earth Orbit
IGSO	Inclined Geosynchronous Orbits
GEO	Geostationary Orbits
NAVSTAR	Navigation Satellite Timing and Ranging
DoD	Department of Defense
GCS	GPS Control Segment
MCS	Master Control Station
MS	Monitoring Stations
IEARS	International Earth Rotation and Reference System Service

USNO	The United States Naval Observatory
GPST	GPS Time
ToW	Time of Week0
SoW	Second of Week
TAI	International Atomic Time
GSA	Global Navigation Satellite System Agency
ESA	European Space Agency
EU	European Union
GIOVE	Galileo In- Orbit Validation Element
IOV	In orbit validation
FOC	Full Operational Capability
GaCS	Ground Control Station
GMS	Ground Mission Segment
GCC	Galileo Control Centers
LEOP	Launch and Early Operation
MEOLUTS	Medium Earth Orbit Local User Terminal
GST	Galileo Time System
GTRF	Galileo Terrestrial Reference Frame
WGS84	World Geodetic System 84 (check)
FDMA	Frequency Division Multiple Access
CDMA	Code Division Multiple Access
GLST	GLONASS Time System
ITU	International Telecommunication Union
SU	Soviet Union
GM	Gravitational Coefficient
LNAV	Legacy Navigation Message
CNAV	Civil Navigation message
MNAV	Military Navigation Message
FNAV	Freely Accessible Navigation Message
INAV	Integrity Navigation Message
SoL	Safety of Life
ECEF	Earth Centered Earth Fixed
ICD	Interface Control Document

CDDIS	Crustal Dynamics Data Information System
RMSE	Root Mean Squared Error

TABLE OF CONTENTS

1. INTRODUCTION

In the history of human development, determining the location of an object on or close to the Earth's surface has been a fundamental activity throughout the ages. Location is an important geographic factor in history that brings a correspondingly larger conception of the environment, which is related to various problems in the human activities. The expertise to use any kind of coordinate system for localization purposes dates since the dawn of humanity, but it was with the great navigations in the 14th century that more complex problems appeared, making Cartography and Geodesy gain an even more restricted scientific path (SEMPLE, 1908). The classical methods to determine someone's position were carried out using compasses and sextants among other mechanical methods assembled with astronomical information. Nowadays with the development of the Global Navigation Satellite System (GNSS) the activities involving time and positioning have changed dramatically (PLAG; PEARLMAN, 2006).

Currently, there are four GNSSs in operation or under implementation: GPS (Global Positioning System) from the United States of America; GLONASS (Globalnaya Navigatsionnaya Sputnikovaya Sistema) from Russia; Galileo from the European Union (EU) and BDS (BeiDou Navigation Satellite System) from China. The last couple of years have been significantly intense for those systems, with GNSS going through a period of significant change: the modernization of the GPS including new signals, Russia deployment of the renewed GLONASS satellites and the start of operations for the European and Chinese systems (MONTENBRUCK et al., 2017).

With the time and positioning capabilities, there is an increasing number of applications for GNSS: agriculture, civil construction, aviation, environmental monitoring, meteorology, and mining are some of the fields that have been using this technology as part of their activities. The new applications bring a huge impact on the development of the economic and industrial aspects of society where using navigation with satellites is constantly (PLAG; PEARLMAN, 2006). With the evolution of the GNSS constellations and its applications, their monitoring opened space for new research topics to be discussed. In 2016 the IGS (The International GNSS Service) launched a research proposal to assess the new systems and technologies. The IGMA (International Monitoring and Assessment) Trial Project is the joint activity of GNSS providers and IGS to promote an international monitoring and assessment of the system with results trusted by all parties worldwide. Considering the outstanding role of IGS in GNSS monitoring,

it is one of the key participants in the Trial Project along with GNSS Providers. It has as main goals the monitoring a number of limited parameters and constellations using existing infrastructure; consolidating monitoring system products, demonstrate the benefits of the combined use of multi-constellation, and promote trust in GNSS data and products. Initially, four GNSS constellations (GPS, GLONASS, Galileo, and BDS) and one regional navigation satellite system (Quasi-Zenith Satellite System - QZSS) will be the focus of the project with four parameters for the initial phase: broadcast ephemeris accuracy, signal in space (SIS) range error, SIS coordinated universal time (UTC) error, and position dilution of precision (PDOP).

The São Paulo State University (Unesp) through the group of space geodesy studies (GEGE) answered the call for participants in 2017 to be one of the analysis centers (AC) for the IGMA trial project. The development of the activities will be presented in the context of this dissertation. For the systems to be monitored it was selected all four global ones and as for the parameters, PDOP and the accuracy of broadcast ephemeris were the chosen ones.

PDOP can be visualized as the volume of the tetrahedron created by the satellites in the adjustment to determine the coordinates of a location with the point of interest, what yields a geometrical characteristic: a larger volume of the tetrahedron provides lower PDOP and also a lower error propagated for the adjusted coordinate. PDOP has been addressed in the literature since the early stages of satellite navigation (KLEUSBERG; TEUNISSEN, 1996) the modernization of the GNSS has brought new perspectives and applications as the inclusion of new satellites and they direct effect on the PDOP values (TENG; WANG; HUANG, 2016). Milbert (2008) highlights the necessity to evaluate the new satellites being added to the adjustment and PDOP because, even though mathematically they will represent an improvement on the geometry, the data can be deteriorated by multiple sources related to the GNSS signal propagation. In his paper Milbert (2008) shows a dilution of precision scaled by the ionosphere and troposphere components, however, the results are obtained from mathematical models using mapping functions without the addition of any physical information, also there isn't any comparison when using standard point positioning (SPP). Won et al. (2012) used a weighting PDOP (WPDOP) from the satellite elevation angle where from field data it is shown that there is a correlation between the length of the path crossed by the signal and the quality on the pseudorange measurement.

With current application such as satellites inter-links (HAN et al., 2014), low orbit satellites (LEO) coordinate determination through Kalman filter and the effects of PDOP as a

control parameter on the adjustment process (BISWAS; QIAO; DEMPSTER, 2017), the multi-GNSS constellation brings up the new applications for dilution of precision values.

As PDOP values, the accuracy of the broadcast ephemeris also will influence directly the quality of the point positioning process due to the fact that from the Keplerian elements the satellite coordinates will be calculated and constrained into the adjustment process. According to IGS, the accuracy of the coordinates obtained from GPS broadcast ephemeris is on the order of 1 meter (LEICK; RAPOPORT; TATARMIKOV, 2014; MONTENBRUCK; STEIGENBERGER; HAUSCHILD, 2014). For multi-GNSS, the applicability of broadcast data gains a new role, as the different systems are conceptualized in different manners and have different quality levels for its navigation data. As an example, early studies showed that for Galileo broadcast ephemeris, the RMS obtained in comparison with the final products is about 4 meters (STEIGENBERGER et al., 2015) which is highly discrepant with the quality of the GPS RMSE (root mean squared error) satellite coordinates.

This research aims to cooperate with the IGMA trial project processing and evaluating PDOP and broadcast ephemeris for the GPS, Galileo, GLONASS, and BeiDou. For PDOP with the data files, it will also be evaluated the dilution of precision with weighting factors considering the elevation angle of the satellites. For the broadcast ephemeris, they will be compared with final IGS products before and after the corrections of the phase center offset (PCO) that connect the center of mass (CoM) and the center of phase (CoP).

1.1 OBJECTIVES

This project has as a main goal the contribution of FCT-Unesp in the activities under development by the IGMA trial project and its efforts on the monitoring of the GNSS constellations proposed by the International GNSS committee.

To achieve the above-mentioned objective, the following specific goals to accomplish:

- To determine the accuracy of the satellites' coordinates from broadcast ephemeris following the standards of the IGMA trial project;
- To evaluate the implications of the CoM and CoP corrections on the broadcast ephemeris accuracy;

- To evaluate the methodology for WPDOP: using the satellite elevation angle as a weighting element;
- To assess the correlation between the WPDOP values with the accuracy of SPP for multi-GNSS positioning;
- To create a tool to keep continuous analyses of the broadcast ephemeris quality using the final MGEX (Multi-GNSS Experiment) products as a base for comparison for the GPS, Galileo, BDS, and GLONASS constellations.

1.2 MOTIVATION AND CONTRIBUTIONS

Even though there are many optimistic expectations presented in recent literature, some considerations are still needed when it comes to the GNSS integration (YANG et al., 2014), which ones need to be deeply understood, the realization and structure of the system such as reference frame, time system, signal propagation and availability, hardware structure for the satellite and receiver, etc. So, with the necessity of an international monitoring network that also includes the in deploying systems, the IGS and the MGEX launched the IGMA trial project. It aims to evaluate and make available information and products on a global scale to all GNSS constellations.

Answering the IGS call, the supervisor of the current project included the FCT-Unesp to work as one of the analyses centers to two of the four parameters and four of the five GNSS constellations. This master's degree dissertation comes as part of the activities that aim to complete the proposed participation. Not only in the scientific contribution, but this research also inserts itself as the inclusion of the Cartography Graduate Program (PPGCC – Programa de Pôs Graduação em Ciências Cartográficas) as part of an international effort in the international cooperation directed by the main GNSS organization.

The results and outcome products will offer reliable information about a multiple number of parameters, allowing to better understand how the GNSS integration works and the open opportunities for new applications. Specifically, for the Galileo and BeiDou systems, this research aims to give information that, when the systems are complete, it will give the background to expand the use of the GNSS in navigation and timing.

2 DEVELOPMENT OF GLOBAL NAVIGATION SATELLITE SYSTEMS

In this chapter it will be presented the characterization of the GPS, Galileo, BDS, and GLONASS systems, focusing on their ground and space segments, the basic concepts of its operation, and the available observables.

Currently, the navigation systems are grouped under one name: Global Navigation Satellite Systems, it is composed of the GPS, that was set operational in 1995. Following the USA efforts, the USSR (Union of The Soviet Socialist Republics), presently, Russia, launched GLONASS also started to be operational in 1995. Summing those, nowadays two other systems on a global scale are under development: the European Galileo and the Chinese BDS (LANGLEY; TEUNISSEN; MONTENBRUCK,2017).

GNSS and regional navigation satellite systems (RNSSs) are composed of three components:

- The space segment: it is the set of satellites transmitting signals inside the radio spectrum;
- The control segment: It consists of a global network for monitoring which is responsible for maintaining the health of the system.
- The user segment: it consists of GNSS receiving equipment both civil and military. This includes receivers on the ground, at sea, in the air, and even in space.

GNSS constellations typically adopt a specific orbital configuration: MEO (medium-altitude Earth orbit) satellites for global coverage; IGSOs (inclined geosynchronous orbits) and GEOs (geostationary orbits) as supplements in regional systems. MEO satellites are often evenly distributed in inclined near-circular orbits over equally spaced orbital planes, forming a constellation known as a Walker constellation. The geometry of a specific Walker constellation is described by the triplet t=p=f, where t denotes the total number of satellites, p the number of equally spaced planes, and f the phase difference between the adjacent orbital planes (XU, 2007).

2.1 GPS

The Navigation Satellite Timing and Ranging (NAVSTAR) GPS is a navigation system developed by the Department of Defense (DoD) of the US with its primary purpose being to

serve military needs. It works 24 hours per day in any given location and weather conditions in the world (LEICK; RAPOPORT; TATARMIKOV, 2014; MONICO, 2008).

GPS consists of 24 MEO satellites in 6 circular orbital planes, 4 satellite each plane with a radius of 20200 km. The planes are inclined 55° in relation to the equator. It started to be developed in 1973 and was declared operational in 1995 with the full constellation (SEEBER, 2003). The constellation parameters are shown in table 1.

Table 1- Characteristics of GPS

Parameter	Value
Number of operational satellites	24
Number of orbital planes	6
Satellites per plane	4
Orbit	Near circular
Eccentricity	e<0.02
Inclination	55°
Orbital height	20200 km
Period	11 h 58 min

Source: Adapted from Seeber (2003, p. 2012)

Until now, 67 GPS satellites have been launched in 6 blocks, out of which 32 are currently operational[1]. The key characteristics of the blocks are presented in table 2.

Table 2 - Key characteristics of GPS Blocks

Parameter	Block I	Block II/IIA	Block IIR/IIR-M	Block II F	GPS III
Operational	0	11	7	12	1
First launch	1978	1989	1997	2010	2020
Manufacturer	Rockwell International	Rockwell International	Lockheed Martin	Rockwell International	Lockheed Martin
Design lifetime (years)	5	7.5	7.5	12	15
Mass (kg)	450	>850	1080	1630	2200
System Power (W)	400	700	1140	2610	4480
Signals	L1, L2	L1, L2	L1, L2	L1, L2, L5	L1, L2, L5
Navigation payload clocks	Rubidium, Cesium	Rubidium, Cesium	Rubidium	Cesium, Rubidium	Rubidium

Source: Adapted from Hergarty in 04/12/2020 (2017)

[1] - Available at < https://www.glonass-iac.ru/en/GPS/index.php>

To monitor the satellites, it was created the GPS Control Segment (GCS), which consists of a global network of ground facilities that track the satellites, analyze their performance and transmit commands and data using up links to the constellation. The GCS is composed of a master control station (MCS) in Colorado Springs, Colorado. Its job is to use the global monitored data to compute precise coordinates, generate and upload navigation messages and clock corrections, analyze system integrity and the satellite health and perform satellite maneuvers. The MCS works 24 hours per day, 7 days per week.

To maintain the system reliability a complete MSC is put as a backup in Vandenberg, California. Monitoring stations (MS) are designed to keep track of the GPS satellites and are shown in figure 1, providing global coverage with 16 sites; 6 from the US Air Force. They track GPS signals from all visible satellites with geodetic quality receivers. The MS is equipped with additional components including meteorological sensors, cesium atomic clocks, communication equipment, and workstations. Pseudorange, carrier-phase measurements, navigation messages, and signal reception quality are collected and sent to the MSC from each MS every 1.5 seconds (HERGARTY, 2017; LEICK; RAPOPORT; TATARMIKOV, 2014; MONICO, 2008).

Figure 1 - GPS control segment

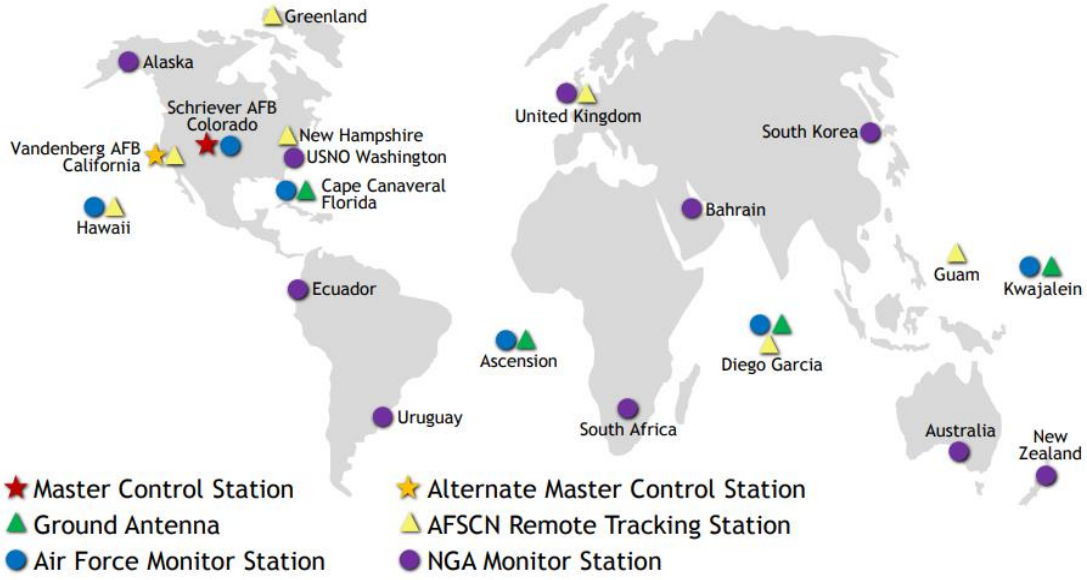

Source: https://www.gps.gov/systems/gps/control/ , Accessed on May 18th, 2018

With its process of modernization GPS constellation currently broadcasts signals in three frequencies: L1, L2, and L5 with a carrier frequency of 1575.42MHz, 1227.6MHz, and

1176.45MHz and a wavelength of approximately 19 cm, 24 cm and 25.5 cm respectively. They are modulated over a fundamental frequency of 10.23 MHz coherently driven from an onboard synthesizer by an atomic clock on the satellites (LEICK; RAPOPORT; TATARMIKOV, 2014; MONICO, 2008).

GPS, as the other GNSS, measures the time interval between the signal broadcasted at the satellite and the signal arrival at the receiver. It is a requisite to introduce a timescale that reflects the accuracy of the needed measurements. Currently, GPS uses atomic quality time reference known as GPS time. Its origin point is on January 6, 1980, by the USNO (The United States Naval Observatory) and equal UTC for that same day. As the GPS time is on an atomic scale, it does not have leap seconds like UTC. In May 2018 the difference between both time systems was 18 seconds, this value is available at the IERS (International Earth Rotation and Reference System Service) bulletins at https://www.iers.org/IERS/EN/Publications/Bulletins/bulletins.html (LEICK; RAPOPORT; TATARMIKOV, 2014; MONICO, 2008).

The GPS time (GPST) is given by a week number and the second of the referred week. The week number was planned to go from 0 to 1023 and start from zero for every new cycle after 1023, currently, we are on the second cycle, but the counting kept going without resetting. For each week we have the SoW (Second of the week) that starts its count from the first second of the week until the end of the week (from 0 to 604800) (MONICO, 2008).

GPST is employed since 1990, it is formed as a composite clock from atomic clocks within the GPS Control Segment (including both the MCS and the MS) as well the clocks onboard of GPS satellites. Using common view time transfer, GPS time is steered to deviate by at most 1μs from UTC, that is, the realization of UTC maintained by USNO. The origin of GPST is January 6th, UTC (USNO). It is permanently offset (late) by a constant amount from TAI (International Atomic Time) (equation 1).

$$t(GPS) = TAI - 19s \quad (01)$$

For the geodetic referential, GPS satellite positions are given within the World Geodetic System (WGS84) reference frame. The MS is periodically readjusted to keep the WGS84 aligned to the International Terrestrial Reference Frame (ITRF).

2.2GALILEO

The Galileo system, an initiative of the European Union (GSA, 2018) of the final orbit constellation of 24 satellites (plus 3 spare) planned. Compared to the two first GNSS systems (GPS and GLONASS) that emerged in the early ’70s, Galileo is relatively new with its basic concepts developed at the end of the 1990s. In 2003 the European Space Agency (ESA) and the European Union (EU) started the first stage of the Galileo Project (MONICO, 2008; NURMI et al., 2015, GSA, 2020).

Table 3 - Galileo orbit parameters

Parameter	Value
Number of operational satellites	24
Number of orbital planes	3
Satellites per plane	8
Orbit	Circular orbits
Eccentricity	0.00
Inclination	56°
Orbital height	23222km
Period	14 h 04 min

Source: Adapted from Falcon; Hahn; Burger (2017); Bartolomé et al (2017)

ESA launched 2 GIOVE (Galileo In-Orbit Validation Element) in 2005 and 2008 to secure the frequencies set to the project by the International Telecommunication Union and as a testbed to some key elements such as atomic clocks and signal generation. The GIOVE satellites were moved to a higher altitude and are no longer available. An in-orbit validation (IOV) phase that aimed to do an initial assessment of the system using a set of 4 satellites with the first generation of Galileo satellites (GSAT010x) was made after. From those, 3 are still operational and serve as part of the main current constellation (GSA, 2018). The IOV campaign was conducted until 2013 and the outcomes were used to set the expected performance of the Galileo system (BARTOLOMÉ et al., 2015).

The third implementation phase is the completion of the full operational capability (FOC) (currently undergoing) financed by the EU. It consists of the design and launch of the remaining satellites and deployment of the full operational ground control segment (FALCONE; HAHN; BURGER, 2017). The satellites are being manufactured by OHB-System AG and are made of 2 main components: the platform and the payload, the IOV satellites have a set of small differences in comparison with the FOC satellites, but in its functionality, they

are very similar (BARTOLOMÉ et al., 2015). The Galileo incrementation deployment timeline is shown in figure 2. Currently (February 2020) there are 22 operational satellites and 2 under testing[2].

Figure 2 - Galileo incremental deployment

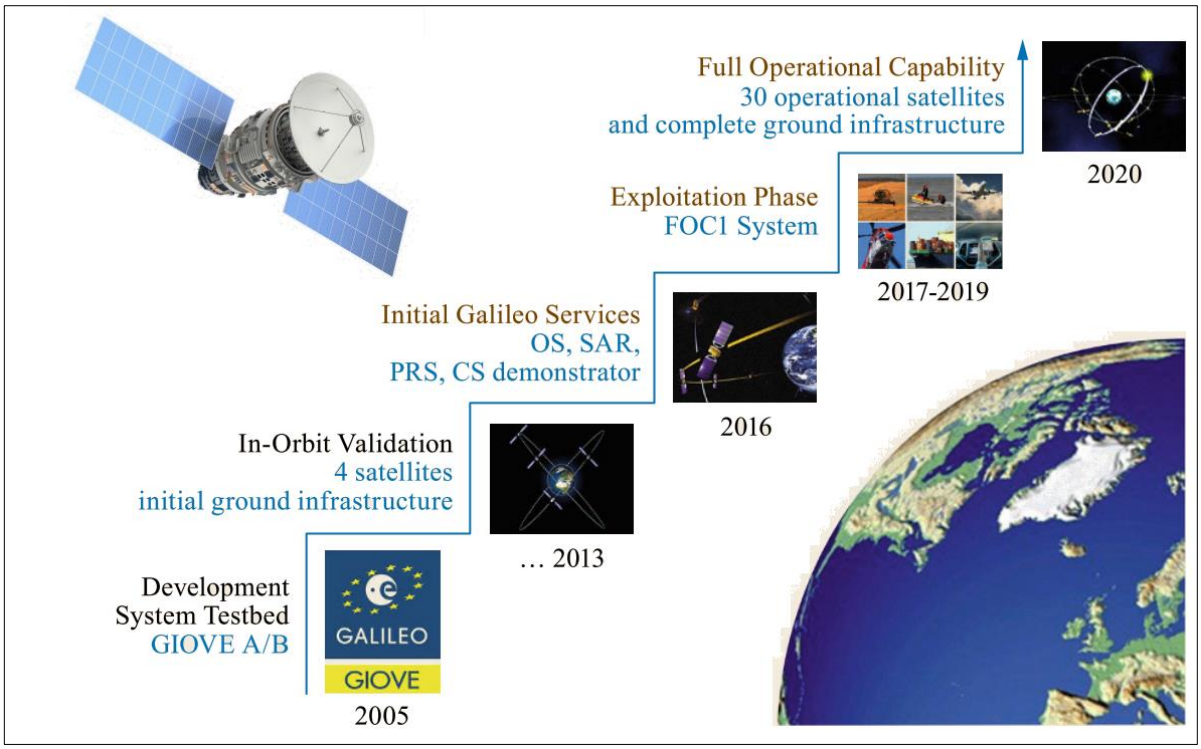

Source: Falcone, M.; Hahn, J.; Burger (2017)

The ground segment for the Galileo constellation is composed of the Ground Control Segment (GaCS) and the Ground Mission Segment (GMS).

The GaCS is responsible for the management of the Galileo constellation during the operation of the system. Further to the monitoring and control data, the GaCS also upload Galileo mission data through the telecommand uplink channel to ensure the continuity of Galileo navigation services. The GaCS elements are located worldwide (BARTOLOMÉ et al, 2015). The GMS measures and monitors the Galileo signals and computes and distributes the navigation messages to the satellites.

There are two Galileo Control Centers (GCC), one in Oberpfaffenhon, Germany, and another one in Fucino, Italy. As part of the ground segment there are still two Launch and Early

[2] – Available at < https://www.gsc-europa.eu/system-service-status/constellation-information>

Operation (LEOP) control centers, one in Toulouse, France, and one in Darmstadt, Germany. They provide the services to take control over the satellites after the separation of the launch vehicles and the Medium Earth Orbit Local User Terminal (MEOLUTS) that is part of the Search and Rescue Service (GSA, 2018b).

Galileo has adopted a uniform time system (GST – Galileo Time System) without any leap seconds. The starting epoch for GST is 00:00 on 22 August 1999 UTC (midnight between 21 and 22 August 1999). GST exhibits a constant offset from TAI of 19 seconds (equation 02). The origin for Galileo time, for consistency, is defined to be identical to that of GPS Time

$$t(Galileo) = TAI - 19. \quad (02)$$

The service providers broadcast the GPS/Galileo time offset in the header of the navigation message, and alternatively, the offset can be determined in a combined receiver with very high accuracy at the very small cost of using one satellite observation during the least square process (BARTOLOMÉ et al., 2015).

Galileo establishes its own Galileo Terrestrial Reference Frame (GTRF). The GTRF is aligned to the ITRF concerning the origin, scale, orientation, and rate, such as to remain within 3 cm (2-sigma) of the ITRF. Although the Galileo Terrestrial Reference Frame (GTRF) is different from the GPS coordinate reference frame (WGS84), both differ less than a few centimeters with respect to the ITRF, hence guaranteeing interoperability for most applications (BEARD; SENIOR, 2017).

2.2.1 Galileo signals and service

Galileo satellites transmit permanently three independent CDMA and Right-Hand Circularly Polarised (RHCP) signals, named E1, E5, and E6. The E5 signal is further sub-divided into signals denoted E5a and E5b. These signals are transmitted in four frequency bands which provide a wide bandwidth for the transmission of the Galileo signals. Table 4 specifies the corresponding carrier frequencies and receiver reference bandwidths for the Galileo signals.

Table 4 - Overview of Galileo signals

Galileo signal	Carrier frequency (MHz)	Subband	Subband frequency (MHz)	Carrier aligned with
E1	1575.420	--	--	GPS L1 C/A, L1C
E6	1278.750	--	--	
E5	1191.795	E5b	1207.140	
		E5b	1176.450	GPS L5

Source: Falcone, M.; Hahn, J.; Burger (2017)

The signals and components are assigned to four types of positioning services:

1. **The Open Service** (OS) results from a combination of open signals, free of user charge, and provides position and timing performance competitive with other GNSS systems. It uses E1, E5a, and E5b.
2. **The Public Regulated Service** (PRS) provides position and timing to specific government-authorized users requiring a high continuity of service, with controlled access. Two PRS navigation signals with encrypted ranging codes and data are available on the frequencies: E1 and E6.
3. **The Commercial Service** (CS) provides access to two additional signals, to allow for a higher data throughput rate and to enable users to improve accuracy. The signals are encrypted and delivered on the E6 frequency.
4. **Search and Rescue (SAR)** is an international satellite-based search and rescue system established by the US, Russia, Canada, and France, capable of locating emergency radio beacons. This support is provided through a forward search-and-rescue repeater as part of the payload, and through an associated data return link embedded into the navigation message of the E1 OS data component. On January 21 2020, the SAR/Galileo Return Link Service (RLS) was declared operational. Now, Galileo not only locates people in distress and makes their position known to the relevant authorities, the SAR/Galileo RLS provides an automatic acknowledgment message back to the user informing them that their request for help has been received.

2.3 GLONASS

GLONASS is the global satellite navigation system from the Russian Federation. The first satellite was launched in 1982 and by 1996, a fully operational constellation of 24 satellites was in orbit. Due to economic issues followed by the ending of the Soviet Union, the system had a short life span. By the early 2000s the constellation had only a few remaining satellites. With the restatement of the Russian government, GLONASS was rebuilt, and on 8 December 2011, full operational capability was again achieved and has been subsequently maintained. The system main characteristics are presented in table 5 (REVNIVYKH et al., 2017).

The constellation of GLONASS satellites is a key element of the entire GLONASS system. Throughout the more than 30 years of its history, three generations of GLONASS satellites have been built and operated: The initial generation of GLONASS satellites first launched in 1982, the subsequent GLONASS-M satellites launched since 2003 and GLONASS-K introduced in 2011 (JEREZ, 2017). Currently (January 19th, 2020) the system has 23 operational satellites, 3 under maintenance, 1 spare, and 1 under tests[3].

Table 5 - Characteristics of GLONASS

Parameter	Value
Number of operational satellites	24
Number of orbital planes	3
Satellites per plane	8
Orbit	Near circular
Eccentricity	e<0.01
Inclination	64.8°
Orbital height	19100 km
Period	11 h 15 min 44 s

Source: Adapted from Revnivykh et al. (2017, p. 221)

The GLONASS satellites are categorized into three blocks: starting in 1982 the first generation GLONASS I/II, in 2003 the second generation GLONASS-M and after 2011 the third generation GLONASS-K1/K2.

GLONASS provides two types of services:

- An open service with unencrypted signals in up to three frequency bands (L1, L2, and recently L3) that is globally available for all users without any limitations;

[3] - Available at < https://www.gsc-europa.eu/system-service-status/constellation-information>

- A service for authorized users, using encrypted signals.

It is important to remark that GLONASS relies on the Frequency Division Multiple Access (FDMA) technique instead of the code-division multiple access (CDMA) one used by other GNSS systems such as GPS or Galileo. Each satellite transmits navigation signals on its carrier frequency, so that two GLONASS satellites may transmit navigation signals on the same carrier frequency if they are in antipodal slots of a single orbital plane (REVNIVYKH et al., 2017). From the channel number (k) is possible to derive the satellite's frequency with the expressions :

$$f_{k1} = f_{01} + k\Delta f_1, \quad (03)$$

$$f_{k2} = f_{02} + k\Delta f_2, \quad (04)$$

where:

f_{01}= 1602 MHz;

f_{02}= 1246 MHz;

Δf_1=562.5 kHz;

Δf_2 = 437.5 KHz.

GLONASS signal evolution plan proposes the inclusion of new CDMA signals to the users as a complement to the FDMA signals. Some of the major reasons for introducing CDMA signals include an improved navigation accuracy, an improved resistance to interference, and the improved separation of open and authorized services. The GLONASS signal evolution plan is based on a phased approach. Since 2011 the first CDMA signal has been available in the L3 band and further signals will be added with each new generation of GLONASS satellites (REVNIVYKH et. al, 2017).

The ground segment is an essential part of the GLONASS architecture providing system operation and ultimate GLONASS performance. There is no formal division between system control and mission control functions. All operational procedures after satellite launching are fulfilled by the Air and Space Defense Forces. If satellites are launched from the Baikonur launch site, the initial active phase of the launcher trajectory tracking is supported by the Russian Federal Space Agency assets (PETROVSKI, 2012).

Core components of the GLONASS ground segment include the GLONASS system control center and the central clocks, the telemetry, tracking and command stations, and the uplink stations, as well as one-way monitoring stations and satellite laser ranging (SLR)

stations. All major ground segment assets are located within the Russian territory at the Air and Space Defense Forces sites (REVNIVYKH et. al, 2017).

Figure 3- GLONASS ground segment sites

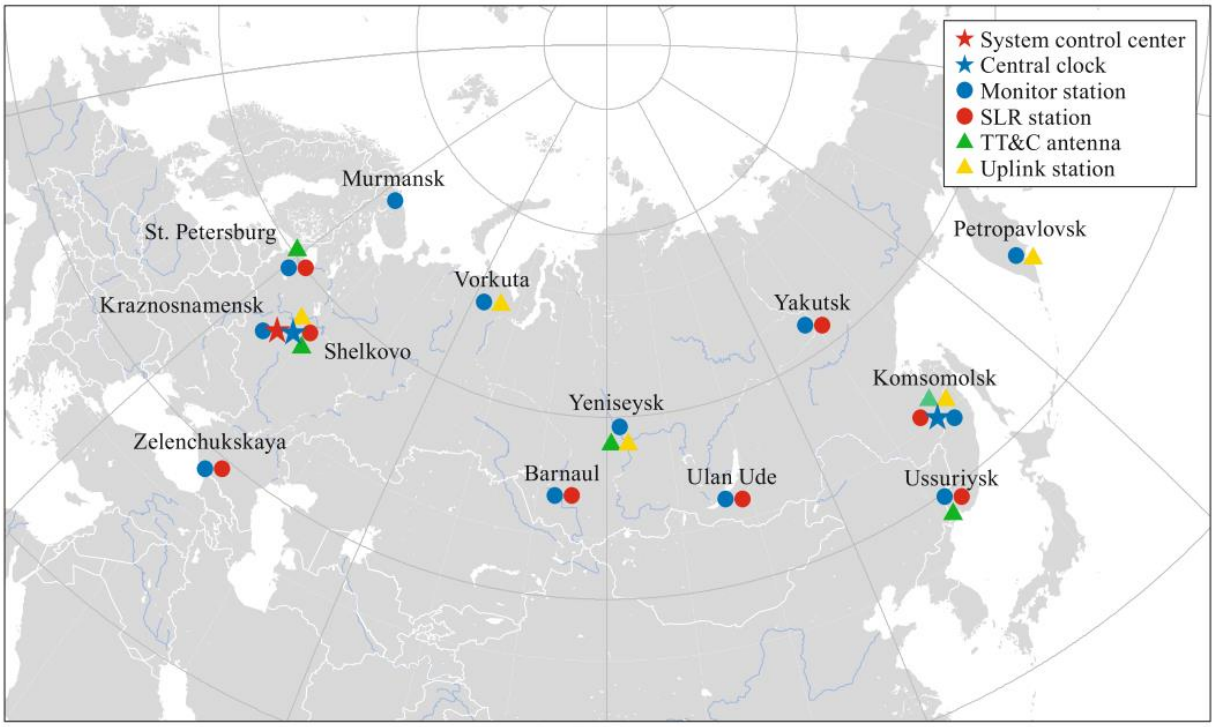

Source: Revnivykh et. al. (2017)

The system control center is located in Krasnoznamensk 40km southwest of Moscow. It performs the planning and coordinates the work of all ground segment elements. Orbit determination and clock synchronization is implemented through the processing of all available sets of data including two-way ranging the telemetry, tracking and command stations, downloaded radio cross-link ranging data, and one-way ranging data from the defense force station monitoring stations. The use of data from the federal space agency monitoring stations is planned to improve orbit and clock information as well as the cross-link ranging data (REVNIVYKH et. al, 2017).

GLONASS Time System (GLST) is the only GNSS time scale that follows the ITU (International Telecommunication Union) recommendation to align a disseminated time scale with UTC. Its origin is chosen as January 1st, 1996 in the UTC(SU) time system, that is, the Russian (formerly Soviet Union, SU) realization of UTC maintained by the Institute of Metrology for Time and Space in Moscow. Besides incorporating leap seconds, GLST is always 3 h ahead of UTC because of the time zone difference between Greenwich and Moscow (equation 05) (JEKELI; MONTENBRUCK, 2017). Thus,

$$t(GLONASS) = UTC + 3\ h. \quad (05)$$

The parameters and data of the Earth Model PZ- 90 are applied for GLONASS satellite orbit determination and ephemeris calculation. The PZ-90 system was established in 1990 and superseded the Soviet Geodetic System (SGS-85) that was used by GLONASS until 1993.

The PZ-90 definition comprises fundamental geodetic constants, parameters of the Earth ellipsoid, and the Earth gravity field, which is defined in accord with common conventions of the IERS and Bureau International De l'Heure. The PZ-90 system originates in the Earth's center of mass including the oceans and atmosphere. Its z-axis is directed to the conventional reference pole and its x-axis points to the intersection of the equatorial plane and the zero meridian as defined by the BIH.

Figure 4 - PZ- 90.11 reference points on the Russian territory (as of 2011)
Source: Revnivykh et. al. (2017)

2.4 BeiDou

The Chinese BeiDou Navigation Satellite System (BDS) had its development structured in a “three-step” strategy. The demonstration system was step one (BDS-1), the regional system (BDS-2), and the global system (BDS-3) (ZHANG et al., 2017). BeiDou-1 development started in 1994 and the operation started in 2000 and presenting its three GEO satellites composing the regional navigation system in 2003, which is a result of research efforts that started in 1980. A fourth satellite was launched in 2007, this first regional system (BeiDou-1) was complemented by a global system. The complete system will include 6 GEO, 10 IGSO, and 27 MEO satellites (YANG et al., 2019). As of January 2020, 35 satellites are operational[4].

The BeiDou Navigation Satellite Demonstration System (BDS-1) provides combined localization and communication service through two geostationary satellites that are called Beidou-West and BeiDou-East, simplified as BeiDou 1A and BeiDou 1B. As a backup, a third satellite (BeiDou1C) was included in 2003. Its main functions comprise: positioning (navigations), short message communication, and timing. Similar to other satellite navigation systems, the BDS- 1 system architecture comprises a space segment, a ground control segment, and the user terminals. The services are achieved by the same channel and this concept is known as radio determination satellite service (RDSS) (YANG et al., 2017).

Figure 5 - Service coverage of BDS-1.

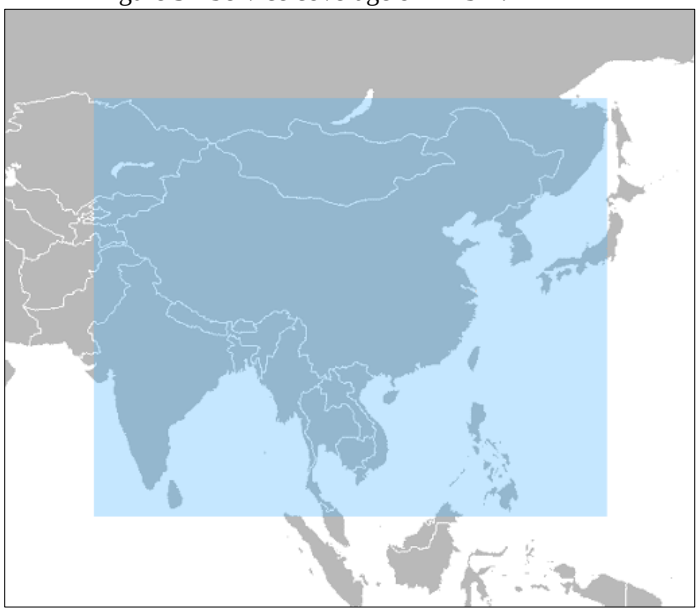

Source: Yang et al. (2017)

[4] - Available at < http://www.csno-tarc.cn/system/constellation>

In 2004, it was initiated the construction of BDS-2 and a first MEO satellite (then known as COMPASS-M1) which was launched in 2007. In 2012 BDS-2 was officially operational and started its regional service. The initial service announcement was accompanied by the release of the first open service interface control document (ICD) for the users of the single-frequency B1 band.

The second-generation of BDS uses a unique constellation design, which is a combination of elements from global systems (GPS, GLONASS, and Galileo) with those of purely regional systems (such as the QZSS and the IRNSS/NavIC). The BDS-2 space segment comprises five satellites in geostationary orbit, five spacecraft in IGSO, and four MEO satellites (YANG et al., 2017).

The BDS-2 satellites transmit a total of six signals in three distinct frequency bands: B1 at a center frequency of 1561:098MHz, B2 at a center frequency of 1207:14MHz, and B3 at a center frequency of 1268:52MHz and each carrier frequency is modulated with two signals. The in-phase components of the B1 and B2 signals are assigned to the BDS-2 open service while the remaining four signals are reserved for the authorized service.

Apart from the standard positioning and timing service available in the entire service area, the BDS-2 open service signals also support an improved, satellite-based augmentation system (SBAS)-like positioning service based on near-real-time corrections transmitted through the GEO satellites. This service is freely available to all users, but limited to a smaller service area centered around the Chinese mainland (YANG et al., 2019).

BDS is composed of three groups of spacecraft, namely the GEO, IGSO, and MEO satellites. The satellites have a specified lifetime of eight years. The platform and navigation payload of all three satellites types are essentially similar, but various complementary payloads are accommodated on the GEO spacecraft.

Table 6- Characteristics of BDS satellites

Parameter	IGSO	GEO	MEO
Number of operational satellites	10	6	27
Number of orbital planes	--	--	3
Orbit	Circular orbits	Circular orbits	Circular orbits
Eccentricity	e=0	e=0	e=0
Inclination	55°	0	55°
Orbital height	36000 km	21528 km	19100 km
Period	23h 56 min	23h 56 min	11 h 15 min 44 s

The Operational Control System (OCS) of BDS, like that of other GNSS, is a key segment for BDS operations. The research on the OCS of BDS demonstration system started as early as the 1980s. The OCS of BDS- 2 has been in place since 2007, when the first BDS-2 satellite was launched.

The workflow of the OCS can be simply described as collecting data related to the satellites and the ground stations, processing and analyzing the collected data, managing communication between satellites and ground stations, uploading operational commands to satellites, satellites, and broadcasting navigation messages to the users.

Figure 6- Location of BeiDou Master Control Station and the monitoring stations

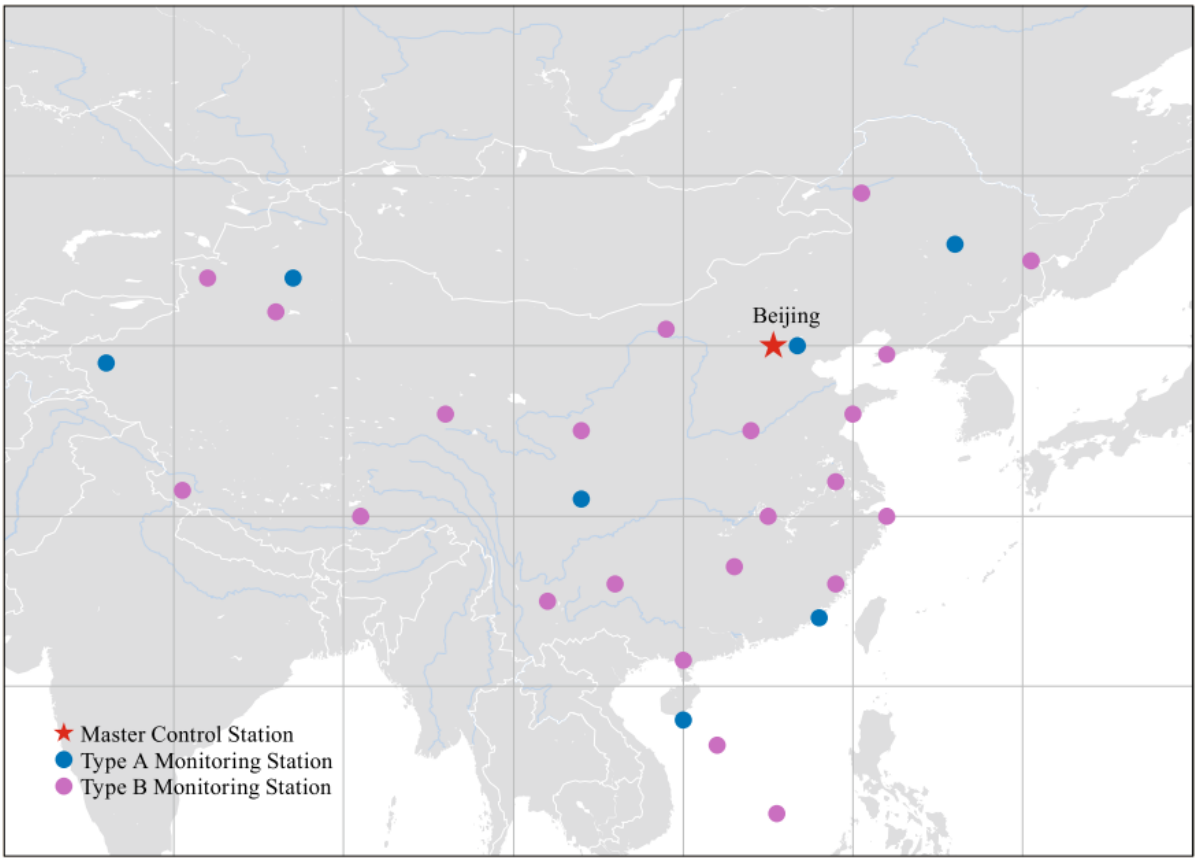

Source: Yang et al. (2017)

The BeiDou Navigation Satellite System (BDS-3) will be completed by 2020. The space constellation will consist of five GEO satellites. BDS-3 will provide an open service and an authorized service in four frequency bands, including B1, B2, and B3. A new S-band signal, Bs (2483:5−2500MHz), is also broadcasted by the newly launched satellites. Compared to the

regional BeiDou system, new and advanced signal structures are employed for better performance, compatibility, and interoperability with other GNSS (YANG et al., 2019).

The time reference for the BeiDou Navigation Satellite System is BeiDou Time (BDT). BDT is a continuous navigation time scale without leap seconds and with the SI second as its basic unit. BDT is commonly represented by the BeiDou week number and the seconds of week (SoW), ranging from 0 to 604.799. The zero point of BDT is January 1st, 2006 (Sunday) UTC is aligned to TAI except for an integer second offset shown on equation 06 (JEKELI; MONTENBRUCK, 2017).

$$t(BDS) = TAI - 33s \tag{06}$$

The BDC system is connected to the China Geodetic Coordinate System 2000 (CGCS2000), which is aligned to the ITRS. CGCS2000 is realized by the China Terrestrial Reference Frame (CTRF). The definition of this coordinate system follows the criteria outlined in the 1996 conventions from IERS. CGCS2000 is a right-handed, orthogonal system. Its origin is the center of the mass of the Earth including the oceans and the atmosphere. Its scale is that of the local Earth frame, in the meaning of a relativistic theory of gravitation. The orientation is initially given by the orientation of the Bureau International de l'Heure Terrestrial System at 1984.0, and the time evolution of the orientation is ensured by using a no-net-rotation condition concerning the horizontal tectonic motions over the whole Earth. The unit of the length is meter. Its z-axis is the direction of the IERS Reference Pole. This direction corresponds to the direction of the BIH conventional terrestrial pole at epoch 1984.0. The x-axis is the intersection of the IERS reference meridian and the plane passing through the origin and normal to the z-axis (TANG et al., 2017).

3 BROADCAST EPHEMERIS: FUNDAMENTALS

This chapter will cover the understanding of broadcast and almanac messages for the GPS, Galileo, GLONASS and BeiDou systems. The almanac and ephemeris algorithms to compute the satellites velocities and coordinates are presented as well as the coordinates corrections for the variations and influence of the satellite attitude.

3.1 EPHEMERIS AND ALMANAC

An important element for every satellite navigation system is the provision of broadcast orbit information that will allow the user to compute the position and velocity of the GNSS satellites in the constellation. This information is important to the navigation solutions as the satellite coordinates are fixed in the adjustment. Two types of parameter sets are commonly distinguished (HUNGENTOBLER; MONTENBRUCK, 2017):

- Almanac: It has a lower accuracy and offer a coarse orbit information with an error in the kilometer order. Each satellite transmits the orbit parameters of all satellites in the constellation with auxiliary health status. The information is also made available online[5].
- Ephemeris: provides meter level orbit information for use in the velocity and position computation. Each satellite only transmits its ephemeris, allowing a shorter message length and a higher repetition rate.

Both ephemeris and almanac, also includes the satellite clock information (offset, drift, and drift rate). The detailed specifications can be found on the interface control documents[6], which provide a description of the navigation message format and contents and the instructions for the use of this information. Despite having common characteristics, care must be taken

[5] GPS: https://www.navcen.uscg.gov/?pageName=gpsAlmanacs
Galileo: https://www.gsc-europa.eu/system-status/almanac-data
GLONASS: ftp://ftp.glonass-iac.ru/MCC/ALMANAC
BeiDou: https://www.glonass-iac.ru/en/BEIDOU/ephemeris.php

[6] GPS: https://www.gps.gov/technical/icwg/IRN-IS-200H-001+002+003_rollup.pdf
Galileo:https://www.gsc-europa.eu/system/files/galileo_documents/Galileo-OS-SIS-ICD.pdf
GLONASS:http://russianspacesystems.ru/wp-content/uploads/2016/08/
BeiDou: http://en.beidou.gov.cn/SYSTEMS/ICD/

because individual constellations employ different reference systems realizations as well as different physical constants. For the reference frame, considering the latest realizations in use today, the differences between them will have an impact of a position offset at a few centimeters level and in most cases, can be neglected in comparison with the broadcast ephemeris precision (LEICK; RAPOPORT; TATARMIKOV, 2014). The use of physical constants should be made as defined by the interface control documents. Special care should be taken for the Earth's gravitational coefficient (GM) since a subtle variation in the GM values would affect the computed mean motion and create position errors that grow linearly over time. The values for GM and ω_e (Earth rotation velocity) for the GNSS systems are presented in table 7 (HUNGENTOBLER; MONTENBRUCK, 2017).

Table 7 - GNSS physical constants values

System	GM (m^3/s^2)	ωe (rad/s)
BDS	398600.4418×10^9	7.2921150×10^{-5}
Galileo	398600.4418×10^9	$7.2921151467 \times 10^{-5}$
GLONASS	398600.4418×10^9	7.2921150×10^{-5}
GPS	398600.5×10^9	$7.2921151467 \times 10^{-5}$
QZSS	398600.5×10^9	$7.2921151467 \times 10^{-5}$

Source: Hungentobler; Montenbruck (2017)

3.2 EPHEMERIS MODELS

The user receiver computes the satellites' coordinates from the information broadcast by the GNSS satellites in the navigation messages. Two different approaches are followed by GPS/Galileo/BeiDou and GLONASS satellites to account for satellite orbit perturbations. Those approaches define their messages contain.

In the case of GPS, Galileo and BeiDou satellites, the orbits are Keplerian in first approximation, and the perturbations are treated as temporal variations in the orbital elements. For GLONASS satellites, the navigation message broadcasts initial cartesian conditions of position and velocity and moon and solar gravitational acceleration perturbation vector components

3.2.1 Keplerian Ephemeris Models

The broadcast ephemeris model has its representation through a perturbed Keplerian orbit for GPS and Galileo and BeiDou constellations. The spacecraft position and velocity can be computed from the given orbital parameters at any desired epoch in the validity interval of the messages. The model has been firstly established to be used with the GPS LNAV (Legacy Navigations Message) and later inherited by most other constellations. It is an extended version of the model used by the almanac with the introduction of additional parameters for a refined representation. These account for differences in the mean motion relative to its Keplerian value, a drift of the orbital inclination, and for perturbations in the radial, along-track, and cross-track direction (HUNGENTOBLER; MONTENBRUCK, 2017).

For GPS, the navigation message is transmitted as the LNAV. Besides the LNAV on L1 C/A, four additional new messages have been introduced by GPS modernization: L2-CNAV (Civil Navigation Message), CNAV-2, L5-CNAV, and MNAV (Military Navigation Message). The legacy and the first three after GPS modernization are civil messages, while the MNAV is a military. The L2-CNAV, L5-CNAV, and MNAV have a similar structure. Those formats allow more flexibility, better control, and improved content. Furthermore, the MNAV includes new improvements for the security and robustness of the military message. The CNAV-2 is going to be modulated in the upcoming L1C, sharing the same band as the legacy navigation message (MONTENBRUCK; STEIGENBERGER; HAUSCHILD, 2014).

The Galileo satellites broadcast two navigation messages: The Freely Accessible Navigation Message (FNAV) and Integrity Navigation Message (INAV). The INAV messages are used in the Safety of Life (SoL). The INAV message structures are transmitted in E5b (1207.14 MHz) and E1 (1575.42 MHz) frequency bands. FNAV is used within the Open Service (OS) and it is transmitted in the E5a frequency band (1176.45 MHz). All orbital elements and parameters within a broadcast navigation message refer to an origin, called time of ephemeris (t_{oe}). The applicability interval for each message type is presented in table 8.

Table 8 - Typical applicability intervals of broadcast ephemerides relative to the t_oe

Constellation	Type	From	To
GPS	LNAV	$t_{oe} - 120min$	t_{oe}
	CNAV	$t_{oe} - 90min$	$t_{oe} + 30min$
Galileo	INAV/FNAV	$\approx t_{oe} + 10min$	$\approx t_{oe} + 180min$
GLONASS		$t_{oe} - 15min$	$t_{oe} + 15min$

continue

conclusion

BeiDou		$t_{oe} - 30min$	$t_{oe} + 30min$

Source : Montenbruck; Steigenberger; Hauschild (2018)

To achieve a higher accuracy, the drifts of the semimajor axis and the mean motion are, furthermore, considered in the CNAV transmitted with the GPS L2C and L5 signals. Also, the CNAV provides the offset of the nodal drift from a reference value rather than the full value to achieve higher precision with a smaller number of data bits. The parameters on the broadcast ephemeris are presented in table 9.

Table 9 - Parameters of Keplerian broadcast ephemeris

Parameter	**Description**
$\sqrt{a}, \Delta a$	Square root of semimajor axis legacy navigation message (LNAV) or semimajor axis offset from the reference value a_{ref} = 26559710 m (GPS civil navigation message (CNAV)).
$\dot{a}$	Rate of change of the semimajor axis (CNAV)
Δn	Correction to mean motion
$\dot{n}_0$	Rate of change of mean motion (CNAV)
e	Eccentricity
i_0	Inclination at reference epoch
$\frac{di}{dt}$	Rate of change of inclination
Ω_0	Rate-of-change of the right ascension of the ascending node (LNAV)
$\Delta\dot{\Omega}$	Rate-of-change of the right ascension of the ascending node relative to a reference value $\dot{\Omega}_{ref} = 4.68 * 10^{-7}°/s$ (CNAV)
$\dot{\Omega}$	Rate-of-change of the right ascension of the ascending node (LNAV)
ω	Argument of perigee
M_0	Mean anomaly at reference epoch
$C_{rc,}C_{rs}$	Amplitude of cosine/sine harmonic correction term to the orbital radius
$C_{uc,}C_{us}$	Amplitude of cosine/sine harmonic correction term to the argument of latitude
$C_{ic,}C_{is}$	Amplitude of cosine/sine harmonic correction term to the inclination

Source: Hungentobler; Montenbruck (2017)

The algorithm to calculate the satellite coordinates starts with the computation of the mean anomaly (SEEBER, 2003):

$$M = M_0 + n(t - t_e), \tag{07}$$

at the epoch of interest from the semimajor axis

$$a \begin{cases} (\sqrt{a})^2 & (LNAV, INAV\ and\ FNAV) \\ a_{ref} + \Delta a & (CNAV)' \end{cases} \tag{08}$$

the perturbed mean motion (n) will be (equation 09):

$$n = \sqrt{\frac{GM}{a^3}} + \begin{cases} \Delta n & (LNAV, INAV\ and\ FNAV) \\ \Delta n + \Delta n(t - t_e) & (CNAV)' \end{cases} \tag{09}$$

the solution of Kepler's equation can be obtained from equation (10), after it will be computed the true anomaly (υ):

$$\upsilon = 2tan^{-1}\left(\sqrt{\frac{1+e}{1-e}}\tan\frac{(E)}{2}\right), \tag{10}$$

and the unperturbed argument of latitude $\bar{u} = \omega + \upsilon$ are obtained. It is used to evaluate the periodic corrections presented on equations 11, 12, and 13:

$$\delta_r = C_{rs}\sin(2\bar{u}) + C_{us}\sin(2\bar{u}), \tag{11}$$

$$\delta_u = C_{us}\sin(2\bar{u}) + C_{uc}\sin(2\bar{u}), \tag{12}$$

$$\delta_i = C_{is}\sin(2\bar{u}) + C_{ic}\sin(2\bar{u}), \tag{13}$$

δ_r is the radius correction, δ_u is the correction of the argument of latitude and δ_i is the inclination correction. The parameters corrected by the perturbations are given by:

$$r = a(1 - e\cos E) + \delta_r, \tag{14}$$

$$u = \bar{u} + \delta_u, \tag{15}$$

$$i = i_0 + \frac{di}{dt}(t - t_e) + \delta_i, \tag{16}$$

r is the perturbed radius, u is the perturbed argument of latitude and i is the perturbed inclination

The Greenwich longitude of the ascending node (λ_Ω) is given by equation (17) and the nodal rate ($\dot{\Omega}$) is either given directly or obtained from the reference for the CNAV, xp and yp are the orbit-plane position (equations 19 and 20) coordinates before transformation to the ECEF (Earth Centered Earth Fixed) coordinate system

$$\lambda_\Omega = \Omega_0 + (\dot{\Omega} - \omega_0)(t - t_a) - \omega_0 t, \tag{17}$$

$$\dot{\Omega} = \dot{\Omega}_{ref} + \Delta\dot{\Omega}, \tag{18}$$

$$xp = r\cos u, \tag{19}$$

$$yp = r\sin u, \tag{20}$$

the earth-fixed position is finally given by equation 21:

$$r_{ECEF} = R_3(\text{-}\lambda_\Omega)R_1(-i)\begin{bmatrix} xp \\ yp \\ 0 \end{bmatrix}, \tag{21}$$

complementary to the GNSS satellite position, its velocity is required as part of the navigation solution process. The velocity can be found by differentiation of the above expressions for the position with respect to time t. The resulting ECEF velocity equations are given by 22, 23, and 24 (THOMPSON et al., 2019):

$$Vx = -xp\dot{\Omega}_k \sin\Omega - yp\left(\dot{\Omega}_k \cos\Omega\cos i - \frac{di_k}{dt}\sin\Omega\sin i\right) + Vx'\cos\Omega - Vy'\sin\Omega\cos i, \tag{22}$$

$$Vy = xp\,\Omega_k \cos\Omega - yp\left(\dot{\Omega}_k \sin\Omega\sin i - \frac{di_k}{dt}\cos\Omega\sin i\right) + Vx'\sin\Omega - Vy'\cos\Omega\cos i, \tag{23}$$

$$Vz = yp\left(\frac{di_k}{dt}\right)\cos i + Vy'\sin i, \tag{24}$$

to fully implement these equations, several additional derivatives are required. These derivatives (equations 25 to 32) are functions of the parameters of the broadcast navigation message and parameters computed by the SV position equations

$$\dot{E} = \frac{n}{1 - e\cos E}, \tag{25}$$

$$\dot{v} = \frac{\dot{E}\sqrt{1 - e^2}}{1 - e\cos E}, \tag{26}$$

$$\frac{di_k}{dt} = \frac{di}{dt} + 2\dot{v}(C_{is}\cos 2u - C_{ic}\sin 2u), \tag{27}$$

$$\dot{u} = \dot{v} + 2\dot{v}(C_{us}\cos 2u - C_{uc}\sin 2u), \tag{28}$$

$$\dot{r} = eA\dot{E}\sin E + 2\dot{v}(C_{rs}\cos 2u - C_{rc}\sin 2u), \tag{29}$$

$$\dot{\Omega}_k = \dot{\Omega} + \dot{\Omega}_k, \tag{30}$$

$$Vx' = \dot{r}\cos\dot{u} - \dot{r}\sin\dot{u}, \tag{31}$$

$$Vy' = \dot{r}\sin\dot{u} + \dot{r}\cos\dot{u}. \tag{32}$$

3.2.2 Cartesian Ephemeris Models

GLONASS has an alternative form for distributing orbit information. Users are provided with a Cartesian state vector: the position (**r**), velocity (**v**), and acceleration (**a**) at the ephemeris reference time. The trajectory in the vicinity of this epoch can then be obtained by numerical integration of the first-order equation of motion (HUNGENTOBLER; MONTENBRUCK, 2017).

$$\frac{d}{dt}\begin{pmatrix} r \\ v \end{pmatrix} = \begin{pmatrix} v \\ a \end{pmatrix}. \tag{33}$$

The GLONASS satellite coordinates shall be computed according to the specifications in the GLONASS ICD (Interface Control Document) document. The elements which are made available in the navigation message are presented in table 10 (GLONASS ICD, 2016):

Table 10 - Parameters of Cartesian broadcast ephemeris

Parameter	**Description**
x, y and z	Satellite position (Km)
Vx, Vy, and Vz	Velocity (Km/sec)
Ax, Ay and Az	Satellite lunar and solar perturbations (Km/sec^2)

continue

conclusion

-TauN	SV clock bias (sec)
+GammaN	SV relative frequency bias
tb	Message frame time in seconds of the UTC week

Source: Hungentobler; Montenbruck (2017)

The initial conditions broadcasted in the navigation message, are in the ECEF Greenwich coordinate system PZ-90. Therefore, and before orbit integration, they must be transformed into an absolute (inertial) coordinate system for an epoch t_e using the following expressions for the position (GLONASS ICD, 2016):

$$x_a(t_e) = x(t_e)\cos\theta_{Ge} - y(t_e)\sin\theta_{Ge}, \quad (34)$$

$$y_a(t_e) = x(t_e)\sin\theta_{Ge} + y(t_e)\cos\theta_{Ge,}$$

$$z_a(t_e) = z(t_e), \quad (35)$$

(36)

and for the velocity following equations 37, 38 and 39:

$$v_{x_a}(t_e) = v_x(t_e)\cos\theta_{Ge} - v_y(t_e)\sin\theta_{Ge} - \omega_e y_a(t_e), \quad (37)$$

$$v_{y_a}(t_e) = v_x(t_e)\sin\theta_{Ge} + v_y(t_e)\cos\theta_{Ge} + \omega_e x_a(t_e), \quad (38)$$

$$v_{z_a}(t_e) = v_z(t_e), \quad (39)$$

the (A_x, A_y, and A_z) acceleration components are the projections of lunisolar accelerations to axes of the ECEF Greenwich coordinate system. Thence, these accelerations must also be transformed to the inertial system by:

$$A_{xa} = A_x(t_e)\cos\theta_{G_e} - A_y\sin\theta_{G_e}, \quad (40)$$

$$A_{ya} = A_x(t_e)\sin\theta_{G_e} + A_y\cos\theta_{G_e}, \quad (41)$$

$$A_{za} = A_z(t_e), \quad (42)$$

where θ_{G_e} is the sidereal time at a chosen epoch t_e, which the initial conditions are referred, in Greenwich meridian:

$$\theta_{G_e} = \theta_{G_0} + \omega_e(t_e - 3\ hours), \tag{43}$$

being θ_{G_0} the sidereal time in Greenwich at midnight (GMT) of a date at which the epoch t_e.

To avoid the necessity for explicit reference system transformations, the equation of motion is presented in the rotating, Earth-fixed reference frame. Accordingly, centrifugal and Coriolis terms are considered in the modeled acceleration (equation 44) (HUNGENTOBLER; MONTENBRUCK, 2017).

$$\begin{pmatrix} A_x \\ A_y \\ A_z \end{pmatrix} = -GM\frac{\overrightarrow{r}}{r^3} - \frac{3}{2}J_2 GMa\begin{pmatrix} x \\ y \\ z \end{pmatrix}\begin{pmatrix} \frac{x-5xz^2}{r^2} \\ \frac{y-5yz^2}{r^2} \\ \frac{3z-5z^3}{r^2} \end{pmatrix} + \omega^2\begin{pmatrix} x \\ y \\ 0 \end{pmatrix} + 2\omega\begin{pmatrix} +Vy \\ -Vx \\ 0 \end{pmatrix}, \tag{44}$$

where:

a = 6378136 m - semi-major (equatorial) axis of the PZ-90 Earth's ellipsoid;

J2 = 1082625.75 10^6 - second degree zonal coefficient of normal potential.

The initial conditions for simplified algorithm integration are the coordinates x = x(tb), y = y(tb), z = z(tb), velocity vector components Vx=Vx(t_b), Vy=Vy(t_b) and Vz=Vz(t_b) and perturbing accelerations Ax, Ay and Az for the SV's center of mass at the instant tb is transmitted within navigation message data. Perturbing accelerations are considered constants on an interval of tb ±15 min. Numeric integration can be executed using for example the Runge-Kutta fourth-order method (MONTENBRUCK; GILL, 2000).

3.2.3 Runge-Kutta Methods

Runge-Kutta is a numerical technique used to solve an ordinary differential equation. Starting from initial values y_0 in a time t_0 a simple approximation can be calculated for y in a later time t_0+h using a first-order Taylor expansion:

$$y(t_0 + h) \approx y_0 + h\dot{y}_0 = y_0 + hf(t_0, y_0), \tag{45}$$

being this referred to as a Euler Step. From an initial point (t_0, y_0) and moving with a time-step of h along the tangent to the graph of y (figure 7). Following this, it is possible to obtain approximate values η_1 of the solution at distinct times (MONTENBRUCK; GILL, 2000).

Figure 7- Approximation solution of a differential equation using Euler steps of size h

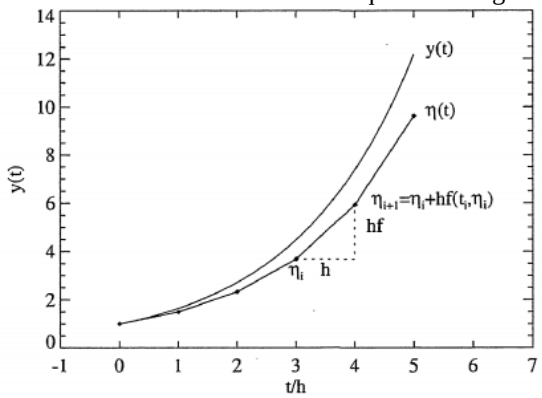

Source: Montenbruck; Gill (2000)

The step size needs to be carefully chosen so the values will follow the curve over several steps and a better approximation. The general notation is given by:

$$y(t_0 + h) \approx y_0 + h\Phi = \eta(t_0 + h), \tag{46}$$

for the approximate solution $\eta(t_0 + h)$, the increment function (Φ) must closely approximate the slope of the secant through (t_0, y_0) and $(t_0 + h, y_0(t_0 + h))$ which may not follow the slope of the tanged used in the Euler step. This problem was solved by Carl Runge and Wilheim Kutta which considers slopes at multiple points inside the integration step. In the 4th order Runge-Kutta, the increment function is calculated as the weighted mean is:

$$\Phi_{RK4} = \frac{1}{6}(k_1 + 2k_2 + 2k_3 + k_4), \tag{47}$$

of four slopes

$$k_1 = f(t_0, y_0), \tag{48}$$

$$k_2 = f\left(t_0 + \frac{h}{2}, y_0 + \frac{hk_1}{2}\right), \quad (49)$$

$$k_3 = f\left(t_0 + \frac{h}{2}, y_0 + \frac{hk_2}{2}\right), \quad (50)$$

$$k_4 = f(t_0 + h, y_0 + hk_3), \quad (51)$$

this formula is used to approximate the solution up to terms of order h^4, if y(t) is sufficiently smooth and differentiable. Its local truncation error is secured by a term of order h^5 (equations 52) (MONTENBRUCK; GILL, 2000).

$$e_{RK4} = |y(t_0 + h) - \eta(t_0 + h)| \leq h^5 \quad (52)$$

3.3 SATELLITE REFERENCE FRAMES: BODY-FIXED FRAME AND LOCAL ORBITAL FRAME

The orientation of the satellite in space is described in a body-fixed reference frame ($\mathcal{R}_{BF}$). This frame is tied to the mechanical structure of the satellite and enables the specification of the antenna relative to the CoM. The principal axes of the spacecraft body provide the natural choice for the definition of the body-fixed frame. The IGS conventions to the axis for the frame was presented by Montenbruck et al. (2015). The conventions are based on the frame assignment for the Block II/IIA of GPS.

The local reference frame ($\mathcal{R}_{RTN}$) is defined by the cross-track (N), along-track (T), and radial (R) components. For a satellite in space with a vector $\boldsymbol{r}$ from the center of mass of the Earth to the satellite and an inertial velocity $\boldsymbol{v}$, the corresponding unit vectors in $\mathcal{R}_{RTN}$ (P_{RNT}) are described in equations 52, 53, and 54 (MONTENBRUCK et al., 2015):

$$\mathbf{e_R} = \frac{\mathbf{r}}{|\mathbf{r}|}, \quad (52)$$

$$\mathbf{e_N} = \frac{\mathbf{r} \times \mathbf{v}}{|\mathbf{r} \times \mathbf{v}|}, \quad (53)$$

$$\mathbf{e_T} = \mathbf{e_N} \times \mathbf{e_R}, \quad (54)$$

from the local frame unit vector (P_{RNT}), the body-fixed frame will be given as:

$$\mathbf{P_{BF}} = \mathbf{A_{BF}^{RTN}} \cdot \mathbf{P_{RNT}}, \tag{55}$$

the transformation between the orbital frame and the body-fixed frame is commonly described by a series of three elementary rotations through the angles ϕ (roll), ϑ (pitch) and ψ (yaw):

$$\mathbf{A_{BF}^{RTN}} = \mathbf{R_1}(\phi)\mathbf{R_2}(\vartheta)\mathbf{R_3}(\psi). \tag{56}$$

Considering the GNSS characteristic of nadir-pointing spacecraft, the pitch and roll angles vanish, and the spacecraft attitude can be fully described by the yaw angle. Figure 8 shows ψ as being the angle between the $\mathbf{e_T}$ and $\mathbf{e_{X,BF}}$, which is the body-fixed frame unit vector for the x-axis (MONTENBRUCK et al., 2015).

Figure 8 - Definition of the yaw-angle

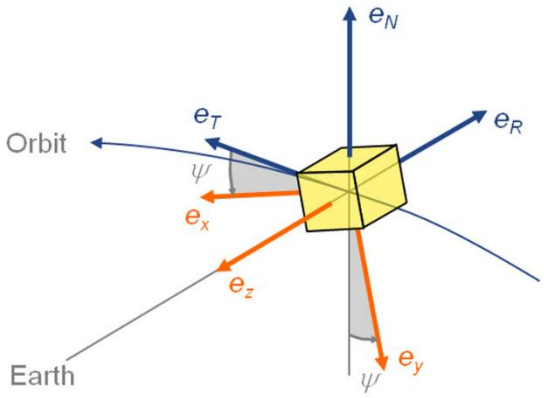

Source: Montenbruck et al. (2015)

For a given Sun elevation β above the orbital plane and an orbital angle μ (measured from the midnight point), the yaw angle can so be calculated by equation 57:

$$\psi = \tan^{-1}(-\tan\beta / \sin\mu). \tag{57}$$

The geometrical representations of the satellite attitude and the angles β and μ are presented in figure 9. β is the complement of the angle between the sun unit vector and the orbit normal vector (e_N). μ will be the angle in the orbit plane between the projection of the sun vector onto

the orbit plane and the satellite position vector. Crossing the orbital normal with the sun unit vector results in the vector $\vec{n}$, perpendicular to both vectors (PENINA; LISA, 2003):

$$\mathbf{n} = \mathbf{e_N} \times \mathbf{r_{sun}}, \tag{58}$$

Montenbruck; Gill (2000) described the algorithm to determine the sun vector. Crossing $\vec{n}$ with e_N it will yield the projection of the sun unit vector in the orbit plane ($\boldsymbol{r_{sun}^{proj}}$):

$$\mathbf{r_{sun}^{proj}} = \mathbf{n} \times \mathbf{e_N}. \tag{59}$$

Figure 9 describes the geometry of β and μ which can then be determined using:

$$\alpha = \tan^{-1}\left(\frac{\mathbf{r_{sat}}.\,\mathbf{n}}{\mathbf{r_{sat}}.\,\mathbf{r_{sun}^{proj}}}\right). \tag{60}$$

Figure 9 - GNSS satellite orientation in nominal yaw-steering mode

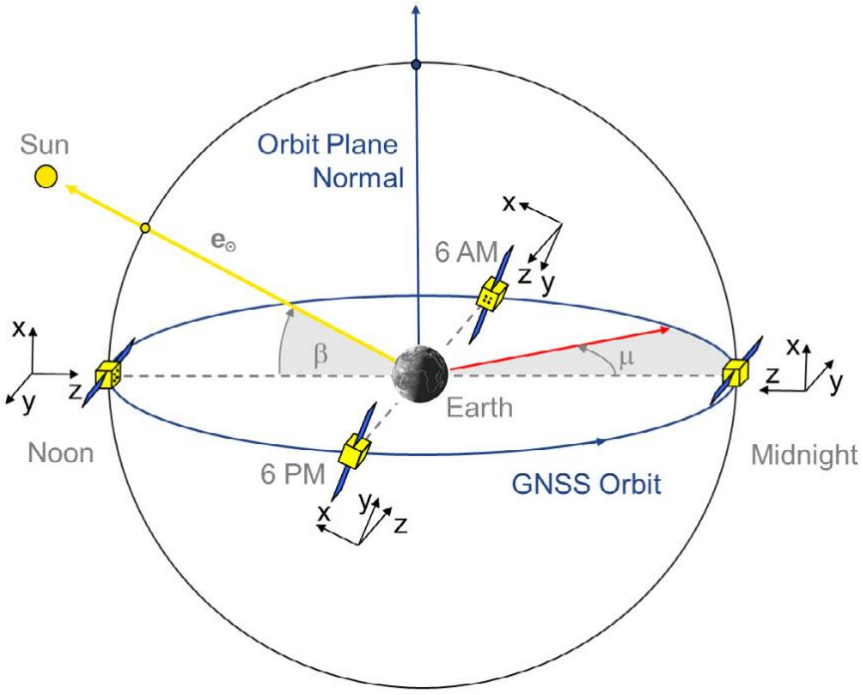

Source: Montenbruck et al. (2015)

The detailed modeling of GNSS satellite attitudes for point positioning and precise orbit determination needs to be done carefully due to different systems involved. By using the IGS-specific body frame orientation, the system can be, to a large extent, unified. The reference

orientation for the IGS body frame is provided by the yaw-steering frame (MONTENBRUCK et al., 2015).

3.4 ATTITUDE

The radio signals transmitted by a GNSS satellite is generated on the phase center of the antenna and in a fixed body coordinate system the CoP has a constant offset from the center of mass, however, it changes in space depending on the instantaneous orientation, or attitude, of the satellite body in an ECEF system (LEICK; RAPOPORT; TATARMIKOV, 2014; MONTENBRUCK et al., 2015).

The changing on the orientation of the satellite relative to the receiver may also have some influence on the observed carrier phase through the wind-up effect. Solar radiation pressure modeling also relies on a proper understanding of the orientation of the spacecraft body and the solar panels relative to the Sun.

The GNSS constellations have different configurations and orbits but a common attitude orientation inherited from the GPS. The inertial attitude of GNSS satellites mostly determined by the need to point the navigation antenna toward the Earth to provide a stronger signal propagation and coverage, while keeping the solar panels oriented to the Sun. Finally, one of the satellites faces perpendicular to the antenna boresight and the solar panel rotation axis should permanently point into the hemisphere opposite the Sun to facilitate thermal stabilization of the atomic clocks (mounted close to the cooling panel). To achieve this, the spacecraft performs a continuous rotation about the Earth-pointing (yaw) axis to keep the solar panel axis perpendicular to the Sun direction. This concept, which was first implemented by the GPS and later adopted by most of the other constellations, is commonly known as yaw-steering (YS) attitude mode (HUGENTOBLER; MONTENBRUCK, 2017).

According to IGS, the axis definitions are given as:

- The +x-, y-, and z-axis form a right-handed coordinate system attached to the satellite body.
- The +z-axis coincides with the antenna boresight direction.
- The y-axis is parallel to the rotation axis of the solar panels. Furthermore, the +y-direction is assigned.

Table 11 presents the nominal attitude for GNSS.

Table 11 - Nominal attitude (orientation of the IGS-specific body frame of individual navigation satellite types outside eclipse periods.

Constellation	Type	Attitude
GPS	I, II/IIA, IIR, IIF	$\mathcal{R}_{BF} = \mathcal{R}_{YS}$
GLONASS	- , M, K1	$\mathcal{R}_{BF} = \mathcal{R}_{YS}$
Galileo	GIOVE-A/B, IOV, FOC	$\mathcal{R}_{BF} = \mathcal{R}_{YS}$
BeiDou – 2	MEO IGSO	$\mathcal{R}_{BF} = \begin{Bmatrix} \mathcal{R}_{YS} \\ \mathcal{R}_{ON+} \end{Bmatrix} for \lvert\beta\rvert \begin{Bmatrix} \geq \\ < \end{Bmatrix} 4°$

3.4.1 Satellite antenna offsets

To compare final satellite coordinates with those acquired from the broadcast ephemeris necessary to correct for the separation between the CoM (where the precise coordinates are calculated) and the CoP (where the GNSS signal is originated and the broadcast ephemeris refer to). One must know the satellite phase center vector and monitor the orientation of the offset vector in space as the satellite orbits the Earth. The correction will be made on a body-fixed reference frame (KOUBA, 2009). The values of the offset can be obtained from the IGS the Antenna Exchange Format (ANTEX) (MONTENBRUCK; STEIGENBERGER; HAUSCHILD, 2018).

3.5 METHODOLOGY FOR ORBIT ACCURACY ANALYSIS

The main goal of this section is to evaluate the accuracy of broadcast ephemeris and the influence of phase center offset corrections in the final accuracy of the broadcast products. It follows up with the IGMA trial project direction, where the results and products may be used in the future to keep track of GNSS.

Four systems were used: GPS, GLONASS, Galileo and BeiDou and they were analyzed for five years (2015,2016,2017,2018 and 2019). For each year, the first 120 days were chosen. This number was chosen due to the researchers processing capabilities, because GLONASS numerical integration had a high computational cost. For the 120 days of 2019 the entire process took over 2 days to be completed.

To process the data, scripts were developed in Python 2.7. The data used was the daily merged broadcast files and final ephemeris downloaded from the Crustal Dynamics Data Information System (CDDIS). After that a first filtering process was carried out to exclude unhealthy satellites. With the remaining health satellites, a second filtering was performed to

exclude duplicated ephemeris. During the merging process of the navigation message done by the CDDIS many satellites had two blocks of ephemeris for the same time of ephemeris. An example is showed in table 12 for the SV E19 on January 23rd, 2015. Even though they have the same toe (in red) the Keplerian elements are not the same.

Table 12 - Duplicated Broadcast ephemeris for Galileo

E19	2015 01 23 00 50 00	2.218445297331E-05	3.410605131648E-13	0.000000000000E+00
	5.210000000000E+02	8.034375000000E+01	3.660152460041E-09	-8.035264774631E-01
	3.617256879807E-06	2.918939571828E-04	5.481764674187E-06	5.440609462738E+03
	4.350000000000E+05	5.215406417847E-08	1.733906234486E+00	-4.470348358154E-08
	9.597571269939E-01	2.198437500000E+02	2.246935609339E+00	-5.972034473493E-09
	5.964534161075E-10	5.130000000000E+02	1.828000000000E+03	
	3.120000000000E+00	0.000000000000E+00	5.820766091347E-09	6.053596735001E-09
	4.349950000000E+05 (tt)			

E19	2015 01 23 00 50 00	2.219260204583E-05	6.963318810449E-13	3.469446951954E-18
	8.500000000000E+01	8.034375000000E+01	3.663366879649E-09	-8.035199879585E-01
	3.622844815254E-06	2.918802201748E-04	5.483627319336E-06	5.440609558105E+03
	4.350000000000E+05	5.215406417847E-08	1.733906196450E+00	-4.284083843231E-08
	9.597571035872E-01	2.198437500000E+02	2.246928757030E+00	-5.974891735366E-09
	5.946676274365E-10	5.130000000000E+02	1.828000000000E+03	
	3.120000000000E+00	0.000000000000E+00	5.820766091347E-09	6.053596735001E-09
	4.376950000000E+05 (tt)			

Due to this problem the selected ephemeris was the one that was the closest to the time of transmission (tt, in green). BeiDou, GPS and Galileo were processed using the equations showed in sections 3.2.1 and 3.2.2, GLONASS was processed using the Runge-Kutta numerical integration in intervals of 15 minutes (following the interval made available by the final ephemeris). The time intervals used for each system's ephemeris is in table 8. Figure 10 shows the processing steps.

Figure 10 - Flowchart for the first part of the processing of the downloaded data

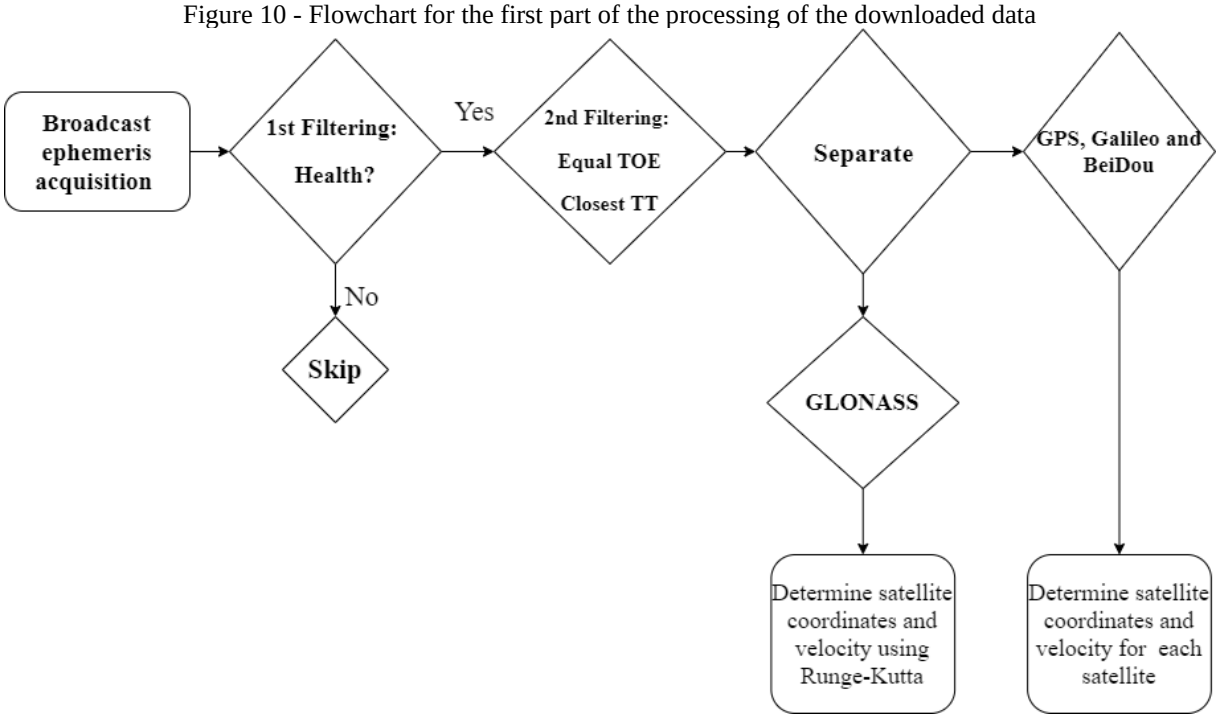

With the calculated coordinates and velocities, a transformation was made to both, broadcast and finals coordinates into the local RAC system (section 3.3). The differences between coordinates were then calculated. Next, the final coordinates were transformed into the IGS body-fixed system (MONTENBRUCK et al., 2015) and the corrections from the IGS ANTEX file 2014 were applied (annexes A) for each satellite taking the coordinates from the CoM (where the coordinates are) to the CoP (where the coordinates will again be used). A second comparison was made, and from these results, it was calculated the standard deviation (equation 61)

$$S_n = \sqrt{\frac{\sum_{i=1}^{n}(dE_i - \overline{dE})}{n-1}}. \tag{61}$$

Where dE_i is the broadcast orbit position error in the any reference direction with respect to IGS final orbit for a satellite at epoch, n is the number of observations, and i is the epoch for the satellite. The RMSE (root mean squared error) is giving as:

$$RMSE = \sqrt{\frac{1}{n}\sum_{i=1}^{n}(dE_i)^2}, \tag{62}$$

and the probability density plot, which t simply means a density plot of probability density function (Y-axis) vs data points of a variable (X-axis). Typically, probability density plots are used to understand data distribution for a variable when it is needed to know the likelihood (or probability) of obtaining a range of values that the variable can assume. By showing probability density plots it is possible to understand the distribution of data visually, know the range of the residuals and have a general idea if the data follow any general statistic model.

Figure 11 - Flowchart for the second part of the processing of the downloaded data

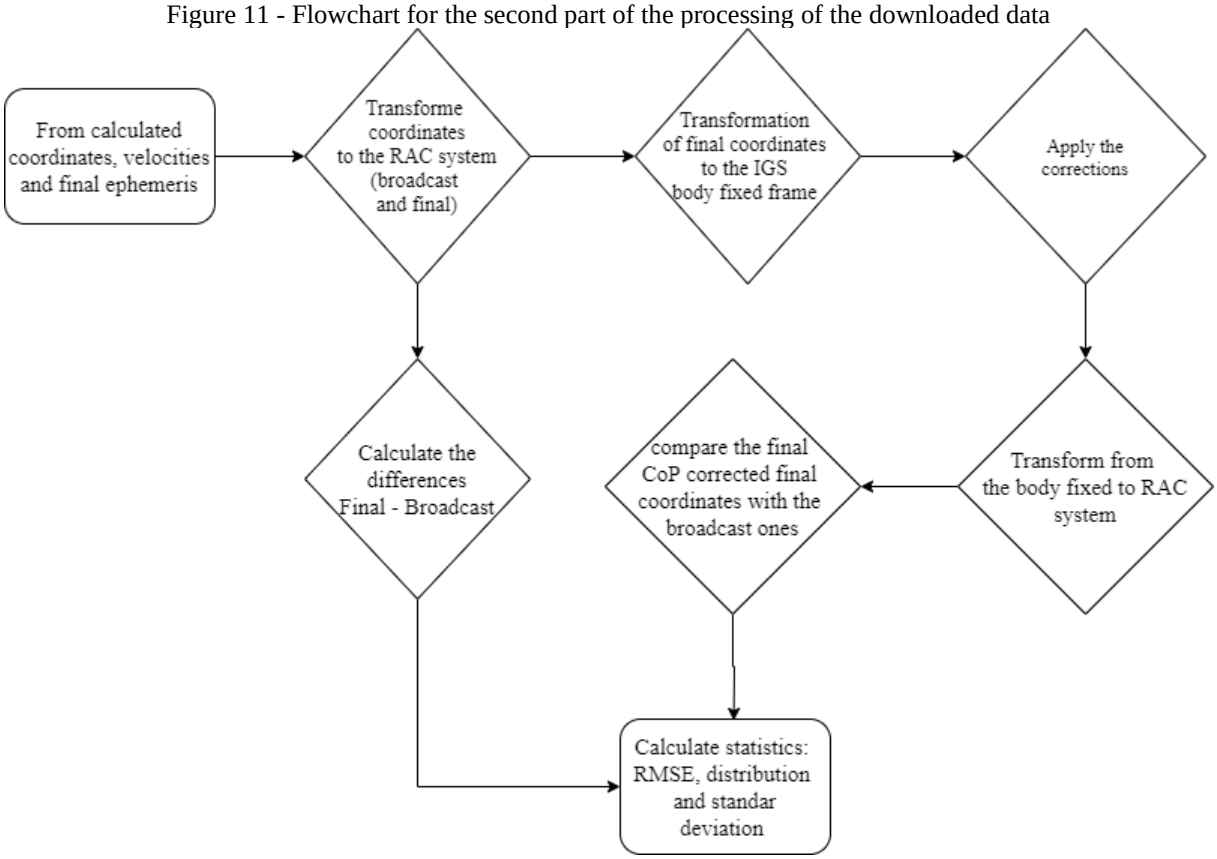

3.6 RESULTS AND ANALYZES

For GPS the probability density plot (figure 12) showed a higher difference for the radial component. Without the corrections of the PCO it did not present a clear distribution and did not have a clear peak. After applying the correction, a closer bell-shape distribution was

presented with a peak around -0.4 m. The other two components (along and cross-track) the distribution did not show a big difference when comparing them.

Figure 12 - Density distribution for the residuals of each component for GPS for the 600 days

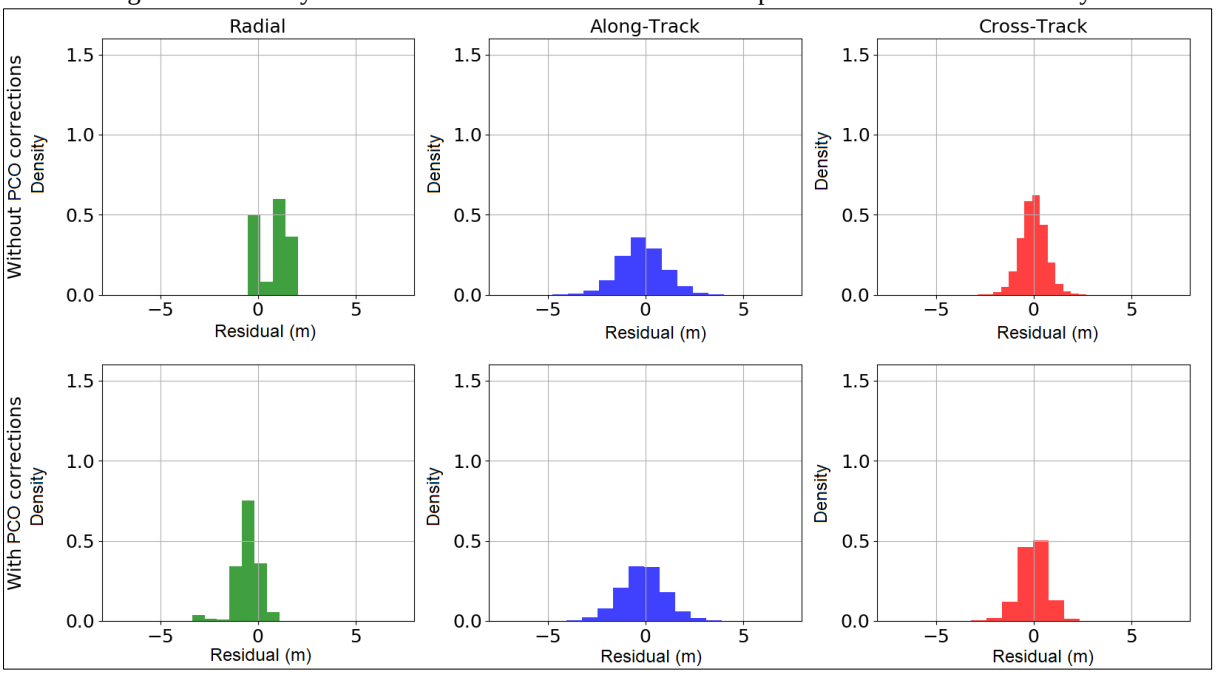

For Galileo (figure 13), when correcting for the PCO the probability density plot on the radial component showed a shift in the mean (peak of the plot), going from 0.4 m to 0.02 m, also it presented a more weighted distribution. For the other two components it did not present such a large difference, both (radial and cross-track) already had a peak around 0. When comparing with the plot in which the corrections were applied, the density around the peak increased.

Figure 13 - Density distribution for the residuals of each component for Galileo for the 600 days

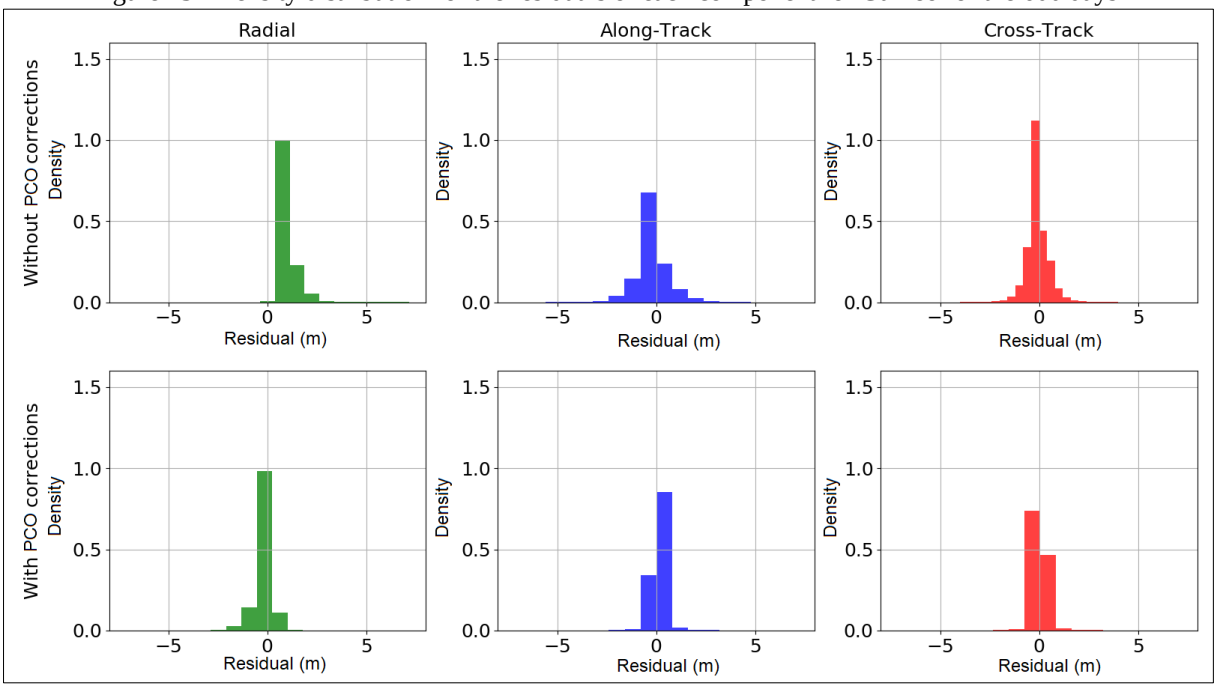

For BeiDou on the probability density plot (figure 14) the radial component was the one that showed the largest difference, a small switch on the peak (mean) appeared when using the PCO correction, going from 0.72 m to -2.10 m. The other two components did not show such a large difference. For the along-track just a small variation on the peak for the cross-track component, but both kept the bell shape of the distribution.

Figure 14 - Density distribution for the residuals of each component for BeiDou for the 600 days

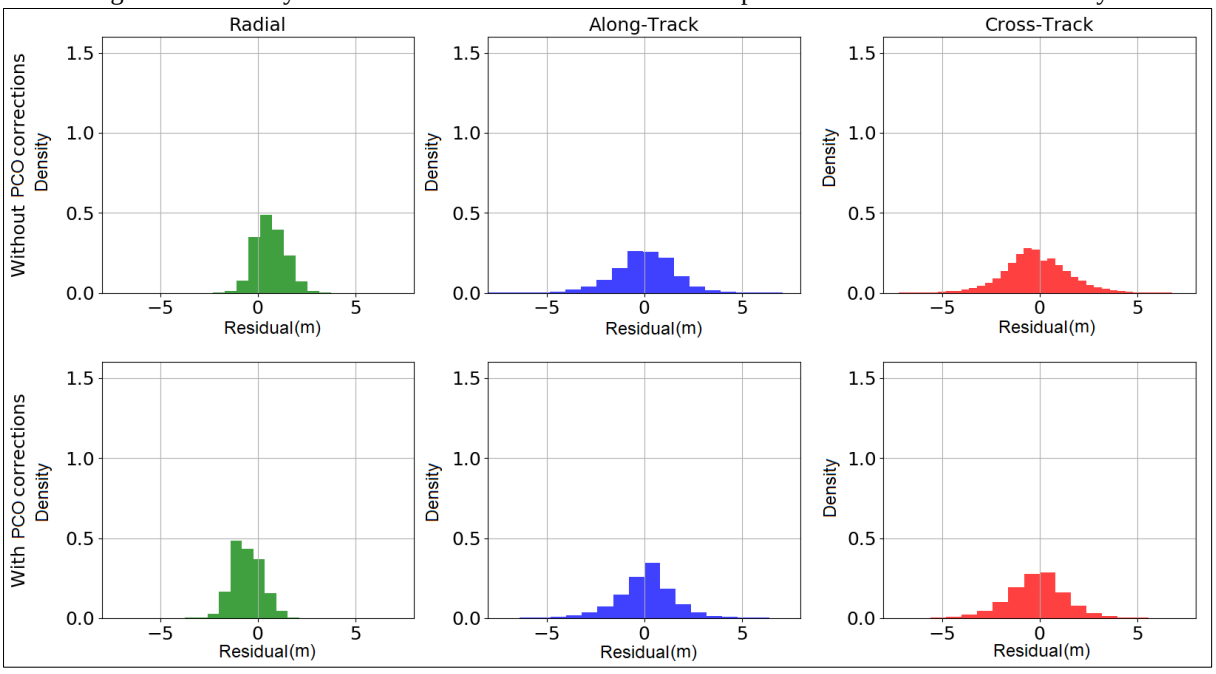

GLONASS probability density plot (figure 15) presented the biggest variation for the radial component. The residuals without the correction present a main tendency around 1.9 and the data was scattered out without a well-distributed graph, after the corrections the component started showing a peak around zero. The along-track did not show any differences when comparing the residuals with and without corrections. For the cross-track component both distributions were close, but the corrected residuals presented a smoother distribution was presented.

Figure 15 - Density distribution for the residuals of each component for GLONASS for the 600 days

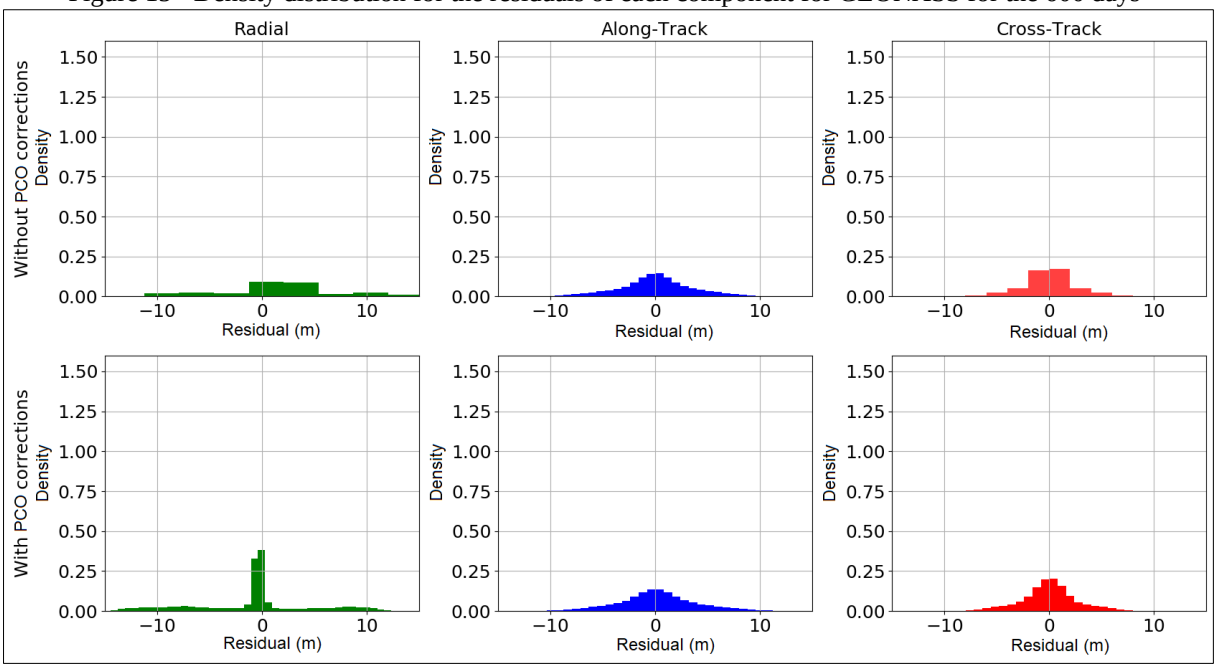

For each system it was calculated the RMSE by year, for the residuals with and without corrections of the PCO. Figure 16 shows the values for GPS, for all years for the three components (radial, along-track, and cross-track) and the final 3D RMSE. When comparing the difference between the RMSE from the residuals with and without corrections the radial component showed the most significant improvement when applying the PCO correction, the largest improvement was of 0.40 m (2016) and the smallest one of 0.25 m (2015). The along-track values were almost the same for both (with and without corrections) for all years, with the most significant improvement being of 0.05 m and the worse value of -0.01 m. For the cross-track component worse values of RMSE were found applying the correction, the biggest

disagreement was of -0.12 m (2018). The 3D component presented an improvement for all five years, the values were between 0.6 m (2018) to 0.17 (2019).

Figure 16 - RMSE for the Radial, Along-track, Cross-track, and 3D by year for GPS. Red (without PCO corrections), black (with PCO correction)

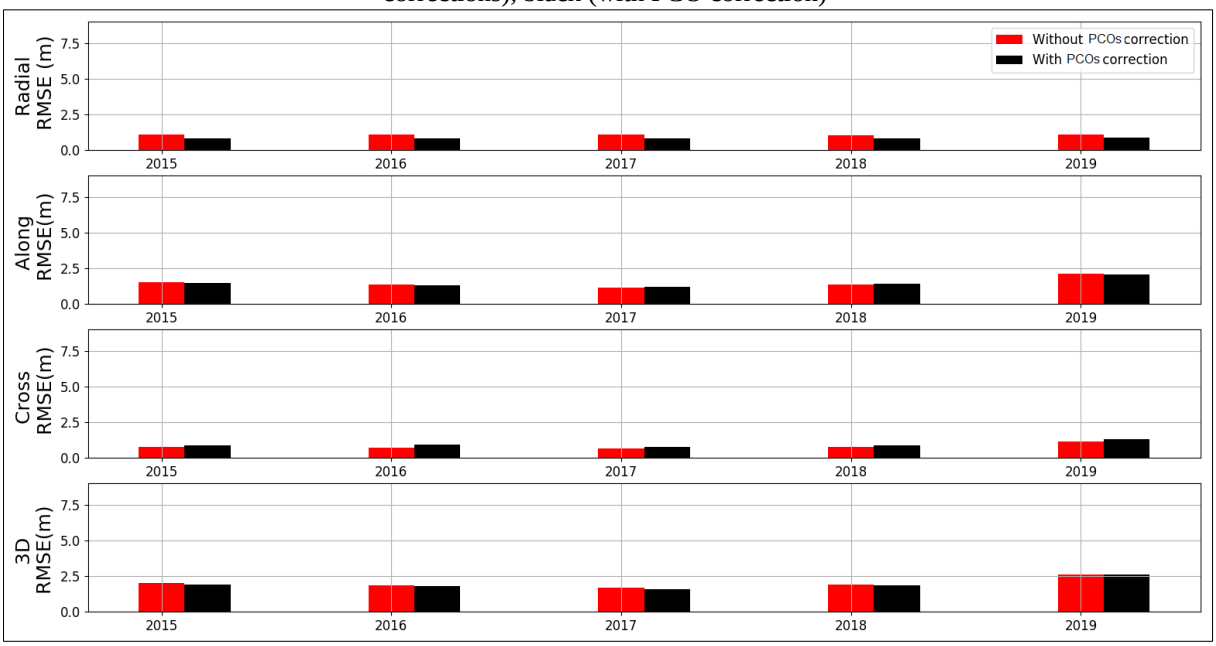

From the 32 satellites, 13 presented a worse value of the 3D RMSE when using the PCO corrections. From those satellites, PRN 22 presented the highest discrepancy (0.34 m). From the remaining 19 the highest improvement when using the PCO corrections was for satellite PRN 16 (0.89 m). One of the reasons for the discrepancy could be during the process of determining the Sun's coordinates and unit vector. As described by Montenbruck and Gill (2000), the algorithm used in this research is considered of low precision, and it may influence the final result during the frames transformation. Another factor that could influence the corrections are the values made available in the ANTEX file, even though they are the official ones released by the IGS there are studies where when they were determined by an adjustment process the values are different from those on the ANTEX file (MONTENBRUCK et al., 2015).

The 13 satellites that did not present good results belong to various blocks of GPS satellites (2 on II-F, 4 on II-R, 7 on IIR-M). For the ones that had a better result with the PCO correction, G04 presented the highest value for the 3D RMSE. However, currently, this satellite is decommissioned, and it was replaced by the first SV of block III – A which was operational

on January 13th, 2020. Table 13 shows the RMSE for all GPS satellites through the 600 days analyzed.

Table 13 - RMSE by satellite for GPS for the components: Radial, Along and Cross-track

SV	Radial	Radial corrected	Along	Along-track corrected	Cross-track	Cross-track corrected	3D	3D corrected
G01	1.13	0.44	1.23	1.38	0.66	1.00	1.80	**1.75**
G02	0.17	0.86	1.17	1.11	0.60	0.58	1.32	**1.52**
G03	1.14	0.52	1.34	1.45	0.66	1.51	1.88	**2.16**
G04	1.49	1.11	6.65	6.54	3.67	4.09	7.74	**7.69**
G05	0.14	0.84	1.01	0.96	0.53	0.51	1.15	**1.37**
G06	1.13	0.41	1.07	1.11	0.66	0.88	1.68	**1.48**
G07	0.13	0.86	1.11	1.05	0.67	0.64	1.30	**1.50**
G08	1.11	0.52	1.90	1.78	0.96	1.05	2.40	**2.13**
G09	1.12	0.46	1.02	1.21	0.61	0.94	1.63	**1.60**
G10	1.10	0.52	1.31	1.42	0.66	0.95	1.84	**1.79**
G11	1.51	0.41	1.54	1.46	0.79	0.76	2.29	**1.69**
G12	0.19	0.91	1.12	1.06	0.63	0.60	1.29	**1.52**
G13	1.62	0.29	1.19	1.12	0.59	0.57	2.10	**1.29**
G14	1.61	0.31	1.37	1.30	0.71	0.68	2.23	**1.50**
G15	0.12	0.66	1.11	1.04	0.63	0.60	1.28	**1.37**
G16	1.64	0.22	1.03	0.97	0.56	0.53	2.02	**1.13**
G17	0.17	0.89	1.48	1.38	0.67	0.64	1.63	**1.76**
G18	1.42	1.08	2.28	2.09	1.27	1.20	2.97	**2.64**
G19	0.11	0.86	1.05	0.99	0.57	0.55	1.20	**1.42**
G20	1.60	0.30	1.07	1.02	0.67	0.65	2.04	**1.25**
G21	1.57	0.24	1.34	1.27	0.71	0.68	2.18	**1.46**
G22	0.15	1.83	1.16	1.11	0.70	0.67	1.37	**1.71**
G23	0.13	0.82	1.12	1.08	0.68	0.66	1.32	**1.50**
G24	1.12	0.50	1.23	1.51	0.65	0.93	1.78	**1.84**
G25	1.11	0.46	1.18	1.24	0.63	0.90	1.73	**1.60**
G26	1.12	0.52	2.07	1.93	0.96	1.00	2.54	**2.23**
G27	1.11	0.48	1.12	1.32	0.66	1.05	1.71	**1.69**
G28	1.52	0.53	1.24	1.17	0.58	0.56	2.05	**1.40**
G29	0.15	0.86	1.47	1.39	0.75	0.72	1.65	**1.78**
G30	1.10	0.48	1.17	1.39	0.62	0.98	1.72	**1.70**
G31	0.14	1.00	1.17	1.12	0.60	0.57	1.32	**1.61**
G32	1.13	0.62	1.85	1.68	0.85	0.94	2.33	**2.03**

Figure 17 shows the values for Galileo, considering all years for the three components (radial, along-track, and cross-track) and the 3D RMSE. When comparing the difference between the RMSE from the residuals with and without corrections the along-track component showed that the best improvement was when applying the PCO correction with the best improvement of 2.32 m (2015) and the worse one of 0.59 m (2019). The radial values were the next to show the best improvement, the highest was 0.79 m (2016) and the smallest was 0.31 m (2017). The cross-track component had the smallest change when comparing the RMSE with and without PCO correction, still it had an improvement, the highest one being of 1.41 m (2015) and the lowest one of 0.23 (2019).

The 3D component presented an improvement for all five years, the difference for the RMSE with and without corrections were between 2.73 m (2015) to 0.97 (2019).

Figure 17 - RMSE for the Radial, Along-track, Cross-track, and 3D by year for Galileo. Red (without PCO corrections), black (with PCO correction)

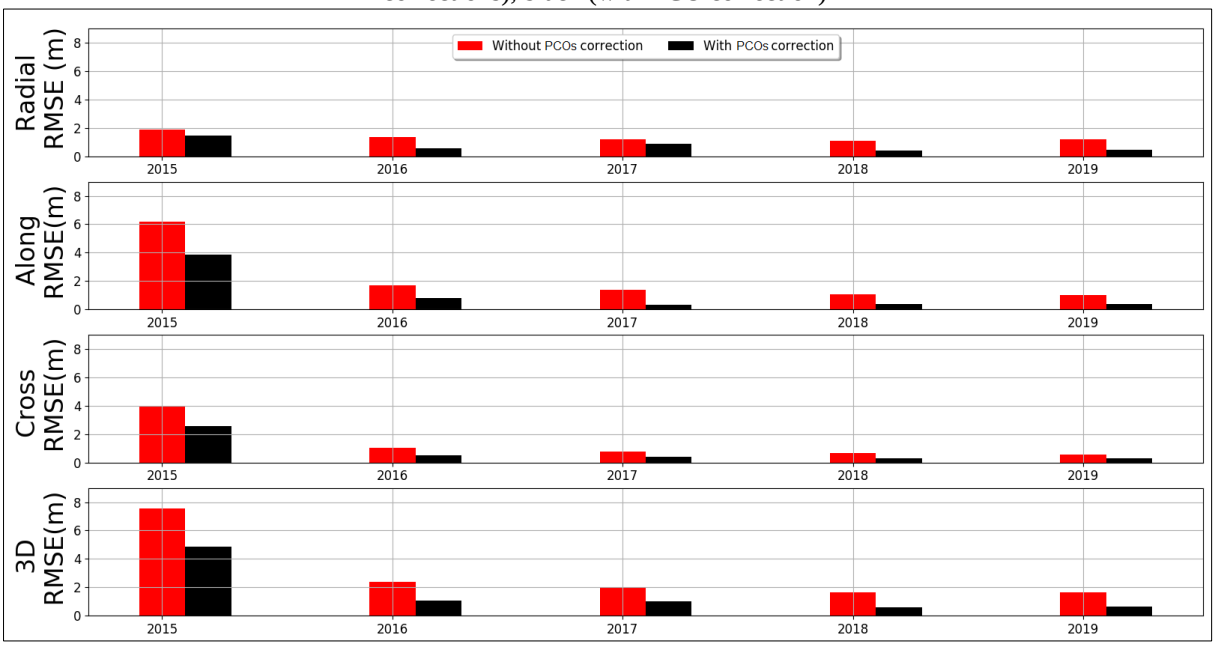

When analyzing each satellite (table 14) all of them improved when the correction was applied. E19 presented the best improvement on the 3D RMSE going from 4.52 m without correction to 2.74 m with corrections and the satellite that presented the smallest improvement was E05, going from 1.33 m to 0.72 m.

Table 14 - Overall RMSE by satellite for Galileo for the components: Radial, Along and Cross-track and 3D

SV	Radial	Radial corrected	Along	Along-track corrected	Cross-track	Cross-track corrected	3D	3D corrected
E01	1.24	0.77	1.35	0.25	0.62	0.22	1.93	**0.84**
E02	0.99	0.40	0.70	0.25	0.42	0.21	1.29	**0.51**
E03	0.98	0.34	0.66	0.26	0.40	0.26	1.24	**0.50**
E04	0.95	0.52	0.76	0.42	0.44	0.27	1.30	**0.72**
E05	1.00	0.36	0.76	0.41	0.45	0.27	1.33	**0.61**
E07	1.00	0.36	1.17	0.23	0.66	0.22	1.68	**0.48**
E08	1.42	0.39	1.26	0.41	0.80	0.29	2.06	**0.63**
E09	1.27	0.43	1.40	0.61	0.93	0.37	2.11	**0.84**
E11	1.28	0.74	2.21	1.41	1.41	0.91	2.92	**1.84**
E12	1.24	1.10	1.65	0.83	1.13	0.68	2.36	**1.53**
E13	1.18	0.41	0.88	0.55	0.48	0.26	1.55	**0.73**
E15	1.13	0.40	0.75	0.24	0.42	0.22	1.42	**0.51**
E19	1.50	0.83	3.59	2.15	2.31	1.49	4.52	**2.74**
E21	1.48	0.88	2.14	0.26	0.66	0.20	2.69	**0.94**
E22	1.10	0.46	1.00	0.32	0.66	0.29	1.62	**0.63**
E24	1.08	0.48	1.24	0.28	0.54	0.24	1.73	**0.61**
E25	1.09	0.35	0.66	0.26	0.37	0.19	1.33	**0.47**
E26	1.40	0.65	1.63	0.32	0.81	0.26	2.30	**0.77**
E27	1.10	0.36	0.70	0.22	0.41	0.21	1.37	**0.47**
E30	1.11	0.52	1.35	0.48	0.75	0.33	1.91	**0.78**
E31	1.07	0.36	0.70	0.28	0.41	0.25	1.35	**0.52**
E33	1.15	0.39	0.75	0.31	0.43	0.21	1.44	**0.54**
E36	1.12	0.38	0.72	0.24	0.40	0.20	1.39	**0.50**

For Galileo is important to point out that the system had an important change over the years. Table 15 shows the RMSE for each satellite in 2015, what was the year that presented the highest RMSE for all components on figure 17. All the satellites presented a better RMSE when applying the correction, but still had a high 3D RMSE, with all of them going over 1.5 m.

Table 15- RMSE by satellite for Galileo for the components: Radial, Along and Cross-track and 3D for 2015

SV	Radial	Radial corrected	Along	Along-track corrected	Cross-track	Cross-track corrected	3D	3D corrected
E11	2.12	1.56	5.49	3.65	3.4	2.24	6.80	**4.56**

continue

conclusion

E12	1.3	0.66	2.42	1.17	2.02	1.21	3.41	**1.80**
E19	2.08	1.82	8.66	5.34	5.52	3.57	10.48	**6.67**

Comparing the values from table 15 and table 16, which presents the results for the year of 2019 it's clear the improvement of the ephemeris for Galileo. Satellite 19 still has the worse RMSE, but it lowered over 8 meters on the RMSE without correction and 5 meters on the RMSE with corrections. Then the final RMSE on table 14 reflects not only the improvement and low values in the final years but also the worse results presented in the early years (2015/2016).

Table 16 - RMSE by satellite for Galileo for the components: Radial, Along and Cross-track and 3D for 2019

SV	Radial	Radial corrected	Along	Along-track corrected	Cross -track	Cross-track corrected	3D	3D corrected
E01	1.03	0.38	0.70	0.23	0.39	0.21	1.31	**0.50**
E02	1.07	0.37	0.71	0.25	0.39	0.22	1.35	**0.50**
E03	1.07	0.35	0.68	0.26	0.40	0.30	1.33	**0.53**
E04	1.06	0.66	0.79	0.25	0.45	0.22	1.40	**0.74**
E05	1.13	0.35	0.69	0.24	0.40	0.20	1.38	**0.47**
E07	0.99	0.36	0.71	0.25	0.44	0.21	1.30	**0.49**
E08	2.13	0.38	1.92	0.58	1.20	0.34	3.11	**0.77**
E09	1.05	0.36	0.71	0.25	0.43	0.19	1.34	**0.48**
E11	1.11	0.47	0.73	0.31	0.52	0.32	1.43	**0.65**
E12	1.18	0.43	0.75	0.29	0.53	0.53	1.50	**0.75**
E13	1.18	0.41	0.88	0.55	0.48	0.26	1.55	**0.73**
E15	1.13	0.40	0.75	0.24	0.42	0.22	1.42	**0.51**
E19	1.11	0.51	1.67	1.22	0.93	0.74	2.21	**1.52**
E21	1.48	0.88	2.14	0.26	0.66	0.20	2.69	**0.94**
E24	1.03	0.38	0.70	0.23	0.38	0.19	1.30	**0.48**
E25	1.09	0.35	0.66	0.26	0.37	0.19	1.33	**0.47**
E26	1.17	0.41	0.72	0.29	0.41	0.23	1.43	**0.55**
E27	1.10	0.36	0.70	0.22	0.41	0.21	1.37	**0.47**
E30	1.03	0.40	0.76	0.21	0.43	0.20	1.35	**0.50**
E31	1.07	0.36	0.70	0.28	0.41	0.25	1.35	**0.52**
E33	1.15	0.39	0.75	0.31	0.43	0.21	1.44	**0.54**
E36	1.12	0.38	0.72	0.24	0.40	0.20	1.39	**0.50**

Figure 18 shows the values for GLONASS, for the years considered in this research in the three components (radial, along-track, and cross-track) and the 3D RMSE. When comparing the difference between the RMSE from the residuals with and without corrections the cross-track component showed the highest improvement. The differences of the RMSE were between 0.25 m (2019) and 0.17 m (2015). The next to present good results was the along-track component, with the difference between 0.09 m (2016) and 0.17 m (2019). The radial component presented worse values with the correction with the differences between the RMSE going from -0.11 (2019) to -0.14 m (2015). The 3D component presented an improvement for all five years, when comparing the RMSE the values were between 0.09 m (2019) and 0.01 (2015).

Figure 18 - RMSE for the Radial, Along-track, Cross-track, and 3D by year for GLONASS. Red (without PCO corrections), black (with PCO correction)

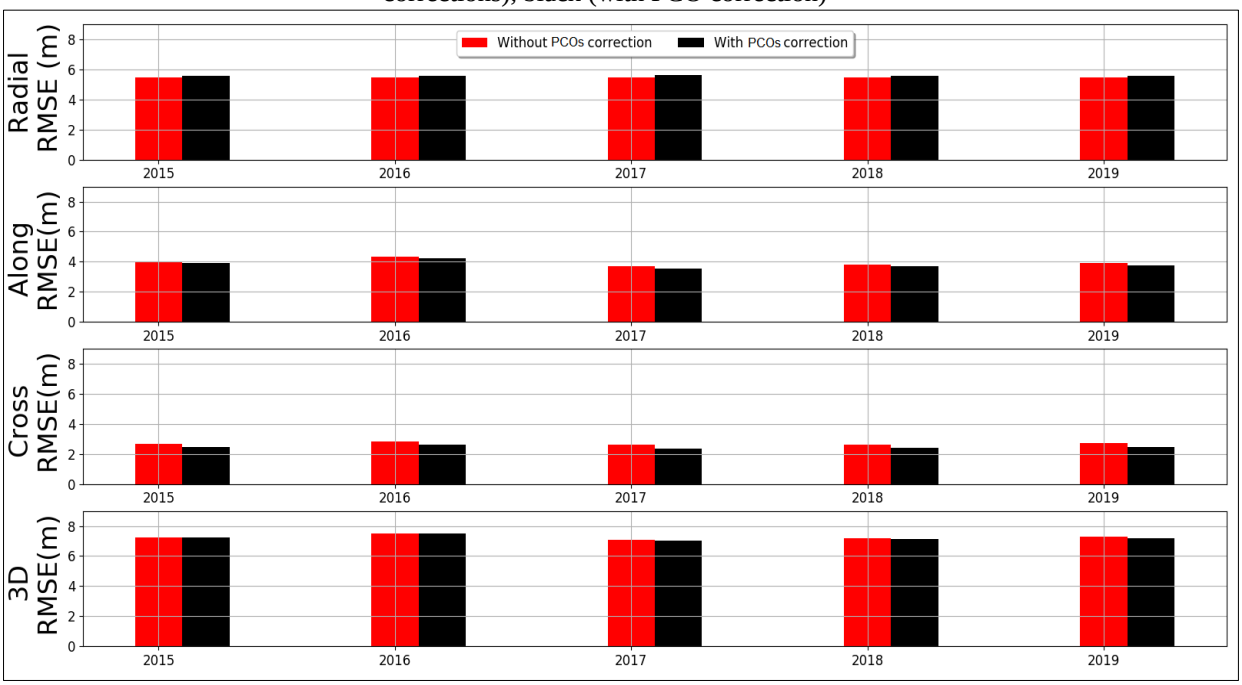

During the evaluation period, all the satellites were fully operational during all the years, even though some are already replaced (SV 04 that started to be operational on 03/01/2020). Table 17 shows the overall results by satellite, from the 24 satellites 3 presented a worse value of the 3D RMSE when using the PCO corrections. As pointed before two main factors could explain these results: the accuracy of the Sun's coordinates determination and the real values of the PCO's that show different values through the literature (MONTENBRUCK et al., 2015), also the orientation of the axis during the frame transformations are not fully comprehended and further tests will be necessary to correctly apply the PCO's. From those satellite 10 presented the highest discrepancy (0.12 m). From the 21 that remained

the highest improvement when comparing the values with and without using the PCO corrections was for satellite 03 (0.14 m).

The 3 satellites that did not present good results belong to the GLONASS-M block. For the ones that had a good result, R21 presented the best result. All satellites presented a high value for the 3D RMSE when compared to the previous systems analyzed.

Table 17 - Overall RMSE by satellite for GLONASS for the components: Radial, Along and Cross-track and 3D

SV	Radial	Radial corrected	Along	Along-track corrected	Cross-track	Cross-track corrected	3D	3D corrected
R01	5.38	5.48	3.68	3.54	2.56	2.36	7.00	6.94
R02	5.43	5.54	3.69	3.57	2.55	2.38	7.05	7.01
R03	5.44	5.51	3.74	3.52	2.60	2.34	7.09	6.95
R04	5.41	5.51	3.52	3.41	2.54	2.36	6.94	6.90
R05	5.39	5.49	3.66	3.56	2.56	2.38	7.00	6.96
R06	5.38	5.47	3.92	3.83	2.71	2.52	7.19	7.13
R07	5.46	5.51	3.55	3.44	2.55	2.36	6.99	6.91
R08	5.41	5.52	3.72	3.51	2.64	2.35	7.07	6.95
R09	5.44	5.42	4.38	4.3	2.61	2.44	7.46	7.34
R10	5.46	5.78	4.93	4.85	2.90	2.73	7.91	**8.03**
R11	5.44	5.55	3.55	3.39	2.57	2.32	6.98	6.91
R12	5.46	5.57	3.71	3.59	2.60	2.44	7.10	7.06
R13	5.46	5.59	4.11	4.01	2.69	2.51	7.34	7.33
R14	5.46	5.7	3.86	3.67	2.67	2.42	7.20	7.20
R15	5.47	5.74	5.85	5.77	3.50	3.26	8.74	**8.77**
R16	5.43	5.56	4.43	4.33	2.82	2.66	7.55	7.53
R17	5.51	5.62	3.70	3.61	2.60	2.44	7.13	7.11
R18	5.53	5.64	3.35	3.22	2.53	2.33	6.94	6.90
R19	5.55	5.68	3.82	3.65	2.67	2.46	7.25	7.18
R20	5.50	5.8	3.39	3.28	2.52	2.34	6.94	**7.06**
R21	5.51	5.63	4.18	4	2.89	2.41	7.50	7.31
R22	5.53	5.66	3.37	3.26	2.51	2.32	6.94	6.93
R23	5.50	5.66	3.58	3.45	2.67	2.43	7.09	7.06
R24	5.57	5.62	3.91	3.78	2.71	2.46	7.32	7.21

Figure 19 shows the values for BeiDou, for all the years in the three components (radial, along-track, and cross-track) and the 3D RMSE. When comparing the difference between the RMSE from the residuals with and without corrections the radial component showed the highest variation. The differences of the RMSE were between -0.68 m (2015) and 0.47 m (2019). Next the along-track component had the differences between -0.51 m (2015) and 0.41 m (2019). The differences for the RMSE for the radial component were between -0.42 (2015) to 0.67 m (2019).

The 3D component presented an improvement for the years 2016,2017, 2018, and 2019 of 0.08 m, 0.26 m, 0.55 m, and 0.67 m respectively. A worsening on the 3D RMSE happened on the year of 2015, when comparing the RMSE with corrections presented a result of 0.81 m higher than the RMSE without corrections.

Figure 19 - RMSE for the Radial, Along-track, Cross-track, and 3D by year for BeiDou. Red (without PCO corrections), black (with PCO correction)

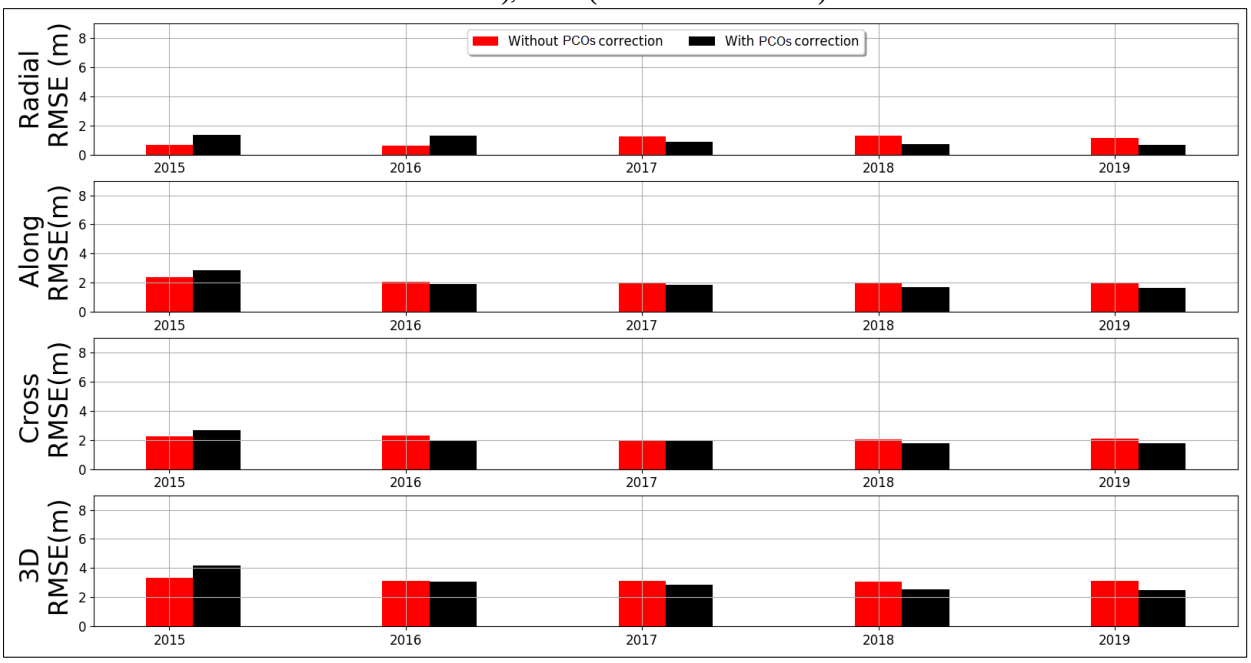

Table 18 shows the RMSE for each satellite in 2015 which is the year that presented the worse results overall. All the satellites had a worse RMSE when applying the correction, but still had a worse RMSE for all components, including the 3D

Table 18 : RMSE by satellite for BeiDou for the components: Radial, Along and Cross-track and 3D for 2015

SV	Radial	Radial corrected	Along	Along-track corrected	Cross-track	Cross-track corrected	3D	3D corrected
C06	0.71	1.30	1.50	2.51	1.94	2.65	2.55	**3.87**
C07	0.64	1.38	2.40	2.51	2.72	3.08	3.69	**4.50**
C08	0.73	1.46	2.53	2.51	2.74	3.82	3.80	**5.66**
C09	0.89	1.47	2.69	2.51	2.88	2.95	4.04	**4.50**
C10	0.76	1.42	2.29	2.51	2.57	2.85	3.53	**4.33**
C11	0.47	1.20	2.33	2.51	1.54	1.79	2.83	**3.22**
C12	0.42	1.19	2.02	2.51	1.42	1.68	2.51	**2.93**
C14	0.45	1.20	2.90	2.51	1.72	1.92	3.40	**3.53**

In comparison, table 19 shows the values for 2019, the year with the best overall RMSE for BeiDou. For 2015 the satellites had an average worsening on the 3D RMSE of 0.77 m, while for 2019 they presented an average improvement of 0.65 m. One of the possible reasons for the worsening is the fact that BaiDou satellites change their attitude when under an elevation angle (β) smaller than 4°, going from yaw-steering to orbital-normal. During the processing phase it was not evaluated if the satellites were in a different attitude, and it was used only the yaw-steering models.

Table 19 - RMSE by satellite for BeiDou for the components: Radial, Along and Cross-track and 3D for 2019

SV	Radial	Radial corrected	Along	Along-track corrected	Cross-track	Cross-track corrected	3D	3D corrected
PC06	1.47	0.48	2.15	1.46	1.85	1.45	3.20	**2.11**
PC07	0.72	0.85	1.74	1.38	2.44	1.87	3.08	**2.48**
PC08	0.90	0.61	1.94	1.57	3.03	2.44	3.71	**2.97**
PC09	1.36	0.45	1.42	1.28	1.67	1.36	2.58	**1.93**
PC10	1.21	0.48	1.28	1.06	1.88	1.51	2.58	**1.91**
PC11	1.01	0.72	2.96	2.41	1.75	1.82	3.59	**3.10**
PC12	0.69	1.02	2.73	2.17	1.56	1.64	3.22	**2.90**
PC13	1.39	0.44	1.34	1.12	2.21	1.67	2.94	**2.05**
PC16	0.68	0.98	1.74	1.49	1.98	1.52	2.72	2.34

Table 20 shows the overall results for all global satellites for BeiDou during the 600 days analyzed. During the evaluation period none of the satellites were substitute. From the 9

satellites, 1 presented a worse value of the 3D RMSE when using the PCO corrections, with a discrepancy of 0.14 m. From the 8 that remained the highest improvement when comparing the values with and without using the PCO corrections was for satellites 03 13 and 16 (0.38 m).

Table 20 - Overall RMSE by satellite for BeiDou for the components: Radial, Along and Cross-track and 3D

SV	Radial	Radial corrected	Along	Along-track corrected	Cross-track	Cross-track corrected	3D	3D corrected
C06	1.33	1.18	1.93	1.92	1.18	2.08	3.19	**3.06**
C07	0.70	1.07	1.89	1.91	1.07	2.11	3.06	**3.04**
C08	1.01	1.05	1.98	2.26	1.05	2.47	3.37	**3.51**
C09	1.28	1.01	2.01	1.91	1.01	2.25	3.49	**3.13**
C10	1.09	0.92	1.58	1.65	0.92	1.93	2.85	**2.70**
C11	0.90	0.95	2.50	2.24	0.95	1.72	3.09	**2.98**
C12	0.79	0.96	2.26	2.06	0.96	1.56	2.76	**2.76**
C13	1.39	0.77	1.94	1.84	0.77	2.66	3.70	**3.32**
C16	0.68	0.98	1.74	1.49	0.98	1.52	2.72	**2.34**

Figure 20 shows the overall RMSE for each system and table 21 the difference between the RMSE without and with corrections for all 600 days analyzed. On the radial component all systems had a lower RMSE when using the corrections with the lowering values between 0.03 m (BeiDou) and 0.59 m (Galileo). On the along-track component GLONASS had a worse RMSE when applying the correction (0.09 m) and the other systems improved, for the cross-track GPS and GLONASS had a worse RMSE (0.12 and 0.21 respectively). Finally, for the 3D RMSE Galileo, BeiDou and GPS had a better result using the corrections (1.09, 0.35, and 0.09 meters respectively). GLONASS, on the other hand showed a final corrected 3D RMSE worse than without correction (0.04 m).

Table 21 - Difference between the 3D RMSE without PCO correction and with PCO corrections

	Radial	Along-track	Cross-Track	3D
Galileo	**0.59**	**0.82**	**0.42**	**1.09**
BeiDou	**0.03**	**0.21**	**0.32**	**0.35**
Glonass	**0.14**	**-0.09**	**-0.21**	**-0.04**
GPS	**0.26**	**0.02**	**-0.12**	**0.09**

Figure 20 - Overall RMSE for each system for the 5 years of analyzes

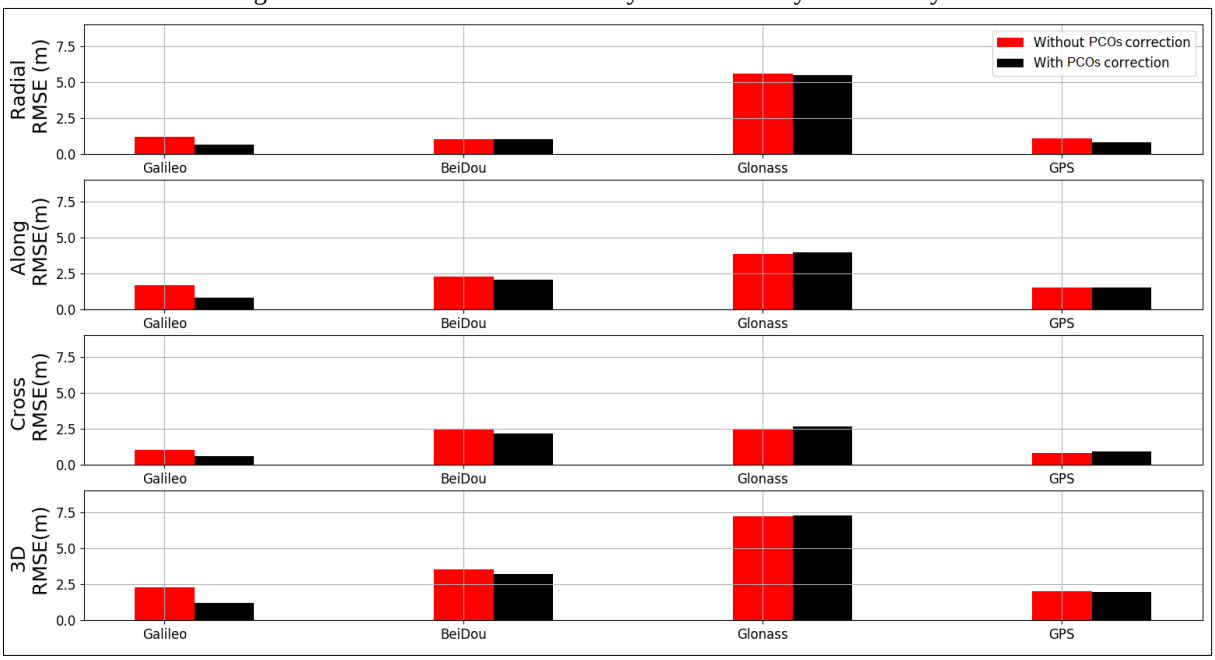

To avoid the excessive use of tables the standard deviations are presented in Appendix A through E. Appendix A shows the standard deviation for each satellite on the GPS constellation. On the radial component most of the satellites kept the same standard deviation 5 satellites presented better and 2 worse standard deviation with the correction of the PCO. Even though there were differences, the values were all smaller than 3 cm for this component. For the radial axis the satellite with the highest standard deviation was G04 (1.01 m) and G20 and G23 the smallest (0.12 m). On the along-track component, all satellites had a lower value for the standard deviation when the correction was used, the average improvement for this axis was of 0.67 meters. Satellite G04 had the largest standard deviation (6.53 m), but also the greatest improvement (2.86 m) having a standard deviation of 3.67 m when corrected. For the cross-track component all satellites had a smaller standard deviation with the PCO corrections. Again, G04 had the biggest standard deviation without correction and the best improvement

when applying the correction (2.34 m) going from 6.43 m to 4.09 m. As it was pointed before, satellite 04 was substituted early this year (2020).

Appendix B shows the standard deviation for each satellite on the Galileo constellation. On the radial component one satellite kept the same values (E02), all other satellites had an improvement when the PCO correction was applied. The highest improvement was 0.68 m (E08). On the radial component the satellite with the highest standard deviation was E19 (0.78 when corrected and 1.06 m without it) and E25 the smallest (0.64 when corrected and 0.25 m without it). On the along-track component, all satellites had a better value for the standard deviation when the correction was used, the average improvement for this component was 0.74 meters. Satellite E19 had the largest standard deviation, but also the greatest improvement when the correction was applied (2.14 m when corrected and 3.14 m without it). For the cross-track axis all satellites had a smaller standard deviation with the PCO corrections. Again, E19 had the biggest standard deviation and the best improvement when applying the correction (1.49 m when corrected and 2.29 m without it). E19 had already presented high values for the RMSE probably due to the fact it is one of the oldest FOC from the constellation, launched in 2012.

Appendix C shows the standard deviation for each satellite on the GLONASS constellation. On the radial component all satellites kept the same standard deviation with values between 5.47 m and 5.30 m. On the radial axis the satellite with the highest standard deviation was R19 (5.47 m with and without the PCO correction) and R01 the smallest (5.30 m with and without the PCO corrections). On the along-track component all satellites had a lower value for the standard deviation when the correction was used. The average improvement for this axis was 0.13 meters. Satellite R10 had the largest standard deviation (4.85 m when corrected and 4.93 m without it), the greatest improvement when the correction was applied appeared on satellite R03 (0.23 m). For the cross-track component all satellites had a smaller standard deviation with the PCO corrections and R15 had the biggest standard deviation (3.26 m when corrected and 3.50 m without it). The best improvement when applying the correction happened for R21 (0.49m), going from 2.87 m to 2.38 m.

Appendix D shows the standard deviation for each satellite on the BeiDou constellation. On the radial component when applying the PCO correction 4 satellites become better, 3 got worse and 2 did not change their standard deviations, with values between 1.09 m and 0.41. On the radial component the satellite with the highest standard deviation was C06 (1.09 m when corrected and 1.11 m without it) and C12 the smallest (0.61 m when corrected and 0.63 m

without it). On the along-track component when the correction was used 7 out of the 9 satellites lowered their standard deviation, the average improvement for this component was 0.07 meters. Satellite C12 had the largest standard deviation (2.06 m when corrected and 2.26 m without it), the greatest improvement when the correction was applied appeared on satellite C16 (0.27 m). For the cross-track component, all satellite had a smaller standard deviation with the PCO corrections, C13 had the biggest standard deviation (2.62 m when corrected and 2.78 m without it) and the best improvement when applying the correction happened for C16 (0.46 m) going from 2.87 m to 2.38 m.

Appendix E shows the standard deviation for each system, one can see that on the radial component all systems improved. GLONASS had the highest standard deviation (5.39 m) and Galileo had the smallest one (0.60 m). On the along-track axis BeiDou and GLONASS had an increase in the standard deviation (0.19 m and 0.12 respectively) and Galileo and GPS had lower the standard deviation (0.81 m and 0.02 respectively). The largest standard deviation was for GLONASS (3.94 m when corrected and 3.82 m without it). Finally, for the cross-track component Galileo, BeiDou and GLONASS presented better standard deviations (an improvement of 0.42 m, 0.48 m, and 0.21 m respectively) and GPS a worsening one on the values of 0.12 m. The biggest standard deviation was for GLONASS (2.47 m when corrected and 3.82 without it). The final 3D standard deviation should not change as the PCO correction is a systematic error, it was the case for GPS, GLONASS and BeiDou, however, for Galileo, it was not the case. Galileo went from a final 3D standard deviation of 2.04 m to 1.17 m when corrected. The attitude of the satellite, the changing in referential and random errors on the broadcast ephemeris could be the cause for such a drastic difference.

The results presented reflect the difficulties in determing the corrections using the PCO's vectors. There are grey zones during the process. The first one is the influence of external factors that are needed to transform from the ECEF to the Body-fixed frame. For this process it is needed to determine the Sun's coordinate, however, using the low precision algorithm could have influenced the discrepant results for GPS that had several satellites with worse 3D RMSE after the correction. Another strong element that needs further analysis is the values available for PCO, the two main sources for this research (Montenbruck et al. (2014) and ANTEX 14) presented different values for the x, y and z corrections for GPS and GLONASS. Lastly it is important to completely understand the satellite attitude, the worsening for BeiDou in 2015 could be caused by the change in the attitude model, that was not considered in this research.

4 PDOP AND WPOP

In this chapter, it will be shown the mathematical fundamental of the position dilution of precision and its applications as well as the weighted DOP.

4.1 LEAST SQUARE ADJUSTMENTS FOR POINT POSITIONING AND ERROR PROPAGATION

As mentioned, the basic measurement made by GNSS receiver, pseudorange, is the time required for the propagation of the signal from the satellite antenna to the receiver antenna. Since GNSS signals are electromagnetic waves traveling at the speed of light it can be converted to a distance range multiplying by *c* (MONICO, 2008)

$$PD_r^s(t) = c\Delta t, \tag{63}$$

Δt is the signal travel time from satellite to receiver's antenna. Considering the pseudorange as a true representation of the geometric distance between receiver and satellite the relation between the coordinates will be:

$$PD_r^s(t) = \sqrt{(X^s(t) - X_r)^2 + (Y^s(t) - Y_r)^2 + (Z^s(t) - Z_r)^2}, \tag{64}$$

$X^s(t), Y^s(t)$ and $Z^s(t)$ are the satellite coordinates, X_r, Y_r and Z_r are the coordinates of the receiver.

At least three satellites will be necessary to determine the position of the receiver. Point positioning uses pseudorange as observable (equation 1), however, it is non-linear concerning the satellite's and receiver's coordinates. Assuming the satellite coordinates as fixed, the solution of the system will require an initial estimated value:

$$\rho_{r0}^s(t) = \sqrt{(X^s(t) - X_{r0})^2 + (Y^s(t) - Y_{r0})^2 + (Z^s(t) - Z_{r0})^2}. \tag{65}$$

X_{r0}, Y_{r0} and Z_{r0} are the initial approximated coordinates to the receiver and ρ_{r0}^{n} is the approximated geometric distance between the n-satellite and the receiver. The receiver's coordinates will be represented as:

$$X_r = X_{r0} + \Delta X_r, \tag{66}$$

$$Y_r = Y_{r0} + \Delta Y_{r,} \tag{67}$$

$$Z_r = Z_{r0} + \Delta Z_r, \tag{68}$$

the initial coordinates are corrected by the $\Delta X_r, \Delta Y_r$ and ΔZ_r which are the unknown values that will be adjusted with at least three satellite's pseudorange measurements. Substituting equations 66, 67 and 68 into equation 65 and using a first-order Taylor's series expansion it yields:

$$\rho_r^s(t) = \rho_{r0}^s(t) + \frac{\partial \rho_{r0}^s(t)}{\partial X_{r0}} \Delta X_r + \frac{\partial \rho_{r0}^s(t)}{\partial Y_{r0}} \Delta Y_r + \frac{\partial \rho_{r0}^s(t)}{\partial Z_{r0}} \Delta Z_{r,} \tag{69}$$

with the partial derivatives as:

$$\frac{\partial \rho_{r0}^s(t)}{\partial X_{r0}} = \frac{X^s - X_{r0}}{\rho_{r0}^s(t)} = a_r^s(t), \tag{70}$$

$$\frac{\partial \rho_{r0}^s(t)}{\partial Y_{r0}} = \frac{Y^s - Y_{r0}}{\rho_{r0}^s(t)} = b_r^s(t), \tag{71}$$

$$\frac{\partial \rho_{r0}^s(t)}{\partial Z_{r0}} = \frac{Z^s - Z_{r0}}{\rho_{r0}^s(t)} = c_r^s(t). \tag{72}$$

Equation 69 assumes that the clock in the GNSS receiver is synchronized with the clocks in the satellites, however, this assumption is not true. The GNSS receiver clock is not synchronized with respect to the satellite clocks, by an unknown amount. Furthermore, the clocks in the satellites are synchronized with each other and to the system timescale within about a millisecond. The range measurements made by the receiver are biased by the receiver and satellite clock errors, dt_r and dt_s,

$$PD = \rho_r^S + c(dt_r + dt_s). \tag{73}$$

The GNSS operators monitor the satellite clocks and determine the offsets and drifts with respect to system time and make the correction available through the navigation or precise ephemeris. A GNSS receiver uses these satellite clock offset values to correct the measured pseudorange. The time correction is highly important, an error of a millisecond would result in a position misleading of over 300 km. However, there is still the receiver clock offset to be determined. One extra unknown will be in the process as:

$$\rho_r^s(t) = \rho_{r0}^s(t) + a_r^s(t)\Delta X_i + b_r^s(t)(t)\Delta Y_i + c_r^s(t)\Delta Z_i + cdt^r. \quad (74)$$

From the equation 74, the model can be written to n satellites as a parametric model of X (GEMAEL; MACHADO; WANDRESEN, 2015; MONICO, 2008):

$$L = AX \quad (75)$$

$$\begin{bmatrix} \rho_{r0}^1 - \rho_r^1 \\ \rho_{r0}^2 - \rho_r^2 \\ \vdots \\ \rho_{r0}^n - \rho_r^n \end{bmatrix} = \begin{bmatrix} a_r^1(t) & b_r^1(t) & c_r^1(t) & 1 \\ a_r^2(t) & b_r^2(t) & c_r^2(t) & 1 \\ \vdots & \vdots & \vdots & \vdots \\ a_r^n(t) & b_r^n(t) & c_r^n(t) & 1 \end{bmatrix} \begin{bmatrix} \Delta x \\ \Delta y \\ \Delta z \\ cdt_r \end{bmatrix}, \quad (76)$$

the vector X can ben estimated as:

$$X = -(A^T W A)^{-1} A^T W L, \quad (77)$$

the matrix W is the weighting factor and is the result of the inverse of Σ_{lb}, which is the covariance matrix from the observed data, times the *a priori* variance (σ_0^2) that is a dimensionless scale factor (equation 78) (GEMAEL; MACHADO; WANDRESEN, 2015). PP is usually set that the *a priori* variance is equal to the variance of the measurements and there are no correlations between the observations. That yields an identity weight matrix and all the satellites will receive a unit weight in the adjustment process:

$$W = \sigma_0^2 {\Sigma_{lb}}^{-1}. \quad (78)$$

Σ_{lb} is the covariance matrix of pseudorange measurements. The variance in which the receiver's coordinates, and clock offset can be determined will be described by the covariance

matrix from the estimated solution (X). This covariance matrix is denoted as Σ_X and follows from 79 applying the error propagation law (GEMAEL; MACHADO; WANDRESEN, 2015):

$$\Sigma_X = \sigma_0^2 (A^T W A)^{-1}, \tag{79}$$

the pseudorange is uncorrelated because of the low correlation of the Golden codes used to generate the PRN for each satellite, also the variance is usually equal for all satellites and them $\Sigma_{lb} = \sigma_{UERE}^2 I$ where I is the identity matrix of order m (the same number of satellites) and σ_{UERE}^2 is the user equivalent range error (UERE). The covariance of the adjusted parameters will be given with the following elements (equation 80):

$$\Sigma_X = \sigma_{UERE}^2 \begin{bmatrix} \sigma_{xx} & \sigma_{xy} & \sigma_{xz} & \sigma_{xt} \\ \sigma_{yx} & \sigma_{yy} & \sigma_{yz} & \sigma_{yt} \\ \sigma_{zx} & \sigma_{zy} & \sigma_{zz} & \sigma_{zt} \\ \sigma_{tx} & \sigma_{ty} & \sigma_{tz} & \sigma_{tt} \end{bmatrix}, \tag{80}$$

the diagonal elements of Σ_X are the estimated variances for the receiver coordinates and clock-offset and the off-diagonal elements show the correlation between the estimated parameters.

UERE is the combination of satellite clock and ephemeris error, atmospheric error, receiver noise and multipath expressed in units of distance and can be divided in signal in space user range error (SISRE) and user equipment error (UEE). SISRE comprises the errors related to the control segment (broadcast and clock errors) as UEE is specific to the user's environment. Table 22 shows usual values for SISRE and UEE, however, those values are mostly illustrations of the level of the error budget since they can change because of multiple factors being difficult to give a universal value (HEGARTY, 2017).

Table 22 - Magnitude of UERE components

Error Source	Contribution (1σ – meters)
Broadcast satellite orbit	0.2 – 1.0
Broadcast satellite clock	0.2 – 1.9
Broadcast Group delays	0.0 – 0.2
Unmodeled ionospheric delay	0 – 5
Unmodeled tropospheric delay	0.2
Multipath	0.2 – 1
Receiver noise	0.1 - 1

Source: Hegarty (2017)

The covariance matrix can give a simple scalar indicator of the overall quality of the least-square solutions and they are referred to as dilution of precision (DOP). The Geometrical DOP (GDOP) will be given by the square root of the trace of the matrix and the position DOP (PDOP) is calculated from the three first elements of the diagonal of $(A^T A)^{-1}$. Desirable values of GDOP are about [0, 5] (LANGLEY; TEUNISSEN; MONTENBRUCK, 2017). The DOP and PDOP definitions is:

$$GDOP = \sqrt{trace(A^T A)^{-1}}, \tag{81}$$

$$PDOP = \sqrt{{\sigma_{xx}}^2 + {\sigma_{yy}}^2 + {\sigma_{zz}}^2}. \tag{82}$$

4.2 WEIGHTED PDOP

WDOP begins with the weighted least squares method where the position is calculated by assigning different weight values according to the included error magnitude for each satellite. The general weighted least squares method sets the W matrix as the inverse of the error covariance matrix of pseudorange measurements. For SPP the weight matrix is usually defined as equation (78) making it equal an identity (I). The idea of giving equal weights for every satellite does not stand along when considering the difference between system and between the physical condition that each satellite signal is under.

Considering the path that the signal travels from the satellite to the receiver, they do not go over the same conditions. The atmospheric propagation delays can be separated into two parts: the ones caused by the troposphere and the ones caused by the ionosphere. The troposphere is that part of the atmosphere that is electrically neutral and stretches from ground level up to a height of 50km, this delay depends on the temperature, pressure, humidity as well as the transmitter and receiver antennas location. The ionosphere is that region of the Earth's atmosphere in which ionizing radiation (principally from solar extreme ultraviolet) cause electrons to exist in enough quantities to affect the propagation of radio waves and goes from 50 km up to 1000 km (LEICK; RAPOPORT; TATARMIKOV, 2014; MONICO, 2008; SEEBER, 2003).

The influence of those elements will be directly related to the length of the path that the signal will go through on the atmosphere. The path will increase with lower satellite elevation angles and will the effects of those two elements, and thus, the position estimation error

increases as lower elevation angle satellites are included. However, as more low-elevation satellites are included, the geometry improves, and thus, the DOP decreases. The reduction of DOP signifies the reduction of the position estimation error due to according to equation 80, and in real situations, there are cases where the opposite occurs. As the DOP does not satisfy the position error changes affected by the satellite elevation angles, a system that employs only the DOP has the limitation of not being able to present the error trends accurately. The proposition of a WDOP that calculates the DOP by setting the weight to reflect the position error trends for a low elevation angle. Figure 21 conceptually illustrates the discussed limitation of standard DOP, showing the DOP, WDOP, and position error change trends as the elevation angle of four visible satellites is gradually reduced (WON et al., 2012).

Figure 21 - (Right) DOP, WDOP, and position error changes according to (left) satellite elevation angle changes.

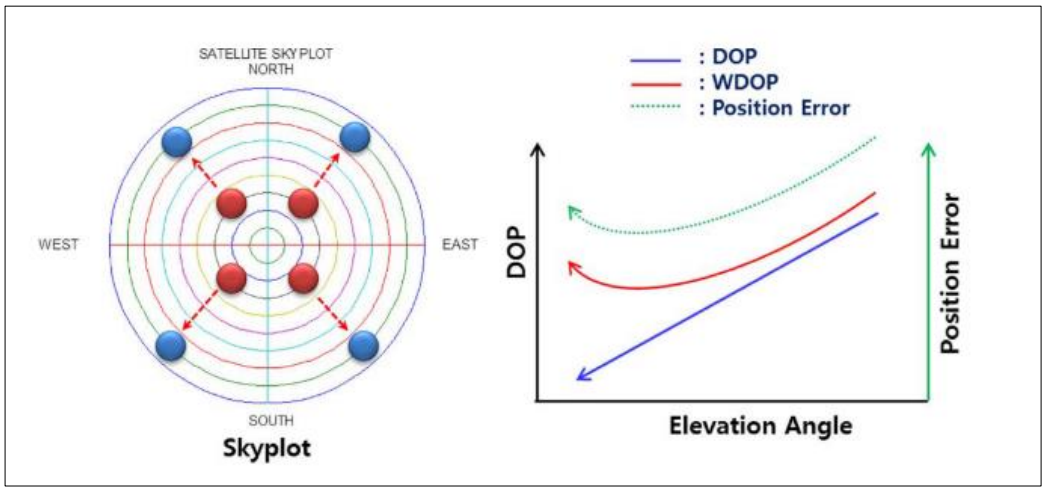

Source: Won et al. (2012)

the proposed WDOP will be driven from the cofactor matrix from equation 83

$$Q = (A^T W A)^{-1}. \tag{83}$$

4.3 METHODOLOGY FOR PDOP AND WPDOP ANALYZES

This study followed the directions from Milbert (2008) and Won et al (2012). The goal was to present a new approach to use the dilution of precision as a weighted element taking into consideration the elevation angle from the satellite. For this, the BRAZ station was chosen from the Brazilian Continuous Monitoring Network (RBMC) as a case of study. The reference

coordinates used were acquired from the description file and are: x = 4114014.0848, y= -4550641.5491 and z = -1741444.0190.

To evaluate the proposed method two years were chosen: 2014 and 2019. They were picked out because of their positions in the solar cycle. 2014 is on the peak of cycle 24, while 2019 is on the lower end of the same cycle as is shown in figure 22. As the weighted model considers the interference that the signal suffers during its traveling through the atmosphere, this is a strong factor to be evaluated.

Figure 22 – International sunspot number S_0= last 13 years and forecasts

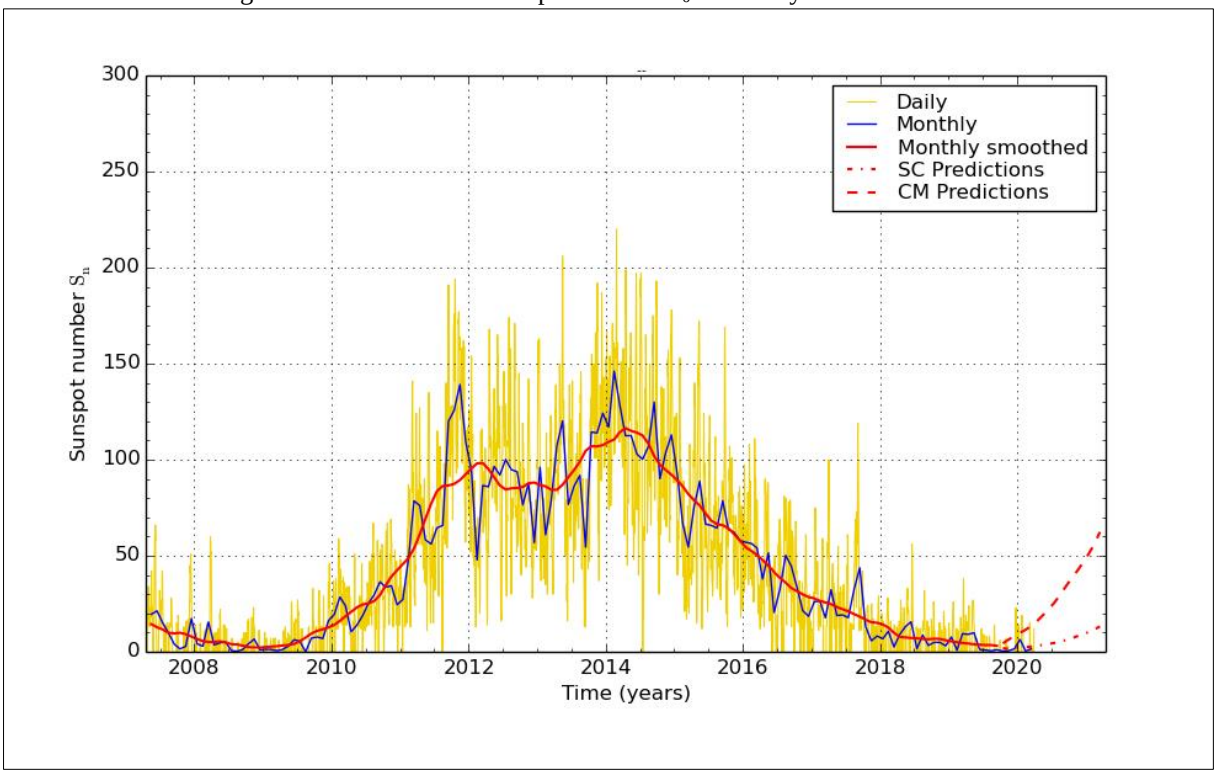

Source: SILSO graphics (http://sidc.be/silso) Royal Observatory of Belgium (04/02/2020)

For each year, six days were analyzed: The summer and winter solstice with the days after and before, they were chosen for their representation of the highest variability on both elements of the atmosphere: troposphere and ionosphere due to the solar zenith angle (PROL, 2015). For 2014 those days were July 20th, 21st (winter solstice for the southern hemisphere) and 22nd and for December they were 19th, 20th (summer solstice for the southern hemisphere), and 21st. For 2019 they were on July 20th, 21st (winter solstice for the southern hemisphere) and 22nd, for December the days were 20th, 21st (summer solstice for the southern hemisphere) and 22nd.

From the downloaded broadcast ephemeris, the coordinates for all satellites were acquired. The azimuth A and elevation angle E or zenith angle z of a satellite Sj as seen from a ground station Bi (BRAZ) can be computed from the coordinates of the ground station ri and of the satellite rj (SEEBER, 2003). The calculations were developed on a Python 2.7 scrip

$$r_j - r_i = \begin{pmatrix} \delta X \\ \delta Y \\ \delta Z \end{pmatrix}, \tag{84}$$

$$A = \tan^{-1} \frac{-\sin \Lambda\, \delta \mathrm{X} + \cos \Lambda\, \delta Y}{-\sin \Phi \cos \Lambda\, \delta \mathrm{X} - \sin \Phi \sin \Lambda\, \delta Y + \cos \Phi\, \delta \mathrm{Z}}, \tag{85}$$

$$z = \cos^{-1} \frac{\cos \Phi \cos \Lambda\, \Delta X + \cos \Phi \sin \Lambda\, \Delta Y + \sin \Phi\, \Delta Z}{(\delta X^2 + \delta Y^2 + \delta Z^2)^{1/2}}, \tag{86}$$

note that ϕ and Λ are the astronomical latitude and longitude. In approximate calculations, ϕ and Λ can be substituted by the ellipsoidal coordinates ϕ and λ (SEEBER, 2003).

With the azimuth and elevation, the PDOP is calculated using the formulas presented in section 4.1. The weighted model for WPDOP was studied by Li (2009) and an experimental model for the weight matrix was proposed by Won et al. (2012), which will be used for this research. For the model definition it was assumed pseudorange measurement error was configured to increase with a decrease in satellite elevation angle (figure 21) and was achieved by analyzing the residual from the measured pseudorange and the geometric distance between station and satellite. Equation 87 shows the estimated variance concerning the elevation angle

$$\sigma_\theta = 5.504 + 35.26\, e^{-\frac{\theta}{10.14}}. \tag{87}$$

With the function represented by equation 87 the WPDOP was determined. Figure 23 shows the flowchart for the calculation process.

Figure 23 - Flow chart for PDOP and WPDOP calculation

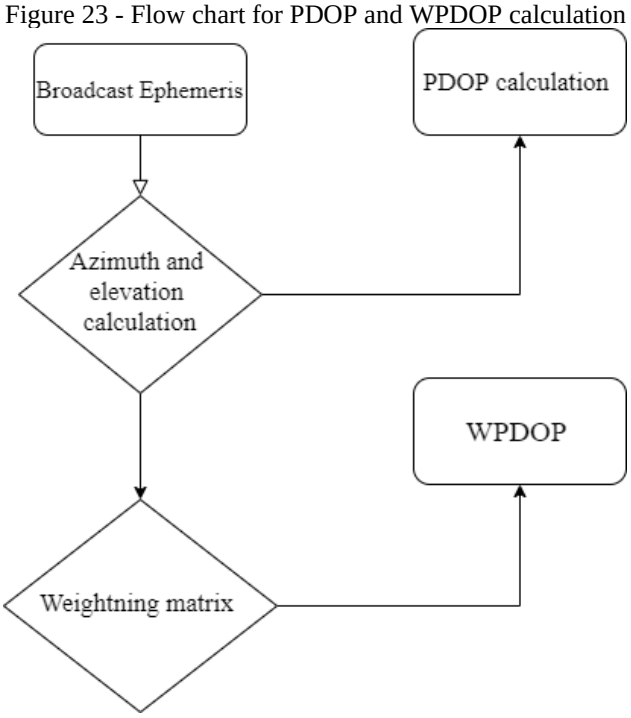

After calculating WPDOP and PDOP, next it was processed the data (SPP) for each day on the reference stations. For this part, it was used the software RTKLib 2.4.2. RTKLIB is an open-source program package for standard and precise positioning with GNSS (global navigation satellite system). RTKLIB consists of a portable program library and several APs (application programs) utilizing the library (TAKASU; YASUDA, 2013). The RINEX files were acquired from the RBMC and the settings for the SPP are presented in table 23.

Table 23 - Settings for the processed (SPP) days on the experiment

	2014	2019
Ephemeris	Broadcast	Broadcast
Elevation mask	10°	10°
Available systems	GPS and GLONASS	GPS, GLONASS, and Galileo
Ionosphere	Broadcast models	Broadcast models
Troposphere	Saastamoinen	Saastamoinen
Epochs	15 min	15 min

The error was determined from the known coordinates on the descriptive file of the station for each epoch being determined as the difference between the known coordinates and the ones estimated. With the errors and values of PDOP and WPDOP the correlation between them was calculated. Equation 88 shows how the correlation between two variables (x and y)

can be calculated, in this study the *x* variable was the 3D error and the *y* variable were the PDOP or the WPDOP.

$$r_{xy} = \frac{\sum(x_i - \bar{x})(y_i - \bar{y})}{\sqrt{\sum(x_i - \bar{x})^2 \sum(y_i - \bar{y})^2}}, \quad (88)$$

where:

rxy – the correlation coefficient of the linear relationship between the variables x and y;

x_i – the values of the x-variable in a sample;

$\bar{x}$ – the mean of the values of the x-variable;

y_i – the values of the y-variable in a sample;

$\bar{y}$ – the mean of the values of the y-variable.

The interpretation for the correlation was used as presented in table 24 (SCHOBER; BOER, 2018)

Table 24 - Conventional Approach to Interpreting a Correlation Coefficient

Absolute Magnitude of the Observed Correlation Coefficient	Interpretation
0.00 – 0.10	Negligible correlation
0.10 – 0.39	Weak correlation
0.40 – 0.69	Moderate correlation
0.70 – 0.89	Strong correlation
0.90 – 1.00	Very strong correlation

Source – Schober; Boer (2019)

Figure 24 shows the steps for the second part of the processing.

Figure 24 – Flowchart for the correlation between 3D error and PDOP or WPDOP

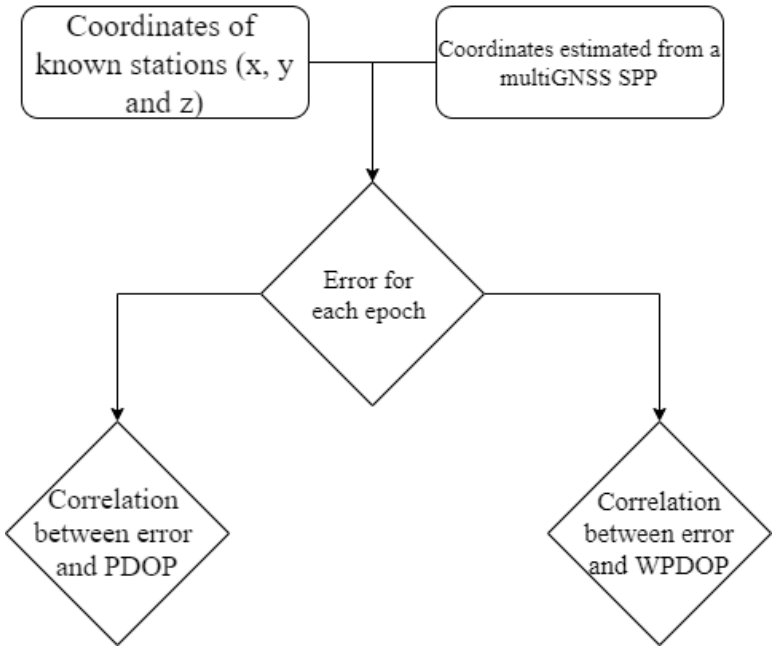

The results for the 6 days of 2014 are summarized in table 25. For the 6 days of processed data, day 171 had the highest 3D RMSE (9.38 m). The correlation between PDOP and 3D error presented a week correlation on 84 % (5) of the days and a negligible correlation for 16% (1). WPDOP had a moderate correlation on 84% of the days and a strong correlation for 16% of them. For the winter the correlation on the WPDOP was higher than the summer in 31 %, that is caused probably due to the effects of the ionosphere during summer in the pick of the solar cycle since the model for WPDOP only considered the satellites' elevation angle and not a physical model of the ionosphere. The 3D RMSE also shows the influence of the ionosphere.

Table 25 - Results for the days in 2014

Year	2014					
Month	July			December		
Day	20 th	21st	22nd	19th	20th	21st
3D RMSE	4.06	2.55	3.27	9.38	8.36	8.20
Mean PDOP	1.55	1.38	1.55	1.21	1.24	1.20
Mean WPDOP	6.71	8.96	6.65	7.54	7.59	8.07
Average n° of satelites	15.99	16.00	15.99	15.73	15.76	16.07
Correlation coefficient (error x PDOP)	-0.15	0.17	-0.06	0.10	0.10	0.05
Correlation coefficient (error x WPDOP)	0.54	0.76	0.50	0.46	0.46	0.45

Figure 25- PDOP, WPDOP and 3D error plot for the days analyzed inf 2014

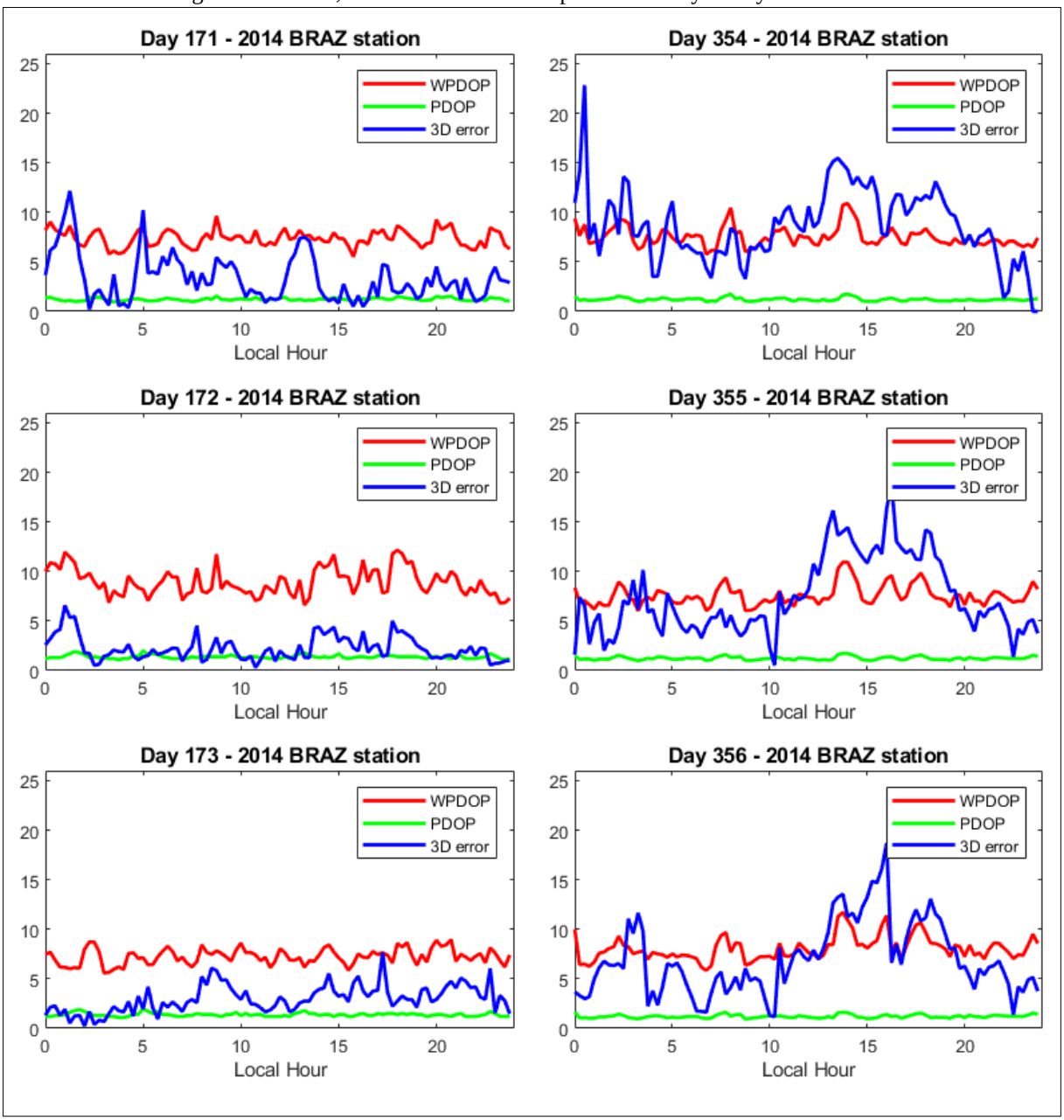

Figure 25 shows the values of PDOP and WPDOP for 2014 through the day for all days. In winter (days 171, 172, and 173) the PDOP was very stable and the 3D error fluctuated between 0.4 m and 13 m, and the correlation coefficient showed that there is a weak connection between the PDOP and 3D error values. WPDOP presented a moderate correlation with a better agreement being capable of indicating the quality of SPP accuracy. For summer the PDOP was also stable showing a very low variability when comparing to winter, however, the 3D error

reached 23.55 m. The higher 3D error can be explained due to the ionosphere, which is more active in the summer. The correlation was still week between PDOP and 3D error but was classified as moderate for the proposed WPDOP.

The results for the 6 days of 2019 are summarized in table 26. For the 6 days of processed data, 355 had the highest 3D RMSE (4.69 m). The correlation between PDOP and the 3D error presented a negligible correlation on 66 % (4) of the days and a week correlation for 36% of the days. WPDOP had a moderate correlation on 84% of the days and a strong correlation for 16% of the days. For 2019 the winter and the summer did not present a high discrepancy on the 3D RMSE, WPDOP values and on the correlation categories, that could be explained by the lower variation of the ionosphere when compared to 2014, what indicates that the proposed model will have a better result when used on a less variable environment.

Table 26 - Results for the days of 2019

Year	2019					
Month	July			December		
Day	20th	21 st	22nd	20th	21st	22nd
3D RMSE	4.69	2.20	3.99	2.56	2.54	2.94
Mean PDOP	1.15	1.01	1.02	1.13	1.18	1.04
Mean WPDOP	6.31	6.52	6.55	6.90	6.19	6.27
Average n° of satelites	22.00	23.20	25.93	21.93	20.91	22.78
Correlation coefficient (error x PDOP)	0.12	-0.01	-0.04	0.21	-0.09	0.05
Correlation coefficient (error x WPDOP)	0.60	0.67	0.58	0.79	0.58	0.42

Figure 26 shows the values of PDOP and WPDOP for 2019 through the day for all days. In winter (days 171, 172, and 173) the PDOP was stable and the 3D error fluctuated between 0.4 m and 13 m, and the correlation coefficient showed that there is a weak connection between the PDOP and 3D error values. WPDOP presented a moderate correlation with a better agreement. For summer the results are close to the ones got from the winter due to the lower variation of the ionosphere.

Figure 26 - PDOP, WPDOP and 3D error plot for the days analyzed inf 2019

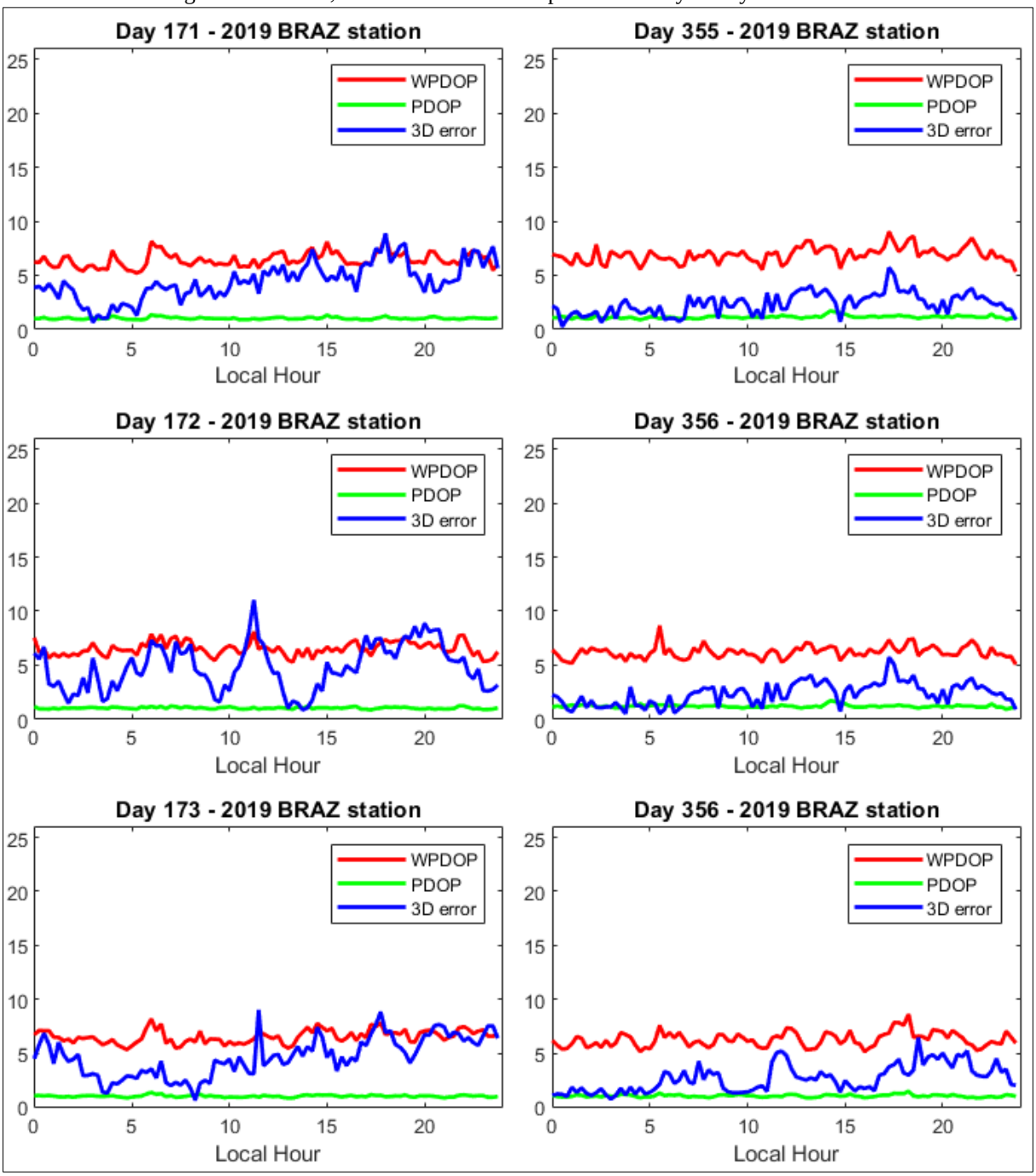

5 DISCUSSIONS, FINAL CONSIDERATIONS AND CONCLUSIONS

The GNSS modernization with the inclusion of BDS and Galileo in the last decade opened the application opportunities on the navigation and timing activities. Galileo specifically has been growing quickly and is already fully operational. The integration between systems however still needs to be fully understood. Each GNSS has its realization, time system, reference frame, and a different structure even for the spacecraft. The IGMA trial project is an initiative that aims to investigate the new systems as well as to update the information about the older ones. This research is part of the IGMA efforts as one of the analysis centers and works with two parameters and four systems.

Chapter 3 presents the analyzes over the accuracy of broadcast ephemeris. Previous studies have been done about this topic (MACIUK, 2016; MONTENBRUCK; STEIGENBERGER; HAUSCHILD, 2014; WARREN, 2002) however a longer period of analyzes was used to access the temporal variation and evaluate its change through the years. The satellites' coordinates were determined using the indicated methods on each ICD system respectively.

Several studies have evaluated the accuracy of the broadcast ephemeris, but most of them did not mention the needed correction between the center of phase, where the coordinates from broadcast messages are calculated, and the center of mass, where the final ephemeris are determined. One of the main goals of this analyzes was to evaluate the influence on the final accuracy when the PCO correction was evaluated in a long-term data set for each system.

Through the years GPS did not present a large variation on the RMSE of the residuals between the calculated coordinates and the finals ephemeris. The cross-track component presented the smallest values of RMSE and the along-track the highest one. During the years the 3D component had RMSE always below 2 m. For the 5 years and computing for the 600 days the system presented an overall 3D RMSE of 2.03, when applying the correction between CoP and CoM the RMSE decreased in 0.09 m reaching 1.94 m.

Galileo presented a large variation on the RMSE of the residuals between the calculated coordinates and the finals ephemeris, starting with a 3D RMSE of 7.58 m (2015) and going down to 1.63 (2019). The cross-track component presented the smallest values of RMSE and the along-track the highest. For the 5 years and computing for the 600 days the system presented an overall 3D RMSE of 2.28; when applying the correction between CoP and CoM the RMSE decreased in 1.09 m. The results for Galileo show why the temporal component is important in

the analyzes of the accuracy of the navigation message. In the period of 5 years the 3D RMSE improved decreasing in 5.95 meters. The improvement increases the reliability of the system and its comparison with a well-stabilized system such as GPS and GLONASS

GLONASS had the highest values of 3D RMSE. The cross-track component presented the smallest values of RMSE and radial the highest. For the 5 years and computing for the 600 days the system presented an overall 3D RMSE of 7.21 m, when applying the correction between CoP and CoM the RMSE decreased in 0.04 m. The results from GLONASS reveal that this system needs further analyzes, one of the causes of the result may be the numerical integration need to calculate its coordinates, mostly when choosing the size of the step that it will go through. In this study it was used a size step of 1 second, decreasing this could improve the final 3D RMSE. GLONASS was later added to the project, so our results are still not aligned to the other members of the group, which can offer feedback on how to properly process the broadcast ephemeris of this system.

BeiDou had a steady 3D RMSE through the years with the radial component with the smallest RMSE and the along-track component with the biggest, however, the results when applying the CoM and CoP correction presented an abnormal behavior. For the first two years (2015 and 2016) applying the correction induced a worsening on the RMSE, however for the remaining years there was an improvement for all components and the 3D RMSE. Further analyzes are needed to evaluate, but BeiDou is the only system that for its attitude model can assume different configurations (yaw steering and orbital normal). To determine the differences, it is needed to evaluate the beta angle, and this was not done during this research. The change in the attitude model may cause the worsening of the RMSE when applying the corrections.

Overall results show that the systems do not have the same quality on its navigation message. Galileo had the smallest RMSE (with correction) of 1.19 m, next GPS (1.94), then BeiDou (3.19 m), and then GLONASS (7.21 m). Although it is not mentioned through many studies, the correction between CoM and CoP when comparing and also when using the ephemeris are highly recommended as for this study all systems had an improvement when doing so.

Chapter 4 addressed the second variable of this study: the dilution of precision (DOP). Likewise, the accuracy of broadcast ephemeris, PDOP, and WPDOP have been evaluated before (MENEGHINI; PARENTE, 2017; MILBERT, 2008; TAHSIN et al., 2015; WON et al., 2012). The goal of this analyzes was to measure the correlation of PDOP and WPDOP with the

3D error of a standard point positioning. For this, two years were chosen and for each year six days were analyzed.

For the days analyzed, PDOP had an average value of 1.30 and never going over 2.00, which indicates a good geometry and a good quality of the solution. Even though the values of PDOP were in the expected range, when comparing its variation through the day with the 3D error of the receiver station (BRAZ), the values showed that they are not correlated. 75% of the analyzed days had a week correlation and the remaining days did not present any correlation. The lack of connection between PDOP and the error during the SPP shows that these values cannot be used as a determinate element to decide if the quality of the positioning process is good or not. Other factors will influence this making the PDOP not even correlated at all with the final error.

Due to the lack of correlation presented before, it was proposed to evaluate the so-called WPDOP, where during the process not only the geometry but also the path done by the traveling signal was accounted for s a factor of influence. The WPDOP was calculated using a function determined in a previous study, its range of value is yet to be categorized. For the correlation it was strong for 16% of the days and a moderate correlation was found for the remaining days. WPDOP had a better agreement but still moderate for most of the experiments. The only significant variation was for the summer during the pick of the solar cycle, which could be due to the influence of the ionosphere, which represented variations on the season and the solar sunspot cycle to see how does will affect the correlation. The results show that determine the quality of an SPP depends not only on the geometry or the path that the signal travels, that are many elements to be accounted for. WPDOP had an overall better correlation with the 3D error of the SPP. PDOP on the other hand almost did not have any correlation.

The results of this dissertation reflect the goals of the IGMA-trial project, which aims to keep track of the GNSS variables. The variation on the quality of navigation message (Galileo as being the best example), the necessity to include a weighting factor on a well-known element (PDOP) to give it a meaningful usage are some of the initial achievements of Unesp's contribution to the project.

The IGMA trial project is still undergoing and therefore some elements need further analyzes for both elements of this research. On the accuracy of the broadcast ephemeris the variation on the standard deviation for Galileo still needs to be addressed as well as its improvement overtime needs to be better explained. GLONASS processing methods need to be better understood and aligned with the other analyzes center. For PDOP a more extended

analyzes needs to be carried out to evaluate the correlation of this element with the quality of the positioning. The proposed WPDOP showed a better correlation but it uses information from a model, higher improvement may be achieved when physical elements are added to the weighting matrix such as the differences in the broadcast messages from each system, broadcast models for the ionosphere and analytical models for the troposphere.

REFERENCES

BARTOLOMÉ et al., Overview of Galileo System. In: Nurmi et al.(Ed.). **GALILEO Positioning Technology**, Spring, 2015. p. 3-8.

BEARD, R.; SENIOR, K. Clocks. In: TEUNISSEN, P.J.G.; MONTENBRUCK, O (Ed.). **Spring Handbook of Global Navigation Satellite System, Spring**, 2017. p.121-164.

BISWAS, S. K.; QIAO, L.; DEMPSTER, A. G. Effect of PDOP on performance of Kalman Filters for GNSS-based space vehicle position estimation. **GPS Solutions**, v. 21, n. 3, p. 1379–1387, 2017.

GEMAEL, C.; MACHADO, A. M. L.; WANDRESEN, R. **Introdução ao ajustamento das observações: aplicações geodésicas**. 2° ed. Curitiba: Ed. UFPR, 2015.

HAN, S. et al. Minimum of PDOP and its applications in inter-satellite links (ISL) establishment of Walker-?? constellation. **Advances in Space Research**, v. 54, n. 4, p. 726–733, 2014.

JEREZ, G. **ANÁLISE DA INTEGRAÇÃO GPS/GLONASS PARA POSICIONAMENTO SOB EFEITO DE CINTILAÇÃO IONOSFÉRICA**. [s.l.] UNIVERSIDADE ESTADUAL PAULISTA "JÚLIO DE MESQUITA FILHO", 2017.

KLEUSBERG, A.; TEUNISSEN, P. J. G. **GPS for Geodesy**. [s.l.] Springer Berlin Heidelberg, 1996.

KOUBA, J. A GUIDE TO USING INTERNATIONAL GNSS SERVICE (IGS) PRODUCTS. 2009.

LEICK, A.; RAPOPORT, L.; TATARMIKOV, D. **GPS SATELLITE SURVEYING**. 4. ed. [s.l: s.n.].

LI, J. The improvement of positioning accuracy with weighted least square based on SNR. n. 3, p. 9–12, 2009.

MACIUK, K. DIFFERENT APPROACHES IN GLONASS ORBIT COMPUTATION FROM BROADCAST EPHEMERIS. **GEODETSKI VESTNIK**, v. 60, n. 3, 2016.

MENEGHINI, C.; PARENTE, C. Advantages of Multi GNSS Constellation: GDOP Analysis for GPS, GLONASS and Galileo Combinations. **Weenect**, v. 7, n. 1, p. 1–10, 2017.

MILBERT, D. Dilution of precision revisited. **Navigation, Journal of the Institute of Navigation**, v. 55, n. 1, p. 67–81, 2008.

MONICO, J. F. G. **Posicionamento pelo GNSS**. 2. ed. São Paulo - SP: Editora Unesp, 2008.

MONTENBRUCK, O. et al. GNSS satellite geometry and attitude models. **Advances in Space Research**, v. 56, p. 1015–1029, 2015.

MONTENBRUCK, O. et al. The Multi-GNSS Experiment (MGEX) of the International GNSS Service (IGS) – Achievements, prospects and challenges. **Advances in Space Research**, v. 59, n. 7, p. 1671–1697, 2017.

MONTENBRUCK, O.; GILL, E. **Satellite Orbits**. Berlin, Heidelberg: Springer Berlin Heidelberg, 2000.

MONTENBRUCK, O.; STEIGENBERGER, P.; HAUSCHILD, A. Broadcast versus precise ephemerides: a multi-GNSS perspective. 2014.

MONTENBRUCK, O.; STEIGENBERGER, P.; HAUSCHILD, A. Multi-GNSS signal-in-space range error assessment – Methodology and results. **Advances in Space Research**, v. in press, p. 20, 2018.

NURMI, J. et al. **GALILEO Positioning Technology**. [s.l.] Spring, 2015.

PENINA, A.; LISA, R. GPS Modeling Summary and Analysis GPS Satellite Predictions Axial Ratio of Research : 2003.

PETROVSKI, I. G. **GPS, GLONASS, galileo, and beidou for mobile devices**. 1. ed. [s.l.] Cambridge University Press, 2012.

PLAG, H.-P.; PEARLMAN, M. **Global Geodetic Observing System: Meeting the Requirements of a Global Society on a Changing Planet in 2020**. [s.l.] Springer-Verlag, 2006.

PROL, F. DOS S. **TOMOGRAFIA DA IONOSFERA A PARTIR DO GNSS E TÉCNICAS ALGÉBRICAS: ESTUDO DE CASO PARA A REGIÃO BRASILEIRA**. [s.l.] Unesp, 2015.

SCHOBER, P.; BOER, C. Correlation Coefficients: Appropriate Use and Interpretation. n. February, 2018.

SEEBER, G. **Satellite geodesy : foundations,methods, and applications**. New York: Walter de gruyter, 2003.

SEMPLE, E. C. GEOGRAPHICAL LOCATION AS A FACTOR IN HISTORY.*. v. 40, n. 2, p. 65–81, 1908.

STEIGENBERGER, P. et al. Galileo orbit and clock quality of the IGS Multi-GNSS Experiment. **Advances in Space Research**, v. 55, p. 269–281, 2015.

TAHSIN, M. et al. Analysis of DOP and its preciseness in GNSS position estimation. **2nd International Conference on Electrical Engineering and Information and Communication Technology, iCEEiCT 2015**, n. May, p. 21–23, 2015.

TAKASU, T.; YASUDA, A. RTKLIB ver. 2.4.2 Manual. n. C, p. 181, 2013.

TANG, X. et al. GPS/BDS relative positioning assessment by zero baseline observation. **Measurement**, 2017.

TENG, Y.; WANG, J.; HUANG, Q. Mathematical minimum of Geometric Dilution of Precision (GDOP) for dual-GNSS constellations. **Advances in Space Research**, v. 57, n. 1, p. 183–188, 2016.

THOMPSON, B. F. et al. Computing GPS Satellite Velocity and Acceleration from the Broadcast Navigation Message. p. 769–779, 2019.

WARREN, D. L. M. **BROADCAST VS PRECISE GPS EPHEMERIDES: A HISTORICAL PERSPECTIVE**. [s.l.] Air University, 2002.

WON, D. H. et al. Weighted DOP with consideration on elevation-dependent range errors of GNSS satellites. **IEEE Transactions on Instrumentation and Measurement**, v. 61, n. 12, p. 3241–3250, 2012.

XU, G. **GPS: Theory, algorithms and applications**. 2. ed. [s.l.] Spring, 2007.

YANG, L. et al. The Analysis on Geometry Dilution of Precision for. p. 762–766, 2014.

YANG, Y. et al. Introduction to BeiDou-3 navigation satellite system. **Navigation, Journal of the Institute of Navigation**, v. 66, n. 1, p. 7–18, 2019.

ZHANG, X. et al. Initial assessment of the COMPASS/BeiDou-3: new-generation navigation signals. **Journal of Geodesy**, v. 91, n. 10, p. 1225–1240, 2017.

APPENDIX A – OVERALL STANDARD DEVIATION FOR GPS SATELLITES (GREEN REPRESENTS A BETTER STANDARD DEVIATION WHEN APPLYING CORRECTION, RED A WORSE AND GREY MEANS NO CHANGE ON THE VALUE)

sv	Radial STD (m)	Corrected Radial STD(m)	Along-track STD(m)	Corrected Along-track STD(m)	Cross-track STD (m)	Corrected cross-track STD (m)
G01	0.19	0.19	1.17	0.62	1.34	0.97
G02	0.13	0.13	1.15	0.6	1.1	0.57
G03	0.26	0.25	1.32	0.66	1.43	1.41
G04	1.01	1.01	6.53	3.67	6.43	4.09
G05	0.13	0.13	1.01	0.52	0.96	0.50
G06	0.18	0.18	1.03	0.6	1.08	0.84
G07	0.13	0.13	1.05	0.67	1.00	0.64
G08	0.28	0.27	1.89	0.94	1.77	1.03
G09	0.18	0.18	0.98	0.57	1.19	0.91
G10	0.26	0.25	1.3	0.66	1.41	0.95
G11	0.16	0.16	1.51	0.79	1.42	0.76
G12	0.14	0.14	1.1	0.63	1.05	0.6
G13	0.13	0.13	1.15	0.59	1.08	0.57
G14	0.12	0.12	1.31	0.71	1.26	0.68
G15	0.12	0.12	1.1	0.63	1.04	0.60
G16	0.14	0.14	1.03	0.56	0.96	0.53
G17	0.13	0.13	1.4	0.67	1.32	0.64
G18	0.41	0.40	2.28	1.27	2.09	1.2
G19	0.11	0.11	1.03	0.57	0.98	0.55
G20	0.12	0.12	1.07	0.67	1.02	0.65
G21	0.14	0.14	1.34	0.71	1.26	0.68
G22	0.15	0.15	1.15	0.7	1.1	0.67
G23	0.12	0.12	1.11	0.68	1.06	0.66
G24	0.23	0.23	1.19	0.59	1.48	0.89
G25	0.17	0.16	1.17	0.63	1.24	0.9
G26	0.28	0.30	2.07	0.95	1.93	1
G27	0.19	0.19	1.12	0.61	1.32	1.02
G28	0.16	0.16	1.22	0.58	1.15	0.56
G29	0.14	0.14	1.47	0.75	1.39	0.72
G30	0.17	0.17	1.15	0.56	1.37	0.95
G31	0.12	0.12	1.17	0.6	1.12	0.57
G32	0.39	0.38	1.84	0.83	1.68	0.92

APPENDIX B – OVERALL STANDARD DEVIATION FOR GALILEO SATELLITES (GREEN REPRESENTS A BETTER STANDARD DEVIATION WHEN APPLYING CORRECTION, RED A WORSE AND GREY MEANS NO CHANGE ON THE VALUE)

sv	Radial STD (m)	Corrected Radial STD(m)	Along-track STD(m)	Corrected Along-track STD(m)	Cross-track STD (m)	Corrected cross-track STD (m)
E01	0.80	0.75	1.35	0.24	0.62	0.22
E02	0.37	0.37	0.69	0.25	0.41	0.20
E03	0.35	0.34	0.65	0.25	0.39	0.26
E04	0.34	0.22	0.76	0.41	0.43	0.27
E05	0.37	0.36	0.75	0.41	0.43	0.27
E07	0.50	0.34	1.17	0.22	0.66	0.21
E08	1.06	0.38	1.26	0.40	0.79	0.29
E09	0.86	0.42	1.39	0.61	0.92	0.37
E11	0.75	0.69	2.20	1.41	1.39	0.89
E12	0.64	0.22	1.64	0.82	1.12	0.66
E13	0.40	0.39	0.87	0.55	0.46	0.26
E15	0.40	0.39	0.74	0.23	0.40	0.22
E19	1.06	0.78	3.59	2.14	2.29	1.49
E21	0.91	0.87	2.13	0.25	0.66	0.20
E22	0.41	0.40	0.98	0.31	0.63	0.29
E24	0.52	0.46	1.22	0.28	0.54	0.24
E25	0.35	0.35	0.64	0.25	0.36	0.18
E26	0.95	0.63	1.61	0.31	0.78	0.26
E27	0.36	0.36	0.70	0.22	0.41	0.20
E30	0.55	0.49	1.34	0.48	0.75	0.33
E31	0.35	0.32	0.70	0.27	0.40	0.25
E33	0.40	0.39	0.73	0.30	0.41	0.21
E36	0.40	0.38	0.68	0.24	0.38	0.20

APPENDIX C – OVERALL STANDARD DEVIATION FOR GLONASS SATELLITES (GREEN REPRESENTS A BETTER STANDARD DEVIATION WHEN APPLYING CORRECTION, RED A WORSE AND GREY MEANS NO CHANGE ON THE VALUE)

sv	Radial STD (m)	Corrected Radial STD(m)	Along-track STD(m)	Corrected Along-track STD(m)	Cross-track STD (m)	Corrected cross-track STD (m)
R01	5.30	5.30	3.67	3.53	2.55	2.36
R02	5.35	5.35	3.67	3.55	2.55	2.37
R03	5.33	5.33	3.74	3.51	2.59	2.34
R04	5.33	5.33	3.52	3.41	2.54	2.35
R05	5.31	5.31	3.66	3.56	2.56	2.37
R06	5.29	5.29	3.92	3.83	2.70	2.51
R07	5.33	5.33	3.55	3.44	2.55	2.36
R08	5.33	5.33	3.71	3.50	2.63	2.35
R09	5.33	5.33	3.95	3.86	2.61	2.44
R10	5.45	5.45	4.93	4.85	2.89	2.72
R11	5.36	5.36	3.54	3.39	2.56	2.31
R12	5.37	5.37	3.71	3.59	2.60	2.44
R13	5.39	5.39	4.11	4.01	2.68	2.50
R14	5.42	5.42	3.85	3.66	2.66	2.41
R15	5.44	5.44	5.83	5.74	3.50	3.26
R16	5.36	5.36	4.40	4.30	2.81	2.65
R17	5.43	5.43	3.69	3.60	2.58	2.41
R18	5.44	5.44	3.35	3.21	2.50	2.30
R19	5.47	5.47	3.82	3.65	2.64	2.43
R20	5.48	5.48	3.39	3.28	2.49	2.30
R21	5.44	5.44	4.18	3.99	2.87	2.38
R22	5.46	5.46	3.37	3.25	2.48	2.29
R23	5.45	5.45	3.58	3.45	2.63	2.39
R24	5.46	5.46	3.73	3.60	2.70	2.45

APPENDIX D – OVERALL STANDARD DEVIATION FOR BEIDOU SATELLITES

	Radial STD (m)	**Corrected Radial STD(m)**	**Along-track STD(m)**	**Corrected Along-track STD(m)**	**Cross-track STD (m)**	**Corrected cross-track STD (m)**
C06	1.11	1.09	1.92	1.91	2.16	2.07
C07	0.62	0.62	1.87	1.91	2.30	2.11
C08	0.84	0.85	1.98	2.26	2.51	2.44
C09	0.96	0.96	2.01	1.9	2.55	2.25
C10	0.81	0.80	1.57	1.55	2.10	1.92
C11	0.70	0.69	2.5	2.24	1.51	1.49
C12	0.63	0.61	2.26	2.06	1.32	1.23
C13	0.77	0.7	1.93	1.82	2.78	2.62
C16	0.54	0.41	1.7	1.43	1.98	1.52

APPENDIX E – OVERALL STANDARD DEVIATION BY SYSTEM (GREEN REPRESENTS A BETTER STANDARD DEVIATION WHEN APPLYING CORRECTION, RED A WORSE AND GREY MEANS NO CHANGE ON THE VALUE)

System	Radial STD (m)	Corrected Radial STD(m)	Along-track STD(m)	Corrected Along-track STD(m)	Cross-track STD (m)	Corrected cross-track STD (m)
Galileo	0.70	0.60	1.64	0.83	1.00	0.58
BeiDou	0.83	0.83	2.09	2.28	2.58	2.10
GLONASS	5.39	5.39	3.82	3.94	2.68	2.47
GPS	0.70	0.64	1.51	1.49	0.81	0.93

ANNEXES I – CORRECTIONS USED FROM ANTEX FILE (2014)

SV	$x_{BF}(mm)$	$y_{BF}(mm)$	$z_{BF}(mm)$		SV	$x_{BF}(mm)$	$y_{BF}(mm)$	$z_{BF}(mm)$
C01	580.00	0.00	3500.00		**G01**	394.00	0.00	1501.00
C02	580.00	0.00	3500.00		**G02**	10.70	10.10	728.00
C03	580.00	0.00	3500.00		**G03**	394.00	0.00	1550.00
C04	580.00	0.00	3500.00		**G05**	-3.30	-0.30	778.00
C05	580.00	0.00	3500.00		**G06**	394.00	0.00	1467.00
C06	580.00	0.00	3500.00		**G07**	-0.40	5.00	822.40
C07	580.00	0.00	3500.00		**G08**	394.00	0.00	1501.40
C08	580.00	0.00	3500.00		**G09**	394.00	0.00	1522.10
C09	580.00	0.00	3500.00		**G10**	394.00	0.00	1515.10
C10	580.00	0.00	3500.00		**G11**	0.70	-1.20	1117.80
C11	580.00	0.00	2120.00		**G12**	10.20	-5.60	767.80
C12	580.00	0.00	2120.00		**G13**	-2.40	-1.60	1348.30
C13	580.00	0.00	3500.00		**G14**	-2.50	-1.70	1305.50
C14	580.00	0.00	2120.00		**G15**	4.50	1.90	622.00
C15	580.00	0.00	3500.00		**G16**	12.60	-6.90	1468.70
C16	580.00	0.00	900.00		**G17**	3.00	1.00	770.90
C17	580.00	0.00	3500.00		**G18**	279.00	0.00	2352.00
C18	580.00	0.00	2560.00		**G19**	8.60	-0.60	808.20
C19	-200.00	0.00	1460.00		**G20**	1.00	3.20	1313.50
C20	-200.00	0.00	1460.00		**G21**	-3.40	2.90	1359.10
C21	-200.00	0.00	1460.00		**G22**	-2.20	2.00	2850.60
C22	-200.00	0.00	1460.00		**G23**	15.40	6.80	766.10
C23	-200.00	0.00	1460.00		**G24**	394.00	0.00	1522.10
C24	-200.00	0.00	1460.00		**G25**	394.00	0.00	1517.40
C25	40.00	-10.00	1100.00		**G26**	394.00	0.00	1503.50
C26	40.00	-10.00	1100.00		**G27**	394.00	0.00	1522.00
C27	40.00	-10.00	1100.00		**G28**	1.40	4.70	999.50
C28	40.00	-10.00	1100.00		**G29**	10.90	-4.50	791.00
C29	40.00	-10.00	1100.00		**G30**	394.00	0.00	1522.10
C30	40.00	-10.00	1100.00		**G30**	394.00	0.00	1522.10
C31	-50.00	0.00	900.00		**G31**	-0.80	5.80	912.50
C32	-200.00	0.00	1460.00		**G32**	394.00	0.00	1534.80
C33	-200.00	0.00	1460.00		**R01**	-545.00	0.00	2306.90
C34	40.00	-10.00	1100.00		**R02**	-545.00	0.00	2413.00
C35	40.00	-10.00	1100.00		**R03**	-545.00	0.00	2517.20
C36	-200.00	0.00	1460.00		**R04**	-545.00	0.00	2333.00
C37	-200.00	0.00	1460.00		**R05**	-545.00	0.00	2333.00
C38	-70.00	-310.00	1990.00		**R06**	-545.00	0.00	2411.00
C39	-70.00	-310.00	1990.00		**R07**	-545.00	0.00	2600.10
C40	-70.00	-310.00	1990.00		**R08**	-545.00	0.00	2323.80
C45	-200.00	0.00	1460.00		**R09**	-545.00	0.00	2083.00

SV	$x_{BF}(mm)$	$y_{BF}(mm)$	$z_{BF}(mm)$
C46	-200.00	0.00	1460.00
C47	-200.00	0.00	1460.00
C48	-200.00	0.00	1460.00
C48	40.00	-10.00	1100.00
C56	-50.00	-300.00	1160.00
C57	-200.00	10.00	1500.00
C58	-200.00	10.00	1500.00
C59	-60.00	-310.00	2090.00
E01	122.00	-9.38	636.11
E02	122.69	-9.25	617.15
E03	116.00	10.00	610.00
E04	123.00	-9.59	604.15
E05	123.00	-9.59	604.15
E07	120.00	-9.18	610.92
E08	121.88	-9.83	606.20
E09	120.84	-8.52	596.95
E11	-169.80	25.85	791.85
E12	-169.51	27.83	781.42
E13	123.16	-7.69	576.44
E14	172.49	-12.41	609.38
E15	120.90	-10.06	600.83
E18	177.38	-12.78	610.84
E19	-171.01	27.94	792.08
E20	-169.76	26.69	806.57
E21	127.06	-10.96	602.85
E22	122.34	-9.50	653.93
E24	119.33	-9.53	628.78
E25	120.85	-10.35	601.00
E26	119.00	-8.46	600.95
E27	121.92	-11.03	635.69
E30	119.58	-8.88	611.48
E31	121.05	-10.28	615.06
E33	122.65	-8.35	608.59
E36	122.51	-9.76	599.06

SV	$x_{BF}(mm)$	$y_{BF}(mm)$	$z_{BF}(mm)$
R10	-545.00	0.00	2325.10
R11	-545.00	0.00	2400.00
R12	-545.00	0.00	2450.00
R13	-545.00	0.00	2375.00
R14	-545.00	0.00	2450.00
R15	-545.00	0.00	2450.00
R16	-545.00	0.00	2361.00
R17	-545.00	0.00	2394.10
R18	-545.00	0.00	2490.20
R19	-545.00	0.00	2443.80
R20	-545.00	0.00	2408.50
R21	-545.00	0.00	2398.90
R22	-545.00	0.00	2347.00
R23	-545.00	0.00	2261.90
R24	-545.00	0.00	2461.00